CHALMERS
UNIVERSITY OF TECHNOLOGY

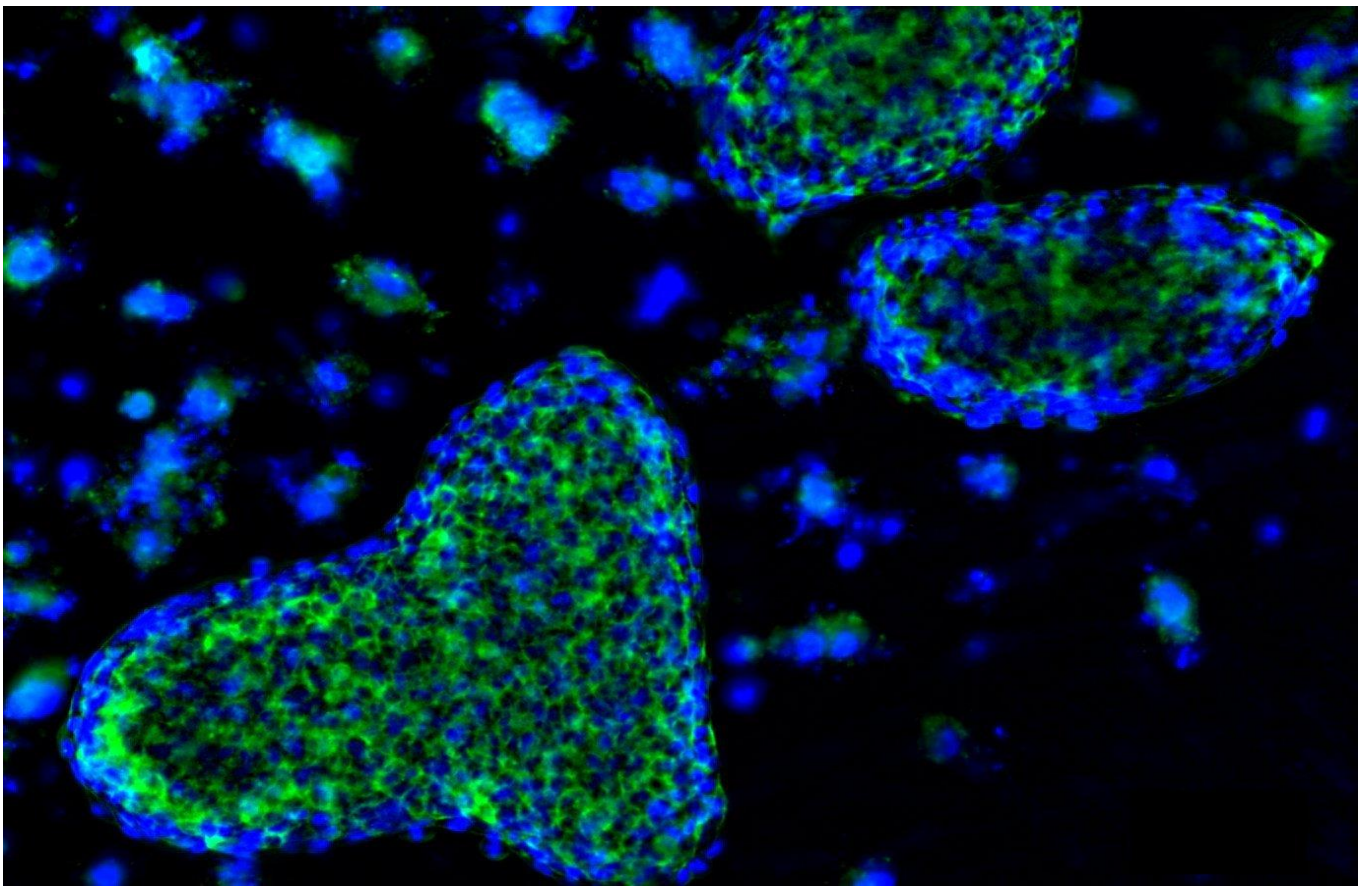

Investigation of 3D Bioprinted Co-cultures as liver tissue models

Master's thesis in Biotechnology

Maram Mohammed

Department of Physics, Division of Biological Physics
CHALMERS UNIVERSITY OF TECHNOLOGY
Gothenburg, Sweden 2019

Master's Thesis 2019

Investigation of 3D Bioprinted Cocultures as Liver Tissue Models

Maram Mohammed

CHALMERS

Department of Physics
Division of Biological Physics
CHALMERS UNIVERSITY OF TECHNOLOGY
Gothenburg, Sweden 2019

Investigation of 3D Bioprinted Cocultures as Liver Tissue Models

Maram Mohammed

© Maram Mohammed, 2019

Supervisors: Itedale Namro Redwan and Duong Nguyen CELLINK AB

Examiner: Julie Gold, Department of Physics

Master's Thesis 2019
Department of Physics
Division of Biological Physics
Chalmers University of Technology
SE-412 96 Gothenburg
Telephone: +46 31 772 1000
Performed at CELLINK AB

Cover: Actin/NucBlue stained 2:1 HepG2 to LX-2 coculture constructs on day 20 of cultivation. Image taken at 10x magnification.

Printed at Chalmers Reproservice
Gothenburg, Sweden 2019

Acknowledgement

I would like to thank my supervisors Itedale Namro Redwan and Duong Nguyen for giving me the incredible opportunity to perform this master's thesis at CELLINK and for all the guidance, support and advice throughout the project. Special thanks Isabella Bondesson for her help in the Live/Dead imaging and analysis. I would like to thank the entire Bioink and Tissue Engineering (BITE) team for their friendship and warm welcome to the team. Last but not least, I would like to thank my family without whom I would not have been able to do this.

Abstract

Liver fibrosis is a strong risk factor for liver cancer and has become a major concern worldwide. All chronic liver diseases (CLD) can lead to liver fibrosis. Nonalcoholic fatty liver disease (NAFLD) and its more severe form nonalcoholic steatohepatitis (NASH) are of particular interest to pharmaceutical companies. One obstacle in the development of efficient therapies is the lack of robust, representative, and biologically relevant *in vitro* models of human liver fibrosis to aid the development phase of pharmaceuticals. This is due to the fact that most *in vitro* models used today are 2D mono layer cultures of stellate cells. These models ignore the importance of the interplay between hepatocytes and stellate cells in liver fibrosis as well as the role played by spatial organization of the different cells.

Bioprinting allows the production of tissue-like structures that mimic the 3D architecture and complexity of native tissue. In this project two different hepatocyte to stellate cell ratios (4:1 and 2:1) in addition to a hepatocyte monoculture were 3D bioprinted to produce liver tissue models. Fibrosis was then induced by addition of the growth factor TGF-β resulting in a fibrotic liver tissue model. Auxiliary proteins supporting liver specific cells were incorporated in the bioink used. The produced fibrotic liver tissue model's viability and functionality were assessed using different assays. Namely, Live/Dead analysis, Celltiter-Blue viability assay, Lactate dehydrogenase (LDH) cytotoxicity assay, Bicinchoninic acid (BCA) protein assay and Actin/NucBlue staining. These assays were originally designed to be used on cells in 2D and not on cells imbedded in a bioink/hydrogel. These assays' applicability for use on cells bioprinted in 3D was therefore evaluated before they were used to analyze the produced bioprinted fibrotic liver tissue models.

It was possible to adapt the mentioned assays to be used with 3D bioprinted constructs. Viability, cytotoxicity and protein deposition results indicated that the 2:1 coculture ratio of HepG2 (Hepatocytes) to LX-2 cells (Hepatic stellate cells) showed greater potential in simulating liver fibrosis compared to the 4:1 ratio of HepG2 to LX-2 cells. There did not seem to be a significant difference between the group in which fibrosis was induced by TGF- β compared to the control group in any of the conditions investigated. This indicates that fibrosis may have in fact not been induced despite the addition of TGF- β as both groups were behaving in a similar manner. Further investigation is needed in this regard.

Keywords: Liver fibrosis, Cocultures, Bioprinting, HepG2, LX-2, 3D model

Table of Contents

1. Introduction 1
2. Aim 1
3. Theory 2
    3.1. The liver 2
    3.2. Liver fibrosis 7
    3.3. Fibrotic liver models 9
    3.4. 3D bioprinted tissue models 10
    3.5. Bioinks 13
    3.5. Assays 14
    3.5. 3D fibrotic liver tissue models 15
4. Materials and Methods 15
    4.1. Cell culture and 2D expansion 15
    4.2. Bioink and Bioprinting procedure 16
    4.3. Culturing of bioprinted constructs 16
    4.4. Construct analysis 17
        4.4.1. Live/Dead analysis 17
        4.4.2. Celltiter-Blue® viability analysis 17
        4.4.3. Lactate dehydrogenase (LDH) Cytotoxicity Analysis 17
        4.4.4. Bicinchoninic acid (BCA) protein concentration analysis 18
        4.4.5. Actin/NucBlue staining 18
    4.5. Image analysis 18
    4.6. Statistical analysis 19
5. Results and discussion 19
    5.1. Viability 19
        5.1.1. Live/Dead analysis 19
        5.1.2. Celltiter-Blue® 22
    5.2. Cytotoxicity 23
    5.3. Protein production 24
    5.4. Morphology 25
6. Conclusion 27

7. Future studies 28
8. Reference list 30
9. Appendix 34

1. Introduction

The liver is one of the most important and complex organs in the human body. It performs a key role in an astounding number of functions from metabolism to storage and even immunity [1-7]. One of the liver's unique characteristics is its impressive ability to regenerate itself after injury. However, this feature becomes destructive to the liver when it is afflicted by a chronic illness. This regenerative capacity causes a strong wound healing response which leads to abundant scar tissue formation. The accumulation of scar tissue (ECM) is referred to as fibrosis [8]. If fibrosis progresses far enough it develops into cirrhosis which in many cases turns into cancer [9]. All chronic liver diseases can lead to liver fibrosis [10]. Lately, nonalcoholic steatohepatitis NASH has garnered a great deal of attention due to its rising prevalence [11-12]. Despite pharmaceutical companies racing to find a treatment, no therapeutic solution has been found yet. One of the major obstacles that are hindering the development of such a treatment is the inefficiency of fibrotic liver tissue models used today [8]. The most widely used fibrotic models are 2D monocultures of stellate cells cultured on petri dishes. These models are not effective in reflecting cellular behavior *in vivo* [13]. Fibrosis is perpetuated by a vicious cycle of hepatocytes and stellate cells activating each other [14]. Therefore, the role of hepatocytes on fibrosis should not be ignored. When designing a truly representative fibrotic liver model one should not only take into account the interplay between different cell types but also the spatial arrangement of these cells that would allow more realistic cell- cell interactions as well as cell-ECM interaction in all directions. 3D bioprinting is a technology that has been gaining a lot of attention recently in the field of tissue engineering. It allows the deposition of cells in a precise and controlled manner [15]. It also involves incorporating customizable biomaterials that support cellular viability and functionality [16]. Bioprinting provides the cells with an environment that is much more similar to their native tissue environment [18]. Thus, allowing the cells to behave in a more realistic manner providing a better disease model for drug screening and testing. Another very important feature of bioprinting is its ability to automatically produce standardized, identical models in a short period of time [17]. This allows for high throughput production of models that is very much needed in the pharmaceutical industry.

2. Aim

The aim of this project was to develop and asses a 3D bioprinted fibrotic liver tissue model using a coculture of hepatocytes and hepatic stellate cells (HSCs). Two coculture ratios (2:1 hepatocyte to HSCs and 4:1 hepatocyte to HSCs) were investigated and compared to a hepatocyte monoculture control. The effect of the addition of the growth factor TGF-β to induce fibrosis on the two different coculture ratios was also investigated. Different assays that can be used to assess the produced fibrotic liver tissue model were evaluated and optimized for use on 3D bioprinted constructs then used to characterize the produced liver model.

3. Theory

3.1. The liver

The liver is the second largest organ and the largest gland in the human body [1]. Over 500 vital functions are performed by the liver [2]. Some of the more well-known functions include:

1. Digestion: Hepatocytes in the liver produce bile continuously. Bile is a yellow green liquid made up of water, bile salts, cholesterol, and the pigment bilirubin. It travels through small tubes or ducts that connect with larger ducts to be stored in the gallbladder. When food containing fats reaches the duodenum, the cells of the duodenum release a hormone to stimulate the gallbladder to release bile. Bile travels through the bile ducts and is released into the duodenum where it emulsifies large masses of fat turning them into smaller pieces that have more surface area and are therefore easier for the body to digest [3].

2. Metabolism: The liver plays a central role in all metabolic processes in the body. The most prominent of which are:
   i) Carbohydrate metabolism is one of the most important metabolic processes performed by the liver. It ensures the maintenance of the concentrations of glucose in the blood within a narrow, normal range which is crucial for human wellbeing. Blood entering the liver through the hepatic portal vein is extremely rich in glucose as a result of carbohydrates being broken down during digestion. In a process called glycogenesis, the excess glucose is turned into glycogen by the hepatocytes and stored in the liver. This process is stimulated by insulin released from the pancreas during the fed state. When blood concentrations of glucose begin to decline, the liver then turns glycogen back into glucose and exports it back into the blood to be transported to all other tissues for generating energy in the form of adenosine triphosphate (ATP). This is known as glycogenolysis. When the liver glycogen reserves have been depleted, hepatocytes in a process called gluconeogenesis, synthesize glucose from amino acids and other non-hexose carbohydrates to build up glycogen reserves in the body [4].
   ii) Fat metabolism is another important process that the liver performs. After digestion fats are transported via blood to the liver. These fats are packaged into protein complexes (lipoproteins) in the liver and then transported to other cells in the body including the fat-storing cells adipocytes. The liver also converts excess carbohydrates and proteins into fatty acids and triglyceride, which are then exported and stored in adipose tissue. Because fats in the form of triglycerides are not water soluble, they cannot be transported by the blood as they are and must be transported to other cells by proteins. These lipoprotein transport molecules are made in the liver. Additionally, the liver synthesizes large quantities of cholesterol and phospholipids. Some of this is packaged with lipoproteins and made available to the rest of the body. The remainder is excreted in bile as cholesterol or after conversion to bile acids [5].
   iii) Protein metabolism also occurs in the liver. Proteins are broken down by the digestive system into their component amino acids and enter the liver through the hepatic portal vein. These amino acids require metabolic processing before they can be used as an

energy source. Hepatocytes first remove the amine groups of the amino acids and convert them into ammonia and eventually urea as ammonia is very toxic and if not rapidly and efficiently removed from the circulation, will result in central nervous system disease. Urea is less toxic than ammonia and can be excreted in urine as a waste product of digestion. The remaining parts of the amino acids can be broken down into ATP or converted into new glucose molecules through the process of gluconeogenesis. Hepatocytes in the liver synthesize non-essential amino acids, plasma proteins particularly, the major plasma protein, albumin, and many of the clotting factors necessary for blood coagulation [3][5].

3. Detoxification: As blood from the digestive system passes through the liver, the hepatocytes monitor the contents of the blood and remove many potentially toxic substances before they reach the rest of the body. The liver transforms fat-soluble toxins into a water-soluble form so they can be released through the kidneys (for elimination through the urine) and into the bile (for elimination through the colon). The liver detoxifies substances such as, drugs, alcohol, medications, food additives, preservatives, food colorings, sweeteners, flavor enhancers, chemicals used in agriculture, volatile organic compounds and many others. The liver even metabolizes and removes hormones produced by the body's own glands, in order to keep their levels within homeostatic limits.

   Hepatocytes metabolize these toxins in three different pathways: Filtering the blood to remove large toxins, enzymatically breaking down unwanted chemicals and synthesizing and secreting bile for excretion of fat-soluble toxins and cholesterol. The enzymatic breakdown of toxins occurs in two different phases: Phase I and phase II. Phase I neutralizes some of the toxins and converts many others into activated intermediates which will then be neutralized by phase II of the enzyme system. Phase II is also called the conjugation pathway because the liver cells add another substance to the toxic chemical to make it less harmful. As a result, it makes the toxin water-soluble and can be excreted from the body through watery fluids such as bile or urine. The intermediates produced in phase I are often much more harmful and toxic than the original substances. Therefore, Phase I and Phase II must be finely balanced to avoid the buildup of the toxic intermediates causing liver damage [6].

4. Storage: The liver acts as a storage facility for many vitamins and minerals obtained from the blood passing through the hepatic portal system such as vitamins A, D, E, K, and B12, and the minerals iron and copper. This way the liver provides a constant supply of these essential substances to the tissues of the body. As stated earlier the liver also stores glycogen that can be converted back into glucose and released into the blood stream when blood sugar levels drop to give the body a quick surge of energy [3].

5. Immunity: The liver is considered part of the immune system as it performs many essential immune tasks. For example, hepatocytes are responsible for the production of 80–90% of the circulating innate immunity proteins in the body. The liver also contains fixed macrophages called Kupffer cells that line the sinusoids where blood passes to reach the central vein. These

cells are therefore constantly exposed to gut-derived bacteria, fungi, parasites, worn out blood cells and microbial and cellular debris. Kupffer cells capture and digest these substances cleaning out large volumes of blood quickly [3] [7].

The liver consists of two main lobes separated by a band of tissue called the falciform ligament (also called the broad ligament) [18]. This ligament also attaches the liver to the diaphragm. The left lobe is smaller and more flattened than the right. The right lobe is much larger; the proportion between them being six to one. Both lobes are made up of eight functionally independent segments. Each segment has its own vascular inflow and outflow and biliary drainage. In the center of each segment there is a branch of the portal vein, hepatic artery and bile duct. The fact that the liver is divided into these independent units allows each segment to be resected without damaging the remaining segments [19] This is crucial for surgeons when resecting tumors or performing live liver transplantation.

As can be seen in Figure1, each segment of the liver is further divided into thousands of lobules. Lobules are the building blocks of the liver tissue measuring from 1 to 2.5 mm. in diameter. They are roughly hexagonal in shape although human Lobules do not have distinct boundaries due to the lack of well-defined connective tissue septum. Each lobule consists of a mass of hepatocytes, arranged in irregular radiating columns between which are blood channels called sinusoids. Situated around the perimeter of the lobule are branches of the hepatic artery, hepatic portal vein and bile duct. These cluster together at the "corners" of the lobule forming what is called the portal triad [20]. Sinusoids receive blood from the circumference of the lobule (the portal triad) and convey it to the center of the lobule (the central vein) after which the blood is transported out of the liver.

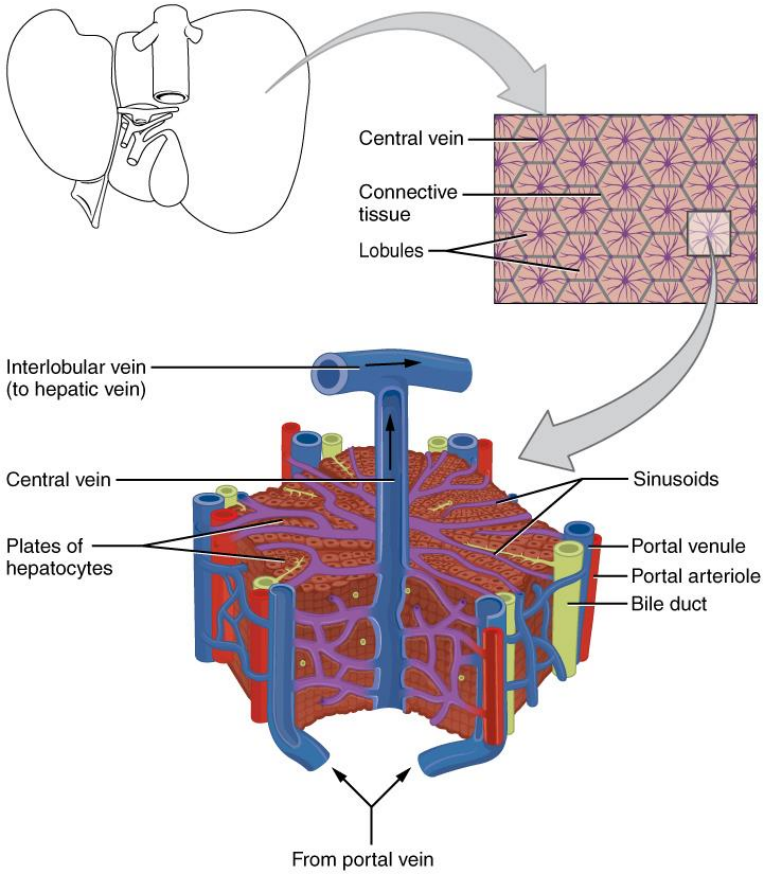

Figure 1. Overview of a hepatic lobule surrounded by the portal triads [21].

The liver has 2 major sources of blood, the portal vein which carries nutrient rich blood from the digestive system and the hepatic artery that supplies the liver with oxygen-rich blood from the heart. Seventy-five percent of the blood flowing into the liver comes through the portal vein, the remaining twenty five percent is oxygenated blood that enters through the hepatic artery. The blood mixes, passes through the sinusoids, bathes the hepatocytes and drains into the central vein. The liver holds about (13%) of the body's blood supply at any given moment and about 1.5 liters of blood exit the liver every minute. [22]

All the blood leaving the stomach and intestines passes through the liver. This blood is not only rich in nutrients but also carries medication and toxic substances. Once it reaches the liver, these substances are processed, stored, altered, detoxified, and passed back into the blood or released in the bowel to be eliminated. As previously mentioned, hepatocytes, the parenchymal cells in the liver, play a key role in all of these processes. Nonparenchymal cells (NPCs) such as hepatic stellate cells, epithelial cells and Kupffer cells on the other hand do not perform specialized liver functions but play a structural and connective role supporting the hepatocytes. The cues, signals and overall interaction of nonparenchymal cells with hepatocytes is vital in supporting and maintaining hepatocyte function.

It is therefore essential to develop representative and reliable liver tissue models that can be used in the fields of pharmacology and pharmacokinetics to aid in the research and development of treatments for various liver diseases and conditions.

Hepatocytes:

Hepatocytes are liver epithelial cells. They are the major parenchymal cells in the liver. They constitute 70–85% of the liver volume and thus give rise to the basic structure of the liver [23]. Hepatocytes range from 20-30 μm in diameter and are polygonal in shape having six or more surfaces. Hepatocytes may have one to two nuclei with prominent nucleoli. They have abundant quantities of both rough and smooth endoplasmic reticulum as well as many stacks of Golgi membranes [24].

As shown in Figure 2, hepatocytes are arranged into plates or columns separated by the sinusoids. Between the sinusoids and the hepatocytes lies the space of Disse where blood plasma is collected. Hepatocytes have many microvilli which project into this space, to increase absorption of proteins and other plasma components [25].

As hepatocytes are extremely metabolically active, *in vitro* hepatocyte models represent very useful systems in research. In fact, Cultures of primary hepatocytes have so far been the gold standard for *in vitro* testing [26]. They have contributed considerably to the understanding of the biochemistry, physiology, and cell biology of the normal and diseased liver and in various application domains [27].

Hepatic Stellate cells (HSCs):

Hepatic stellate cells are liver-specific mesenchymal cells. They are found in the space between the hepatocytes and the sinusoids or what is known as the space of Disse (Figure 2). Stellate cells store vitamin A in characteristic lipid droplets. Eighty percent of the body's vitamin A is stored in the stellate cells. They also help to define the molecular and structural microenvironment of the parenchymal compartment and space of Disse by producing soluble and insoluble cues, including growth factors, inflammatory cytokines, and deposition of extracellular matrix (ECM) and therefore modulate the liver's response to both acute and chronic injury [28].

In a normal healthy liver, hepatic stellate cells are quiescent constituting 5-8 % of the total number of liver cells [29]. When the liver is damaged or injured, stellate cells become activated into a myofibroblast-like cells that synthesize large amounts of extracellular matrix (ECM) components including collagen, proteoglycan, and adhesive glycoproteins [30]. In chronic liver disease, prolonged and repeated activation of hepatic stellate cells causes liver fibrosis characterized by widespread scar formation that changes liver architecture and function. The end stage of fibrosis is called cirrhosis and it is a leading cause of death worldwide [31].

The cells lines HepG2 and LX-2 were used to represent hepatocytes and stellate cells respectively in this project. Cell lines might not always accurately reflect how primary cells behave *in vivo*. They might also exhibit altered functions and properties if they are cultured for too long. Despite these drawbacks, cell lines are still very widely used in research instead of primary cells. This is due to their cost effectiveness, ease of use and more importantly they provide a pure culture that

produces consistent and reproducible results. It is therefore advisable to start research with cell lines and confirm the findings using primary cells [32] [33].

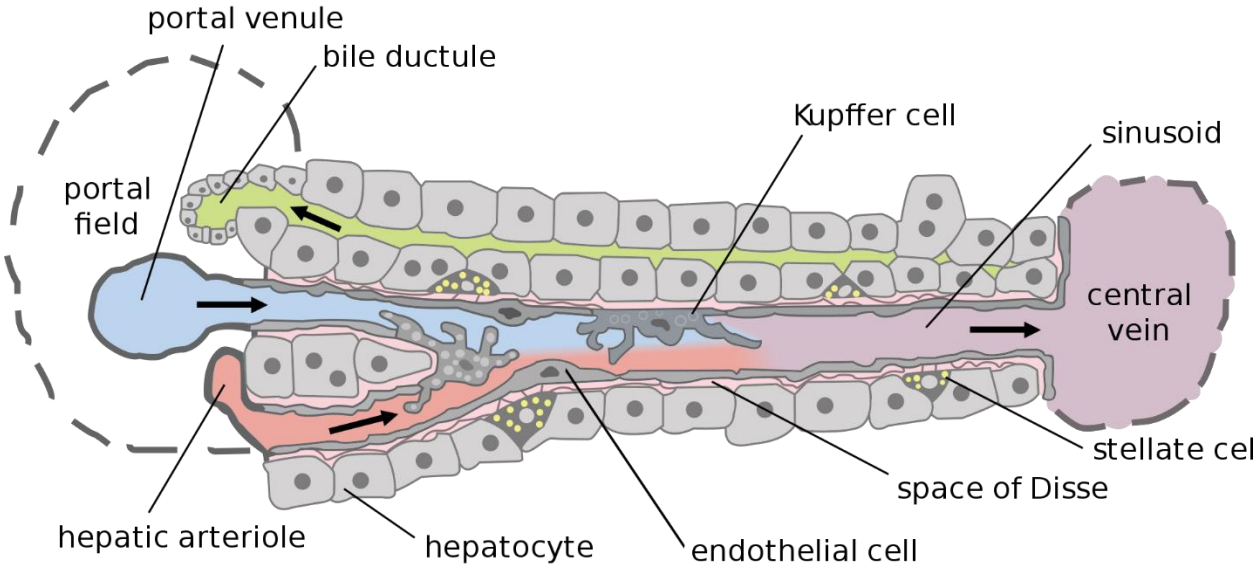

Figure 2. Different cell types in a mammalian liver lobule [34].

3.2. Liver Fibrosis

The liver has a strong regenerative capacity which in acute cases is beneficial as the liver can restore its mass and shape even after the destruction of a large part of it. However, in chronic liver diseases where the liver is continuously injured this regenerative capacity causes necrosis and apoptosis of hepatocytes due to strong inflammation and wound healing response (scar tissue formation) [8]. The accumulation of scar tissue (ECM) is referred to as fibrosis while the more advanced form cirrhosis represents the distortion of hepatic architecture and blood flow.

Liver fibrosis is associated with major changes in both the quantity and composition of the ECM particularly fibrillar collagens (collagen I and collagen III) compared to healthy liver tissue [35]. In advanced stages, the liver contains approximately 6 times more ECM than normal. Accumulation of ECM results from both increased synthesis and decreased degradation [14].

Liver fibrosis is sustained and modulated by an intense cross-talk between different hepatic cell populations that involves the synthesis and release of several mediators, including growth factors, cytokines, chemokines, reactive oxygen species, plasma proteins, and many others [9].

The most prominent agents of liver fibrosis are:

- ***Hepatic stellate cells (HSCs)***
  HSCs are dominant contributors to liver fibrosis. Following multiple injuries and/or exposure to inflammatory cytokines such as transforming growth factor (TGF-β), HSCs are activated or transdifferentiated into myofibroblast-like cells, acquiring contractile, proinflammatory, and fibrogenic properties [35]. HSC activation is a critical event in initiation and progression of hepatic fibrosis and a major contributor to collagen deposition. Activation of HSCs is characterized by cell proliferation and migration, contraction after transforming into myofibroblasts, generation of a large amount of collagen and other ECM components that replace a large part of the hepatocytes and lead to interruption of the blood flow which ultimately causes liver failure and fibrosis [36].

- ***Hepatocytes***
  Chronic liver diseases either promotes apoptosis or triggers compensatory regeneration of hepatocytes. Different modes of cell death such as apoptosis, necroptosis, and necrosis, may exist side by side in acute and chronic liver disease. Whereas apoptosis causes a low inflammatory state, necroptosis and necrosis lead to a high level of inflammation [8]. Damaged hepatocytes release reactive oxygen species (ROS) and fibrogenic mediators, induce activation of HSCs, and stimulate the fibrogenic actions of myofibroblasts. Hepatic cell death is a common event in liver injury and contributes to tissue inflammation, fibrogenesis, and development of cirrhosis. In the last fibrotic stage or cirrhosis, hypoxic hepatocytes become a predominant source of TGF-β1, further intensifying hepatic fibrosis [36]. Therefore, a vicious cycle in which inflammatory and fibrogenic cells stimulate each other is likely to occur [14].

- ***TGF-β***
  TGF-β is the strongest known inducer of fibrogenesis in hepatic fibrosis. The expression level of TGF-β1 is increased in a fibrotic liver and reaches a maximum level at cirrhosis. The effect TGF-β1 has on liver fibrosis is complicated and involves many aspects. The primary effect of TGF-β1 is to stimulate activation of HSCs, and the TGF-β1 autocrine loop in activated HSCs is an important positive feedback to the progression of liver fibrosis. TGF-β1 induces expression of the genes responsible for producing ECM and inhibits degradation of ECM by downregulating expressions of ECM degrading enzymes MMPs and promoting their inhibitors, leading to excessive deposition of collagen and promoting the development of liver fibrosis. In addition, TGF-β1 has been shown to inhibit DNA synthesis and induces apoptosis of hepatocytes. This is thought to be the reason behind the tissue loss and decrease in liver size observed in cirrhosis [36].

Liver fibrosis and cirrhosis are strong risk factors for liver cancer and have become a major concern worldwide. In fact, almost all cases of primary liver cancer are marked by the presence of cirrhosis [9]. The main causes of liver fibrosis in western countries include chronic hepatitis C infection, alcohol abuse, and nonalcoholic fatty liver disease (NAFLD) and its more severe form nonalcoholic steatohepatitis (NASH) [14].

NASH represents the hepatic manifestation of a metabolic syndrome, which is characterized by obesity, insulin resistance, type II diabetes, hypertension and hyperlipidemia [37]. It is associated with a doubling of the risk of dying from cardiovascular disease, and a tenfold increase in the chance of developing cirrhosis or cancer of the liver. It is estimated that 20-30 million people in the United States could have NASH today and the number is expected to increase by 63% by 2030 [11]. NASH is expected to become the leading cause of liver transplantation by 2020 [12]. Financial analysts predict that by 2025, the drug market for NAFLD including NASH will be worth $20 billion to $35 billion a year. So far, no drug has been developed for treating this disease. Pharmaceutical companies are therefore racing to be the first to develop such a treatment [11].

One obstacle in the development of efficient therapies is the lack of robust, representative, and biologically relevant *in vitro* models of liver fibrosis to aid the development phase of pharmaceuticals [8].

3.3. Fibrotic liver models

To date the most used and described *in vitro* fibrosis models consist of mono-layer cultures of freshly isolated rodent HSCs in flat and stiff polystyrene dishes which leads to spontaneous HSC activation. These models are limited due to the use of cells of rodent origin in addition to the absence of hepatocytes and the effect they have on the process of fibrosis. Another drawback is and the uncontrolled activation of the HSCs. Spontaneous activation of HSCs prevents the ability to analyze the initial stages of compound induced fibrosis contributing to these models being less suitable for pharmaceutical and toxicity testing [13].

In many cases, drug candidates that showed efficiency when tested in different 2D *in vitro* models did not produce similar successful results when tested on *in vivo* animal models. Most drug candidates that did make it through *in vivo* animal testing failed by showing toxicity or lack of effectiveness during the most expensive phase of pharmaceutical development i.e. clinical trials. In fact, it has been shown that 9 out of 10 drug candidates that made it through animal testing failed in human clinical trials [9].

It has been estimated that only a 10% improvement in drug failure prediction would save a pharmaceutical company $100 million [38]. Therefore, there is a real need for liver tissue models to exclude ineffective or toxic compounds as early in the drug development process as early as possible preferably before the animal testing stage [9].

A reliable *in vitro* model would be a multicellular system that includes functional hepatocytes that can be damaged by a compound or another form of injury and HSCs that can respond to damage and become myofibroblasts [8].

Due to the importance of the interplay between hepatocytes and HSC in the development of fibrotic liver models, many attempts have been made to generate functional fibrotic models by culturing different ratios of hepatocytes and HSCs together and then inducing fibrosis by exposure to different compounds such as allyl alcohol, free fatty acids (FFA), methotrexate, thioacetamide and TGF-β [28] [13] [39] [40] [41].

Spatial organization of different cell types is an important and often defining determinant of tissue function [42]. Therefore, the perfect *in vitro* fibrotic liver model would attempt to replicate HSC activation *in vivo* not only in terms of the interaction with hepatocytes but also in terms of the complex 3D organization of the cells and ECM [8]. In fact, spatial patterning of liver cells has been shown to be critical in both normal liver functions and in liver diseases [43].

A wide variety of techniques are currently used to form 3D spheroid hepatic models. These methods include micro molds of non-adherent materials, techniques that depend on gravitational aggregation using hanging drop cultures, rotation of concave 96 well cell-repellent plates, or even the use of stirred bioreactors [8]. Another approach to culturing liver cells in 3D is the sandwich culture system. In this approach, cells are first seeded onto the surface of a 2D hydrogel substrate and cultured until full cell attachment is achieved. Another hydrogel layer is then added on top of the cells sandwiching the cells in between two hydrogel layers [44].

Despite these many attempts, hepatic fibrosis *in vitro* is not easily achieved. Spheroids are limited in size due to diffusion barriers in their dense structures, limiting nutrient and oxygen supply [45]. Sandwich cultures although successful in long term maintenance of hepatocyte function cannot be used to construct actual 3D models [46]. Other drawbacks of these invitro models include requiring multistep fabrication methods, missing complex and hierarchical tissue structure, absence of a specific ECM environment. The resulting *in vitro* tissue models are therefore limited in terms of cell viability and functionality [47].

The appearance and progression of the basic features of fibrosis such as inflammation, tissue remodeling, collagen accumulation, and compensatory regeneration of hepatocytes are best detected and interpreted in a 3D tissue environment. These characteristics can be considered parameters to define a successful invitro fibrotic liver model and are required in order to fully understand the quantitative and sequential relationships underlying liver fibrosis [28].

3D bioprinting provides a means of fabricating 3D tissue models that are sufficiently three-dimensional allowing for histological as well as biochemical assessment [43]. Also, the incorporation of HSCs into 3D bioprinted constructs allows them to go back to their quiescent state after being activated from being cultured in 2D. This enables the model to be used in compound exposure experiments to analyze events in the early stages of fibrosis something that has not been possible using other approaches [28].

3.4. 3D fibrotic liver tissue models

There have been several attempts to produce representative *in vitro* 3D fibrotic liver tissue models. *Thiele et al.* used precision cut liver slices (PCLS) from rats, mice and human livers [48]. Ethanol was used to induce fibrosis to investigate the pathophysiology of alcohol induced liver fibrosis. Although this method showed fat accumulation and activation of HSCs after 24 hours, the PCLS retained viability for a maximum of 96 hours. *Westar et al.* used PCLS to test the efficiency of several antifibrotic compounds. In this case the PCLS remained viable for only 48 hours [49]. PCLS are not able remain viable long enough to evaluate the progression of events in fibrogenesis. They also develop early onset fibrosis regardless of treatment, which results in unreliable results when conducting chronic exposure studies.

Leite et al. and *Prestigiacomo et al.* used hepatocytes and non-parenchymal cells (NPC) cultured as 3D spheroids that displayed fibrotic features after exposure to different profibrotic compounds such as TGF-β, Allyl alcohol and Methotrexate. The spheroids were able to reproduce key cellular and molecular events of fibrosis such as hepatocellular injury, HSC activation, collagen secretion and deposition and remained viable for 21 days [13] [41]. However, as mentioned earlier, they are limited in size and have little to no additional ECM components eliminating cell–matrix interactions that are vital for tissue formation and function. This greatly limits their ability to mimic native fibrotic liver tissue.

A few attempts have been made to produce 3D bioprinted liver tissue models. *Nguyen et al.* incorporated several liver cells types to produce a 3D bioprinted liver tissue model for the purpose of modeling drug induced liver injury (DILI). Non-parenchymal (endothelial and hepatic stellate) cells were mixed into one bioink that was used to bioprint a compartment border wall in the center of which Hepatocytes were bioprinted [43]. *Norona et al.* continued on this work using the developed 3D bioprinted liver tissue models to examine the progression of liver injury in response to pro-fibrotic compounds namely, methotrexate, thioacetamide and TGF-β [28]. The 3D bioprinted constructs were successfully able to simulate compound induced fibrogenesis at the cellular, molecular, and histological levels. However, production of these 3D bioprinted models required the use of a huge number of cells. The non-parenchymal cells were mixed in with the bioink at a cellular density of $150e^6$ cells/ml of bioink. Hepatocytes were not mixed in with a bioink, instead, a 100% cellular paste, was generated by compaction of the cells. This obviously requires an enormous number of cells. As high throughput production of tissue models is required to satisfy the needs of the pharmaceutical industry, this may not be the most practical approach to meet this need.

In this project, a bioink customized to support liver specific cells was used to 3D bioprint liver tissue models that allowed cell interaction in all directions with neighboring cells as well as ECM components. Hepatocytes (HepG2) and stellate cells (LX-2) were bioprinted in two different ratios (4:1 and 2:1). The 4:1 ratio resembles the natural hepatocyte/ non-parenchymal cell (NPC) ratio found in a healthy human liver and has therefore been used in the literature in the development of hepatocyte/ (NPC) spheroid cocultures. [41]. The 2:1 hepatocyte, stellate cell ratio was found by *Riccalton-Banks et al.* to produce higher number of spheroids when compared to other coculture ratios. It was found that the spacial arrangement at this ratio was optimal in providing effective and efficient cell–cell interaction necessary for spheroid formation [50]. There have also been other attempts to produce hepatic spheroid cocultures models using a 2:1 hepatocyte/NPC ratio [51][52]. Fibrosis was then induced by exposing the constructs to the growth factor TGF-β. This resulted in a tissue-like structures that remained viable until the experiment was ended at 20 days.

3.5. 3D bioprinted tissue models

Bioprinting is the layer-by-layer spatial deposition of biomaterials that are mostly hydrogels (bioinks) and living cells via a computer-controlled dispensing system to fabricate tissue engineered constructs [15].

Unlike other 3D tissue model fabrication methods such as 3D spheroid formation or sandwich culture systems, bioprinting allows the production of complex tissue-like structures in an additive manner that is both automated and standardized [17]. It is an efficient and reproducible process that establishes key cell architectural relationships that mimic the 3D architecture and complexity of native tissue and preserves tissue-level functions over prolonged periods of time [28]. Bioprinting can therefore be used for establishing standardized models for drug screening, toxicity testing, disease modeling etc.

3D bioprinting allows for customized structure, stiffness, and material composition all of which facilitates cell–cell and cell–matrix interactions that are vital for tissue formation and function. Bioprinting enables cell interaction in all directions with ECM components and neighboring cells allowing tissue-like structures to form [53]. Bioprinted 3D fibrotic liver tissue models also enable the chronological assessment of the progression of fibrosis by revealing specific patterns of collagen deposition by the bioprinted HSCs that are analogous to patterns described in human biopsy samples [28]. Hence, pharmacological studies are increasingly turning to 3D bioprinted *in vitro* models such as Fibrotic liver models.

Different 3D bioprinting technologies have been developed. A summary of the characteristics of the different bioprinting methods can be seen in Table 1 [54] [55] [56]. The most prominent of which are:

- Inkjet 3D bioprinting uses a non-contact technique that may utilize thermal, piezoelectric, or electromagnetic forces to expel successive drops of bioink onto a substrate, replicating a CAD design. Benefits of inkjet bioprinting include high speed, availability, and relatively low costs. Disadvantages include inconsistency in droplet size and placement, the need for low viscosity bioinks which may vary depending on the system used but with a typical threshold of around 30 mPa/s. This eliminates several effective bioinks from being used. Also, when using the piezoelectric mechanism, the vibrating frequency and power employed lie within the ranges of (15–25 kHz) and (10–375 W) respectively. These are known to disrupt cell membrane and cause cell lysis [54] [55 [57].
- Extrusion 3D bioprinting is the most common bioprinting method. It uses mechanical or pneumatic forces to dispense bioink through a nozzle that follows a computer-generated pattern producing continuous streams of material. Advantages of this method include being able to print high viscosity bioinks as well as high cell densities. One of the major disadvantages is the loss of cell viability due to the shear stresses and pressure used to extrude the bioink [54] [55].
- Laser-assisted 3D bioprinting is a non-contact, nozzle free printing process directs laser pulses through a “ribbon” containing bioink. The bioink and cells are suspended on the bottom of the ribbon and when vaporized by the laser pulse, droplets are propelled to the

receiving substrate. The main advantage of laser bioprinting is the high degree of precision and resolution possible of the printed structures as well as the ability to print a very high density of cells. Additionally, the lack of a nozzle creates more options for bioinks that may be used with no concern for viscosity limitations or clogging. The major disadvantages of laser bioprinting are low printing speed, as well as the lengthy process of ribbon preparation [54] [55].

- Stereolithography is a process where a UV light or laser is directed in a pattern over a path of photo-sensitive liquid polymer, cross-linking and thus solidifying the polymer into a hardened layer. This technique is mainly applied to fabricate structures from curable acrylics and epoxies. This is a nozzle free technique which eliminate nozzle clogging problems. Other advantages include short printing time, higher fabrication accuracy when compared to other 3D bioprinting technologies. The main drawbacks for stereolithography is that it is limited to photocrosslinkable polymers and the necessity of using a high intensity ultraviolet light which harms cellular DNA [54] [55].

Table 1. Characteristics of the different bioprinting technologies.				
	Inkjet	Extrusion	Laser-assisted	Stereolithography
Viability	~90 %	40–80 %	>95 %	>90 %
Viscosity	>30 mPa/s	30– 6 × 107 mPa/s	1-300 mPa/s	No limitation
Resolution	20–100 µm	100-200 µm	>20 µm	~1.2–200 µm
Speed	Fast	Slow	Medium	Fast
Cost	Low	Medium	High	Low
Advantages	High speed, low cost, Ability to introduce concentration gradients in 3D constructs, Ability to print high resolution	Compatible with wide range of bioinks, ability to use high viscosity bioinks, can print high cell densities	Nozzle free, ability to print high resolutions, ability to use high viscosity bioinks, can print high cell densities	Nozzle free, highest resolution, low printing time, high accuracy
Disadvantages	Possibility of clogging, thermal and mechanical stress to cells, limited printable materials (low viscosity only), inconsistency in droplet placement and size, low cell densities, cannot produce continuous flow	low resolution, lower viability due to shear stresses, can only be used with viscous materials.	High cost, tedious and time-consuming ribbon preparation; risk of metallic particle contamination from the metal film	Applicable to photopolymers only, possibility of harm to DNA and human skin by UV

Extrusion bioprinting is the most utilized bioprinting method in biomedical research, as it allows for bioink and tissue customization in addition to its many other advantages [53]. To print a successful 3D tissue model, it is important to not only choose the right bioprinting technology but also to choose the most suitable bioink for each specific application.

3.6. Bioinks

Bioinks are biomaterials that are printed along with living cells during the printing process. They are usually hydrogels that vary in viscosity depending on the bioprinting technology used. In addition to containing cells, bioinks sometimes contain nutrients and ECM components in different variations [15]. Formulating suitable bioinks is one of the major challenges in the production of

3D bioprinted tissue models. The ideal bioink should satisfy both biomaterial and biological requirements.

Biomaterial requirements include good printability, good mechanical stability relative to the tissue being printed, good rheological properties such as shear-thinning behavior, high zero-shear viscosity, rapid gelation that enables high shape fidelity and avoids deformation of the 3D bioprinted construct [15] [58] [59] [16]. Biological requirements on the other hand refer to biocompatibility of the bioink with the specific cell type being bioprinted, non-toxicity, mimicking the *in vivo* microenvironment for specific cell types and the ability to support and promote cellular activities such as adhesion, migration, proliferation, and differentiation bioactivity of cells after printing [15] [58]. Other important desirable properties for a relevant bioink are permeability of oxygen, nutrients and metabolic waste transport, low cost, availability, industrial scalability with minimal batch to batch variations [58] [59].

Current biomaterials used in the production of bioinks fulfill either the biomaterial requirements or the biological requirements but typically not both [53]. Bioinks are produced from either natural or synthetic biomaterials alone, or a combination of the two as hybrid materials depending on the specific application.

Among the different biomaterials used, naturally derived hydrogels are the most prominent materials used as bioinks in 3D bioprinting. These include agar, agarose, collagen, gelatin methacryloyl (GelMA), alginate, chitosan, hyaluronic acid, fibrin/fibrinogen, and silk [15]. These natural materials have various advantages over synthetic materials, mainly due to the fact that they mimic ECM composition and structure, self-assembling ability, biocompatibility, biodegradation properties etc. [58]. By contrast, using synthetic-based bioinks, such as polyurethane (PU), polyethylene glycol (PEG), and polylactic acid (PLA) provide their own advantageous properties which are not present in natural polymers such as controllability of mechanical stability, photo crosslinking ability, pH and temperature responses and many others [15] [58].

Naturally derived biomaterials may act as a homogenous substrate supporting tissue growth. However, the ECM is not only made up of large structural macromolecules but also contains many other proteins that enhance mechanical resilience, phenotype specific cell adhesion sites, growth factor and morphogen binding sites, and maintain physiological conditions for specific enzyme activities. This has led to the fabrication and commercialization of specialized bioinks that incorporate auxiliary proteins found in the native ECM such as laminin or fibronectin to generate bioinks that preferentially support the adhesion and functionality of certain cell types [16].
The bioink used in this project was fabricated using a combination of gelatin methacryloyl (GelMA) and alginate. GelMA and alginate are known as structural bioinks. They support cell adhesion, are cross-linkable through covalent or ionic interaction and are resistant to dissolution under cell culture conditions [16]. Xanthan gum was also added as a thickener.

Laminins 111 and 121 were included as auxiliary proteins. In adults, laminin α1 chain expression is present in some epithelial basement membranes, mainly found in tissues such as the eye, liver and kidney. Laminin 111 supports the survival, proliferation and differentiation of many different cell types *in vitro* and induces different cell signaling cascades [60]. Laminin 121 is particularly useful for hepatic and neural differentiation. laminin121 has high affinity to integrin receptors and

therefore influences integrin-laminin stability and downstream effector activation in cell signaling cascades [61].

3.7. Analysis methods of 3D bioprinted constructs

Characterization of 3D bioprinted constructs is essential for the evaluation of their development and functionality. Biological components of 3D bioprinted constructs are inherently variable and it is critical to investigate their status in order to assess the quality and functionality of the bioprinted construct. The development of quality monitoring tools is particularly important for scale up of biofabrication and tissue engineering to production scale processes needed in the pharmaceutical industry [62]. There is however, an unmet need for a consistent set of tools for the evaluation of 3D bioprinted constructs [63].

Histology and immunohistochemistry are widely used techniques for validation of 3D cell cultures [28] [41] [43]. However, sectioning and staining of the bioprinted construct can alter construct characteristics such as cell morphology [63]. Other techniques often employed to assess 3D cell cultures at specific time points include quantitative polymerase chain reaction (qPCR) and electron microscopy. These are all destructive methods that do not allow for assessments of tissue development in the same construct over time [64]. Additionally, sample processing for these techniques is too time consuming and labor intensive for high throughput applications required in drug screening and testing. Easier and faster technique that may be used nondestructively are available for investigating cellular proliferation and functionality. However, these biochemical assays are well established in characterizing 2D, monolayer cell cultures of low cellular densities. Therefore, evaluation and optimization of these assays is needed to affectively assess 3D bioprinted cultures of much higher cellular density [65].

Unfortunately, little literature has been published so far on methods for the non-destructive determination of the quality of 3D cultured constructs [66]. Nevertheless, there have been some recent efforts on the development of non-destructive assessment methods. For example, molecular probes have been investigated to detect biomarkers within the growing 3D cellular structure or in the secreted extracellular matrix [67]. Dielectric impedance spectroscopy has been investigated for the purpose of measuring changes in the cellular constituents of a biofabricated construct by assessing changes in the dielectric properties of the cells within the construct [62]. Attempt have been made to corelate metabolic rates i.e. oxygen uptake, glucose consumption, and lactate production to the cellularity of tissue-engineered constructs [66]. Genetically modified cells have been developed to produce fluorescent protein molecules that can be detected by different techniques for the qualitative and quantitative evaluation of cell growth in a biomaterial without destruction of the sample [68].

In this project, several assays a few of which are nondestructive were investigated and used to characterize the resulting constructs. To assess viability and proliferation, CellTiter-Blue® was used in addition to Live/Dead Staining. The CellTiter Blue® assay is a homogeneous, fluorescent method for monitoring cell viability. The assay is based on the ability of living cells to convert a redox dye (resazurin) into a fluorescent end product (resorufin) which is then excreted by the cells into the medium. Nonviable cells rapidly lose metabolic capacity and thus do not generate a

fluorescent signal. The reagent is generally nontoxic to cells, allowing extended incubation periods [69]. Although Celltiter blue reagent is nontoxic, manufacturers recommend that CellTiter-Blue® be used as an endpoint assay as some reports in the literature show that resazurin affects cell viability, depending on the concentration and duration of incubation.

Live/Dead Staining using Calcein AM and Propidium iodide (PI) will allow simultaneous fluorescence staining of viable and dead cells. Calcein AM is a cell-permeant dye that can be used to determine cell viability in most eukaryotic cells. In live cells the non-fluorescent Calcein AM is hydrolyzed by endogenous esterase into the highly negatively charged green fluorescent Calcein. Green fluorescent Calcein is retained in the cytoplasm in live cells as dead cells lack active esterases, only live cells are labeled. If the cells are functioning normally and the cell membranes are intact, they will emit green fluorescence [70]. PI cannot pass through a viable cell membrane. It reaches the nucleus by passing through disordered areas of dead cell membrane, and intercalates with the DNA double helix of the cell to emit red fluorescence [71].

To assess cytotoxicity of bioprinted cells, the Lactate Dehydrogenase (LDH) Cytotoxicity Assay measures extracellular LDH in culture media. LDH is a cytosolic enzyme that is an indicator of cellular toxicity. This assay uses an enzymatic reaction that results in a red formazan product which can be measured spectrophotometrically. Briefly, LDH catalyzes the conversion of lactate to pyruvate via reduction of NAD+ to NADH. Then, diaphorase uses NADH to reduce a tetrazolium salt (INT) to a red formazan product. The level of formazan formation is directly proportional to the amount of released LDH in the medium and is thus indicative of the cellular cytotoxicity [72].

Cellular protein production was evaluated using Bicinchoninic acid (BCA) protein assay. It is a two-component, high-precision assay set to measure the proteins produced by the cells compared to a protein standard. The BCA Protein Assay combines the well-known reduction of Cu2+ to Cu1+ by protein in an alkaline medium to form a light blue complex with the highly sensitive and selective colorimetric detection of the cuprous cation (Cu1+) by bicinchoninic acid resulting in an intense purple-colored reaction product. The BCA/copper complex is water-soluble and exhibits a strong linear absorbance at 562 nm with increasing protein concentrations [73].

ActinGreen/NucBlue staining is used to visualize cellular morphology. ActinGreen utilizes fluorescently-labeled phalloidin peptide that binds specifically to F-actin to visualize the cell's cytoskeleton. NucBlue uses a Hoechst stain that fluoresces blue when it binds to DNA [74] [75].

4. Materials and Methods

4.1 Cell culture and 2D expansion

Cells, bioinks and bioprinted constructs were all handled in a sterile laminar air flow bench and constructs were cultured and incubated at 37°C with 5% CO_2.HepG2 and LX-2 cells were grown to 80% confluency to obtain 12.5 million HepG2 cells and 2.7 million LX-2 cells for each of the three replicate experiments.

The medium used for culturing HepG2 cells was MEM (1X) + GlutaMAX™-I (Gibco) supplemented with 10% Fetal Bovine Serum (FBS) (Gibco, 1% MEM Non-Essential Amino Acids

(100X) (Gibco), 1% of Anti-Anti(100X) (Gibco) and 1% of Sodium Pyruvate 100mM (100X). IMDM (1X) (Gibco) supplemented with 10% (FBS) (Gibco), 1% MEM Non-Essential Amino Acids (100X) (Gibco), 1% of Anti-Anti(100X) (Gibco) and 1% of L-glutamine (200mM) (Gibco) was used for culturing LX-2 cells. The culture media were prepared following manufacturer's instructions and were changed every 2-3 days. Cells were passaged when the required confluency was reached.

4.2. Evaluation of GelXA bioink and crosslinking method

Compatibility of GelXA LN121 and GelXA LN111 with HepG2 and LX-2 cells respectively was investigated using Live/Dead staining. Effect of two crosslinking methods; submersion in $CaCl_2$ and exposure to UV, on cellular viability was also assessed.

The cells were mixed in with the bioink at a concentration of 10M cells /ml of bioink. The Bio X bioprinter (CELLINK) was used to bioprint 6mm diameter concentric disks with an approximate volume of 10-15µl each in 48 well plates. See figure 3. The printing protocol outlined in Appendix 9.1.1 was followed.

Briefly, cell-laden bioink was prepared by mixing in 50 µl of cell suspension with 450 µl of GelXA (Cellink). The cell-laden bioink was then transferred into a UV shielding cartridge which was loaded onto the bioprinter. After the constructs were printed, half were crosslinked by submersion for 2 minutes in 50 mM $CaCl_2$ (Sigma-Aldrich). The crosslinking agent was aspirated and the appropriate culture media were added. The other half were crosslinked by placing each construct under a 450 nm LED for 15-30 seconds after which the appropriate culture medium was added.

Triplicate samples from each condition were transferred to a 96 well plate containing appropriate medium on days 2,7 and 9 following printing. Live/Dead staining was performed using Calcein AM (Invitrogen eBioscience) and Propidium iodide (PI) (Sigma-Aldrich) to image live and dead cells respectively. Inverted fluorescent microscope (Olympus IX73) was used to image the cells in the constructs. The extended staining protocol followed can be seen in Appendix 9.1.2

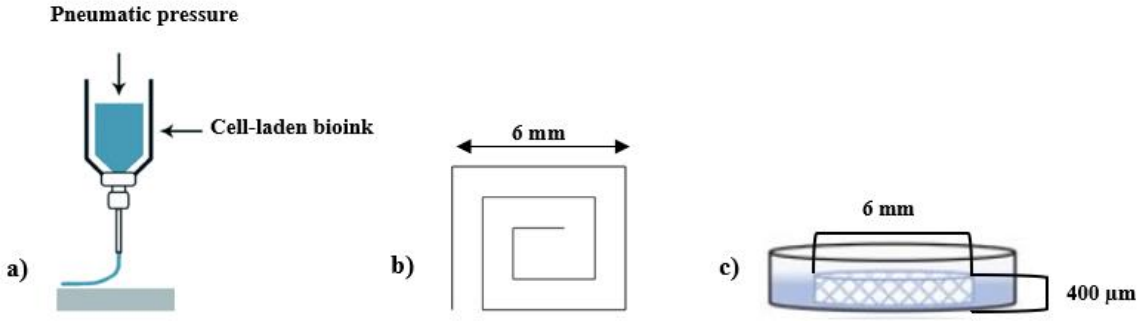

Figure 3. a) Schematic drawing of pneumatic extrusion based bioprinting b) Printing pattern used c) Dimensions of bioprinted construct

4.3. Bioink and Bioprinting procedure

Cells were mixed in with the GelXA LN 111+121 (CELLINK) bioink at a concentration of 10M cells /ml of bioink. Three different cell-laden bioinks were generated ((i) HepG2, (ii) 4:1 ratio of HepG2 and LX-2 and (iii) 2:1 ratio of HepG2 and LX-2). The Bio X bioprinter (CELLINK) was used, in three different print sessions, to bioprint 6mm diameter concentric disks with an approximate volume of 10-15µl each in 48 well plates. (Figure 3). The constructs were crosslinked by submerging them for 2 minutes in 50 mM CaCl2. The crosslinking agent was aspirated and the appropriate culture media were added.

4.4. Culturing of bioprinted constructs

The bioprinted constructs were cultivated for 20 days in culture medium of 1:1 of HepG2 and LX-2 media for the coculture constructs and HepG2 medium for the HepG2 constructs. The media were changed every 2-3 days.

After culturing the constructs for 7 days, fibrosis was induced by adding 0.25µl/mL of the growth factor TGF-β (Sigma-Aldrich) at every medium change (final concentration of 5ng/ml). Medium without TGF-β was used for controls. This resulted in 6 different conditions to be analyzed (Table. 2). Samples were taken on day 1 and day 7 and every 4 days after induction (Figure 4).

Table 2. Resulting conditions to be analyzed

HepG2		2:1		4:1	
Induction (I)	Control (C)	Induction (I)	Control (C)	Induction (I)	Control (C)

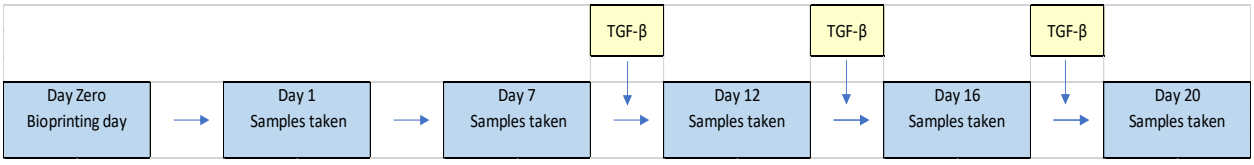

Figure 4. Experimental set up timeline

4.4. Assay optimization

Live/Dead analysis protocol had already been developed by Cellink AB and did not require further optimization. See Appendix 9.2.2

4.4.1. Celltiter-Blue® viability assay

4.4.1.1. Applicability of using Celltiter-Blue® on 3D bioprinted HepG2 and LX-2 cells

The applicability of using Celltiter-Blue® (Promega) to convey changes in cellular densities of bioprinted HepG2 and LX-2 cells, was evaluated. The two cell types were bioprinted separately into 6mm diameter concentric disks in four different cell densities (1.25,2.5,5 and 10 M cells/ml bioink). Controls not containing cells were also printed. The day after bioprinting, 6 constructs samples for each cellular density were transferred to a 96 well plate containing appropriate medium. The cells in one set of triplicates for each cellular density were lysed by incubation with lysis buffer (ThermoFisher Scientific) for three hours, while cells in another set of triplicates were kept alive. Celltiter-Blue® analysis was performed on the bioprinted constructs following the protocol found in Appendix 9.1.3

Briefly, Celltiter-Blue® was added to the constructs to be analyzed. The constructs were incubated overnight and fluorescence was recorded the next day at 560/590 nm using a plate reader (VICTOR Nivo). The reading from the no cell control was deducted from sample readings.

4.4.1.2. Assessing the optimal incubation time for bioprinted constructs with Celltiter-Blue®

A set of triplicate 6mm concentric disks with a cellular density of 10 M HepG2 cells /ml bioink were incubated with Celltiter-Blue® and fluorescence was recorded at 560/590 nm at different time point. Specifically, 4,8,24,48,72,96 hours.

4.4.2. Lactate dehydrogenase (LDH) Cytotoxicity assay

4.4.2.1. LDH cytotoxicity assay validation with HepG2 & LX-2 cells in 2D

Applicability of using the Pierce LDH Cytotoxicity Assay (ThermoFisher Scientific) on HepG2 and LX-2 cells was evaluated. HepG2 and LX-2 cells were plated separately in a series of densities specifically, (2000,4000,6000,8000,10000,12000,20000 cells/well). The cells were incubated overnight at 37°C, 5% CO_2. Cells in one set of triplicate wells for each cellular density were lysed by incubation with lysis buffer for 45 minutes, while cells in another set of triplicates were kept alive. Pierce LDH Cytotoxicity Assay Kit was used to analyze the LDH levels in spent medium. LDH levels in fresh medium was also measured to be used as control.

The protocol found in Appendix 9.1.4 was followed. Briefly, Reaction mixture was prepared and added to medium samples to be analyzed. The plate was incubated for 30 minutes then stop solution was added before measuring the absorbance at 490 nm and 680 nm using a plate reader (Epoch). Readings were transferred to Microsoft Excel and analyzed.

4.4.2.2. LDH cytotoxicity assay validation with HepG2 & LX-2 cells in 3D

Applicability of using the LDH cytotoxicity assay kit on HepG2 and LX-2 cells bioprinted into 3D constructs was evaluated. HepG2 and LX-2 cells were bioprinted separately into 6mm concentric discs in a series of densities (1.25,2.5,5,10 M cells/ml bioink). The constructs were incubated overnight at 37°C, 5% CO_2.The day after bioprinting, 6 constructs samples for each cellular density were transferred to a 96 well plate. The cells in one set of triplicates for each cellular density were lysed by incubation with lysis buffer for three hours, while cells in another set of triplicates were kept alive. The Pierce LDH Cytotoxicity Assay Kit was used to analyze the LDH levels in spent medium. Absorbance was measured at 490nm and 680 nm. Readings were transferred to Microsoft Excel and analyzed.

4.4.2.3. Validating effectiveness of LDH cytotoxicity assay to detect change in LDH levels due to cellular distress

10 M HepG2 cells /ml of bioink were bioprinted and cultured for 19 days. On day 10, the constructs were doused with a series of concentrations of DMSO (40%,20%,10%,5%). A control condition where the constructs were not doused with DMSO was also analyzed. Spent medium was collected and frozen every 2 days and the LDH Cytotoxicity assay was performed on collected medium. Absorbance was measured at 490nm and 680 nm. Readings were transferred to Microsoft Excel and analyzed.

4.4.3. Bicinchoninic acid (BCA) protein concentration analysis

4.4.3.1. BCA protein concentration analysis on bioprinted constructs

To analyze the applicability of using Pierce™BCA Protein Assay (ThermoFisher Scientific) to measure protein deposition inside the bioprinted constructs. LX-2 cells were bioprinted in a series of densities (1.25,2.5,5,10 M cells/ml bioink) into 6mm diameter discs and cultured for 4 days. Bioprinted constructs were lysed by incubation with PBS -/- (Gibco) for 3 hours and pipetting until constructs disintegrated. Working reagent and protein standards were prepared according to manufacturer's instructions.

The different procedures (Microplate and Test tube) and protocols (Standard 37°C and enhanced 60°C) presented in the manufacturer's assay manual were implemented with different incubation times. Namely, incubation for 30 minutes at 37°C using manufacturer's microplate method, incubation for 90 minutes at 37°C using the microplate method, incubation for 60 minutes at 60 °C using the microplate method and incubation for 60 minutes at 60°C using the manufacturer's test tube method.

BCA Protein analysis was also implemented on 2:1 and 4:1 HepG2 and LX-2 bioprinted cocultures. The constructs had a cellular density of 10 M cells/ ml of bioink and were cultured for 20 days. A sonication step using VWR® sonicator was added to improve lysing of the constructs. Samples were incubated for 30 minutes at 60°C using the manufacturer's microplate method.

Following incubation, absorbance was measured at 580nm using the plate reader (VICTOR Nivo). The data was transferred to Microsoft Excel, a standard curve was generated from the protein standards and used to calculate protein concentrations for the samples.

4.4.3.2. BCA protein concentration analysis on spent medium

To analyze the applicability of using the BCA Protein Assay in nondestructively measuring protein deposition in spent medium. HepG2 cells with a cellular density of 10 M cells/ ml of bioink were bioprinted into 6mm diameter discs and cultured for 9 days. Medium samples were collected over the course of 9 days. Fresh medium control was also used.

Different procedures (Microplate and Test tube) and protocols (Standard 37°C and enhanced 60°C) presented in the manufacturer's assay manual were implemented with different incubation times. Namely, incubation for 30 minutes at 37°C using the microplate method, incubation for 90 minutes at 37°C using the microplate method, incubation for 60 minutes at 60 °C using the microplate method and incubation for 60 minutes at 60°C using the test tube method.

Spent medium taken after culturing 2:1 and 4:1 HepG2 and LX-2 coculture constructs as well as HepG2 monoculture constructs was also analyzed. Constructs were bioprinted with a cellular density of 10 M cells/ ml of bioink. Spent medium was collected on days 1 and 7 of culture and diluted with PBS to ratios of 1:5,1:20,1:50. Medium control was also diluted. The manufacturer's microplate method was used on samples incubated at 37°C for 30 minutes and at 60 °C for 60 minutes.

4.4.4. Actin/NucBlue staining

The amount of ActinGreen™ (Invitrogen™ ThermoFisher Scientific™) required to successfully stain cells imbedded in bioink was investigated. The effect of keeping the constructs in HBSS +/+or Ethanol after fixation, on staining and the quality of produced images was also investigated.

3D bioprinted,6mm concentric discs with a density of 10 M LX-2 cells/ ml bioink and cultured for 7 days were used. Samples were fixed for 24 hours in 4% paraformaldehyde (PFA) (Sigma-Aldrich) diluted in 100mM $CaCl_2$ (Sigma-Aldrich) and kept in either HBSS+/+ or Ethanol until staining. Constructs were washed and one drop of Actin staining solution was added to one set constructs while two drops were added to the other set. Constructs were incubated in the actin stain overnight. Actin staining solution was removed and one drop of NucBlue staining solution was added in which the constructs were incubated for 1 hour. The samples were washed and Fluorescent microscope (Olympus IX73) was used to image the cells

4.5. Construct analysis

4.5.1. Live/Dead analysis

Samples for all 3 replicate experiments were collected in duplicates on days 1,7 and 20 following printing. The construct samples to be analyzed were transferred to 96 well plates containing appropriate medium. Live/Dead staining was performed using Calcein AM (Invitrogen eBioscience) and Propidium iodide (PI) (Sigma-Aldrich) to image live

and dead cells respectively. Fluorescent microscope (Olympus IX73) was used to image the cells in the constructs. The extended staining protocol followed can be seen in Appendix 9.1.2

4.5.2. Celltiter-Blue® viability analysis

Samples were collected in triplicates for experiment 3 on days 1,7,14,21. The constructs to be analyzed were transferred to 96 well plate containing appropriate media. CellTiter-Blue® viability assay was conducted. A fourth print was conducted to validate the Celltiter blue results. Construct were not induced with TGF-β. Samples were collected on days 1,7 and 14.

Celltiter-Blue® was added to the constructs to be analyzed. The constructs were incubated overnight and fluorescence was recorded the next day at 560/590 nm using a plate reader (VICTOR Nivo). The full protocol can be seen in Appendix 9.1.3.

4.5.3. Lactate dehydrogenase (LDH) Cytotoxicity Analysis

Pierce LDH Cytotoxicity Assay Kit) was used to analyze the LDH levels in spent medium. Medium samples for all 3 experiments were collected in triplicates on days 1,7,12,16 and 20 following printing.

Reaction mixture was prepared and added to medium samples to be analyzed. The plate was incubated for 30 minutes then stop solution was added before measuring the absorbance at 490 nm and 680 nm using a plate reader (Epoch). Readings were transferred to Microsoft Excel and analyzed. Extended protocol can be seen in Appendix 9.1.4

4.5.4. Bicinchoninic acid (BCA) protein concentration analysis

4.5.4.1. BCA protein concentration analysis on bioprinted constructs

Pierce™BCA Protein Assay (ThermoFisher Scientific) was used to analyze protein deposition in the constructs. Construct samples for all 3 experiments were collected in triplicates on days 8,12,16 and 20.

Bioprinted constructs were lysed by incubation with PBS -/- (Gibco), in addition to sonication using VWR® sonicator and pipetting until constructs disintegrated. Working reagent and protein standards were prepared according to manufacturer's instructions. Construct sample solutions and protein standards were transferred to a 96 well plate and working reagent was added to each sample well. Plate was incubated at 60°C for 30 minutes before absorbance measured at 580nm using the plate reader (VICTOR Nivo). The data was transferred to Microsoft Excel, a standard curve was generated from the protein standards and used to calculate protein concentrations for the samples. Extended protocol can be seed in Appendix 9.2.5

4.5.4.2. BCA protein concentration analysis on spent medium

Spent medium was collected for all 3 experiments in triplicates on days 1,7,12,16 and 20. Medium samples were diluted with PBS to a ratio of 1:20. Working reagent and protein standards were prepared according to manufacturer's instructions. Diluted medium samples and protein standards were transferred to a 96 well plate and working reagent was added to each sample well. Plate was

incubated at 60°C for 30 minutes before absorbance measured at 580nm using the plate reader (VICTOR Nivo). The data was transferred to Microsoft Excel, a standard curve was generated from the protein standards and used to calculate protein concentrations for the samples.

Actin/NucBlue staining

Samples from experiment 3 were collected on days 8, 18 and 21. ActinGreen™ (Invitrogen™ ThermoFisher Scientific™) was used for actin staining. NucBlue™ (Invitrogen™ ThermoFisher Scientific™) was used to stain the nuclei.

Samples were fixed in 4% paraformaldehyde (Sigma-Aldrich) diluted in 100mM $CaCl_2$ (Sigma-Aldrich) for 24 hours. Constructs were washed and Actin staining solution was added. Constructs were then incubated in the actin stain overnight. Actin staining solution was removed and NucBlue staining solution was added in which the constructs were incubated for 1 hour. The samples were washed and Fluorescent microscope was used to image the cells. The extended protocol can be seen in Appendix 9.2.6

4.6. Image Analysis

Live/Dead and Actin/NucBlue images were taken using inverted fluorescent microscope (Olympus™ IX73) after placing the construct samples in medium in a 96 well plate. Actin/NucBlue staining images were taken using the green (FITC/488) and blue (DAPI/360) channels with an exposure time of 100-200ms and 300-500ms respectively. Two z-stacked images were acquired per construct. The images were processed, adjusted and combined using the image analysis software ImageJ to provide one single image per construct.

Live/Dead images were taken using the green (FITC/488) and red (TexasRed/570) channels with an exposure time of 100-200ms and 600-800ms respectively. Two z-stacked images were acquired per construct. The image analysis software ImageJ was used to adjust and process the images, count number of live and dead cells and combine the two z-stacked images to provide a single image per construct. Image cell counts were transferred to Microsoft Excel where total cell count, viability and standard deviation were calculated.

4.7. Statistical Analysis

Data was expressed as means ± standard derivation (SD) of three independent experiments. Statistical significance was calculated by two-way ANOVA test. P values < 0.05 were considered to be statistically significant.

5. Results and discussion

5.1. GelXA compatibility and crosslinking method evaluation results

Construct samples were collected in triplicates for live/dead analysis on days 2,7, and 9 for each of the four conditions (LX-2 cells crosslinked with $CaCl_2$, LX-2 cells crosslinked with UV, HepG2 crosslinked with $CaCl_2$ and HepG2 cells crosslinked with UV). The average cell count and viability values can be seen in table 3 and are also presented in the form of bar graphs (figures 5-8) Images depicting viability can be seen in figures 9 and 10.

Table 3. Average live/dead cell count and viability (%)

		Avg. cell count		Avg. Viability (%)
LX-2 (CaCl2)		Live	Dead	
	Day 2	408	175.67	70.55
	Day 7	351.67	388.67	48.88
	Day 9	429.33	330	55.00
LX-2 (UV)		Live	Dead	
	Day 2	100.33	172.33	38.43
	Day 7	162.33	183.33	46.70
	Day 9	278.00	353.00	45.58
HepG2 (CaCl2)		Live	Dead	
	Day 2	101.67	89.33	52.62
	Day 7	186.33	168.00	48.76
	Day 9	536.33	398.67	57.04
HepG2 (UV)		Live	Dead	
	Day 2	88.00	57.67	57.76
	Day 7	313.00	138.00	71.95
	Day 9	120.67	129.00	48.49

Average live/dead cell count and viability (%) on days 2,7 and 9 for (10M/ml) HepG2 & LX-2 cells bioprinted in GelXA LN 111, 121 and crosslinked withCaCl2 or UV

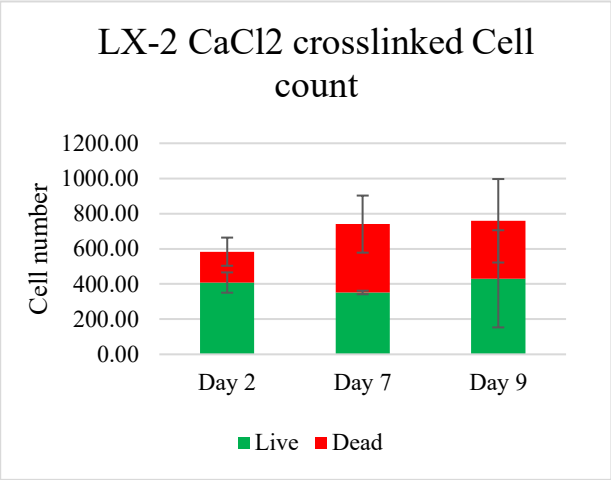

Figure 5. Average live (green) and dead (red) cell count on days 2,7 and 9 for (10 M/ml) LX-2 cells bioprinted in GelXA LN 111 crosslinked with $CaCl_2$.

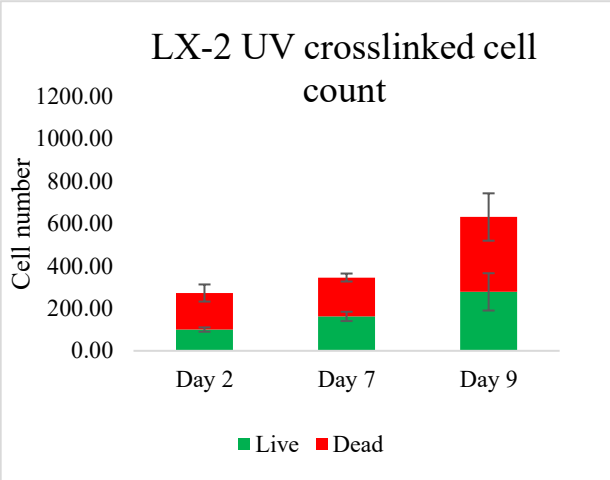

Figure 6. Average live (green) and dead (red) cell count on days 2,7 and 9 for (10 M/ml) LX-2 cells bioprinted in GelXA LN 111 crosslinked with UV.

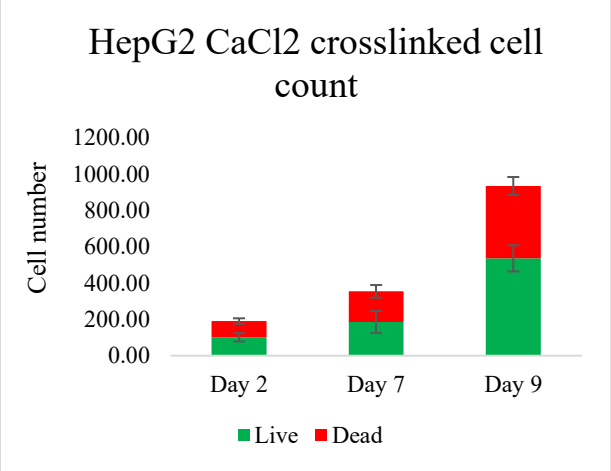

Figure 7. Average live (green) and dead (red) cell count on days 2,7 and 9 for (10 M/ml) HepG2 cells bioprinted in GelXA LN 121 crosslinked with $CaCl_2$.

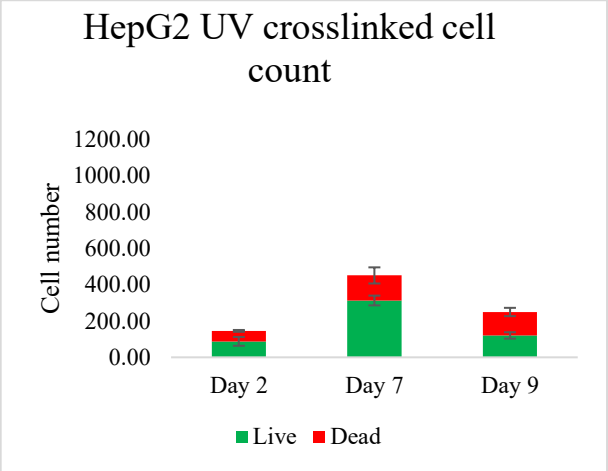

Figure 8. Average live (green) and dead (red) cell count on days 2,7 and 9 for (10 M/ml) HepG2 cells bioprinted in GelXA LN 121 crosslinked with UV.

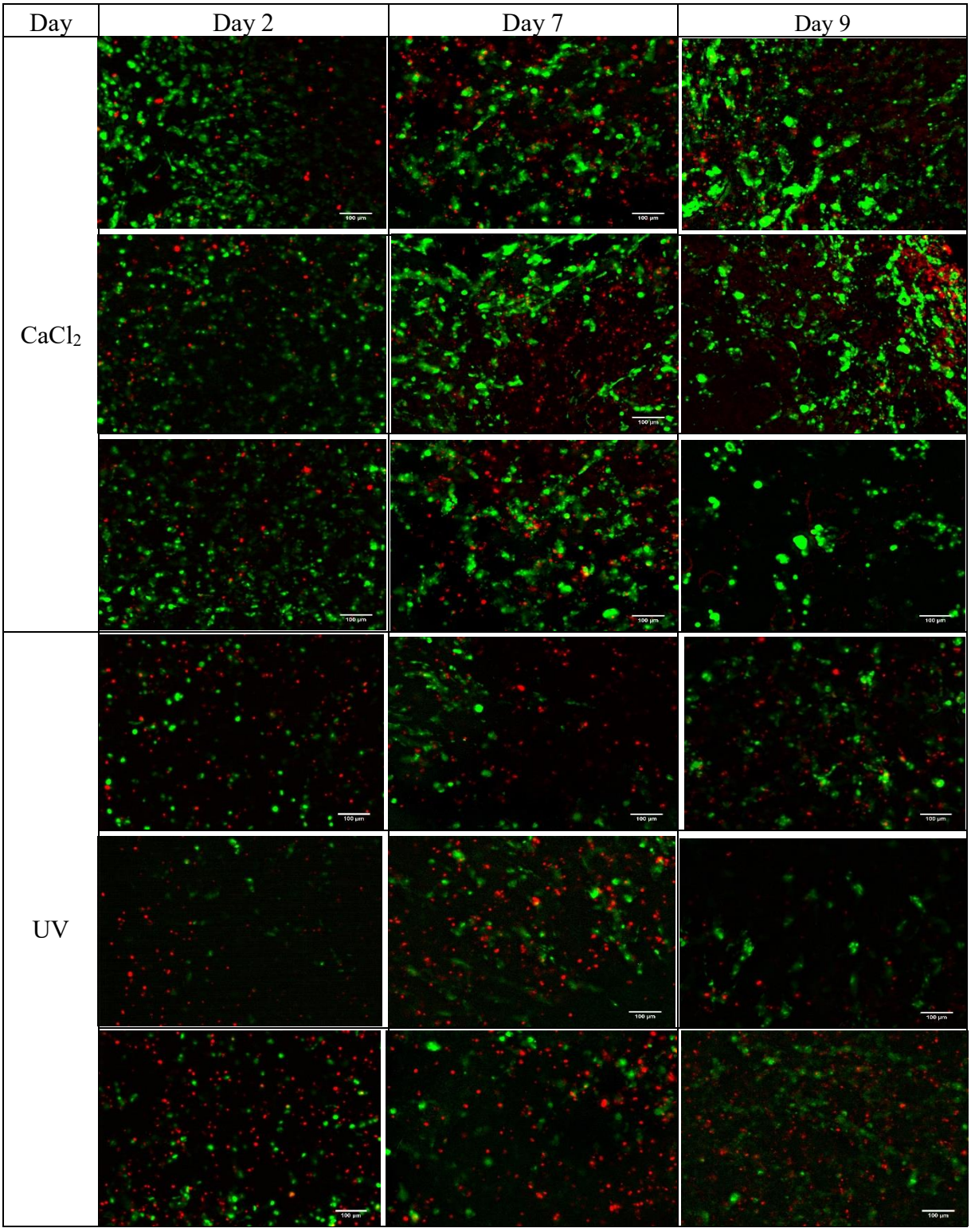

Figure 9. live/dead images of (10M/ml) LX-2 cell printed in GelXA LN111 crosslinked with $CaCl_2$ and UV respectively. Images were taken at 10x magnification

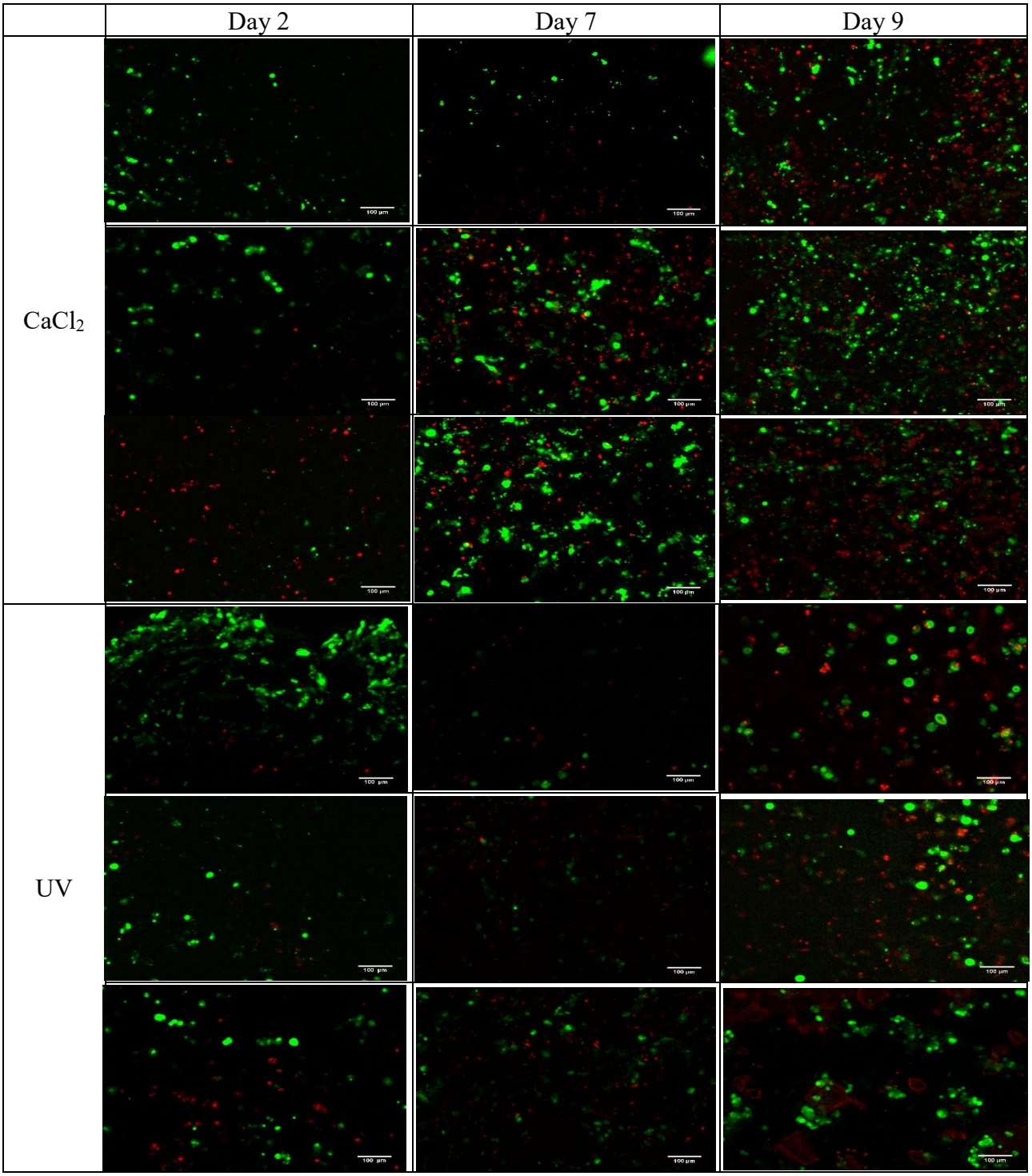

Figure 10. live/dead images of (10M/ml) HepG2 cell printed in GelXA LN121 crosslinked with CaCl2 and UV respectively. Images were taken at 10x magnification.

Viability ranged between 40-70% throughout the culture period in almost all conditions of the experiment. Viability is probably higher than the numbers shown in table 3, as can be seen from the images in figures 9 and 10 but the image analysis software used, counts cell clusters as single cells. As the cells were stretching and clustering, as can be seen from the images, the software could not count them correctly.

Cell count and viability numbers as well as the images in figures 9 and 10 confirm that the GelXA bioink is compatible with both HepG2 and LX-2 cell types. The obtained numbers and images also show that crosslinking by submersion in $CaCl_2$ results in a higher cellular viability compared to crosslinking by exposure to UV. This is not surprising as UV exposure is known to cause cellular DNA damage by initiating a reaction between two neighboring thymine molecules. The resulting thymine dimer although stable, can usually be repaired by the cell. However, extensive damage raises the risk of incorrect repairs. If cellular processes are disrupted because of an incorrect repair or remaining damage, normal cellular responses are interrupted which eventually leads to cell death [55][76]. Therefore, crosslinking using $CaCl_2$ was utilized in the following experiments.

5.1. Assay optimization results

5.1.1. Celltiter-Blue® viability assay

5.1.1.1. Applicability of using Celltiter-Blue® on 3D bioprinted HepG2 and LX-2 cells

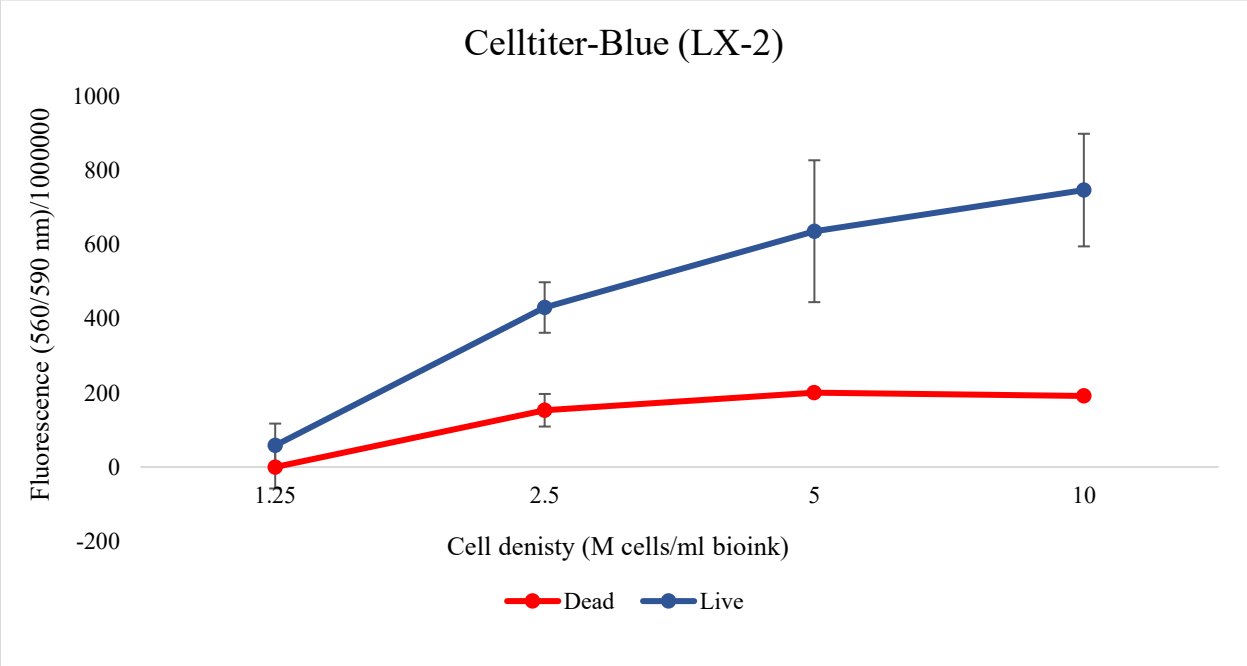

Figure 11. Average Celltiter-Blue® fluorescence values and standard deviations /1000000 recorder at (560/590 nm) for LX-2 cells bioprinted in 4 different cell densities. The cells in one set of triplicates was lysed (red)while the cells in the other set were kept alive (blue).

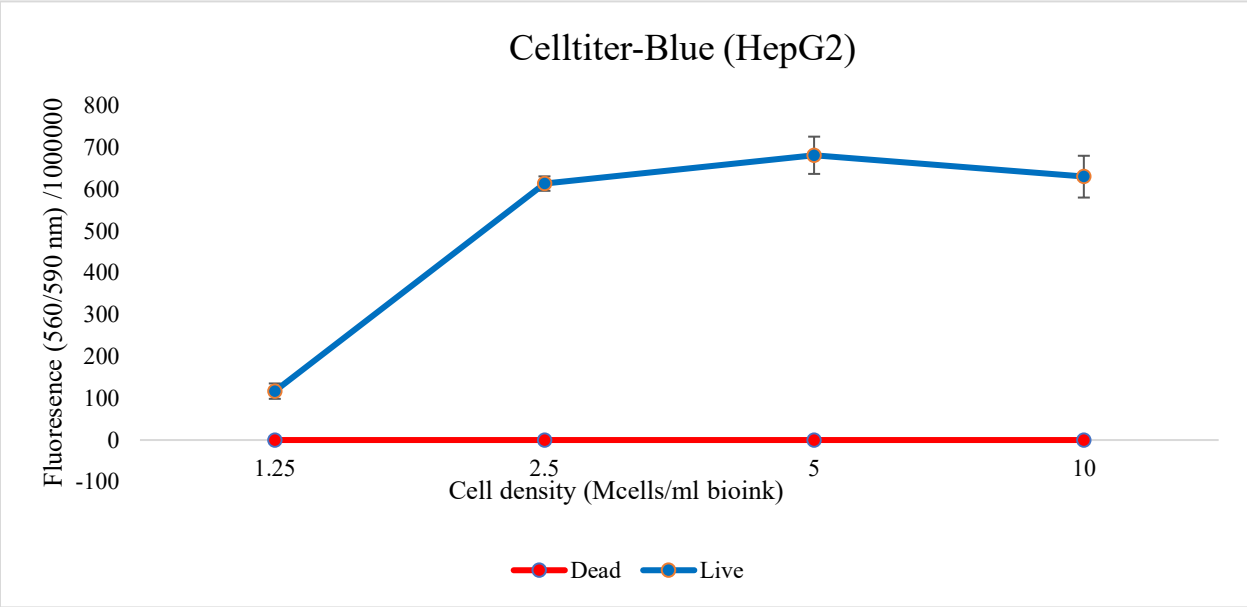

Figure 12. Celltiter-Blue® fluorescence values and standard deviations /1000000 recorder at (560/590 nm) for HepG2 cells bioprinted in 4 different cell densities. The cells in one set of triplicates was lysed (red)while the cells in the other set were kept alive (blue)

Figures 11 and 12 depict expected results. Celltiter Blue was effective in conveying the increase in cellular density as can be seen from the blue lines in both figures. There was also a very clear and significant difference between lysed dead cells and the live cells. The red lines which depicts the constructs that contained lysed/dead cells remained almost flat for the LX-2 cells and completely flat at 0 nm for the HepG2 cells. The lysed LX-2 cells still exhibited some fluorescent signal despite the fact they the cells were supposed to be dead and therefore no resazurin should have been converted to the fluorescent resorufin. This might indicate that despite being incubated with the lysis buffer, some cells may not have been dead when the Celltiter Blue assay was performed. Despite this, Celltiter Blue seemed to be an effective method for demonstrating cellular viability for HepG2 and LX-2 cells imbedded in bioink and can therefore be used to investigate cellular proliferation in 3D bioprinted constructs over a period of time in conjunction with or instead of Live/Dead analysis.

In fact, Celltiter blue is most probably superior to Live/Dead staining in representing cellular viability and proliferation. After Live/Dead staining, bioprinted constructs are imaged through fluorescent microscopy, which although provides high resolution images, poses the challenge of limited area images as well as limited depth of penetration [77]. Therefore, the captured images are not reflective of the whole structure. Additionally, cell counts obtained from these images depend on software programs that are sometimes incapable of accurately counting cells. The quality of captured images depends on the experience and imaging skills of the user. Due to all of these limitations Live/Dead staining might not be a reliable method for monitoring cellular density and proliferation in 3D bioprinted constructs.

Celltiter Blue on the other hand accounts for cells in the entire construct. With the right incubation time, the solution should penetrate into the whole structure. Also, CellTiter-Blue® analysis is much faster, less labor intensive and does not rely on the skills of the user, reducing room for human error. Therefore, this method would be useful for applications where speed and accuracy are essential such as quality control.

5.1.1.2. Assessing the optimal incubation time for bioprinted constructs with Celltiter-Blue®

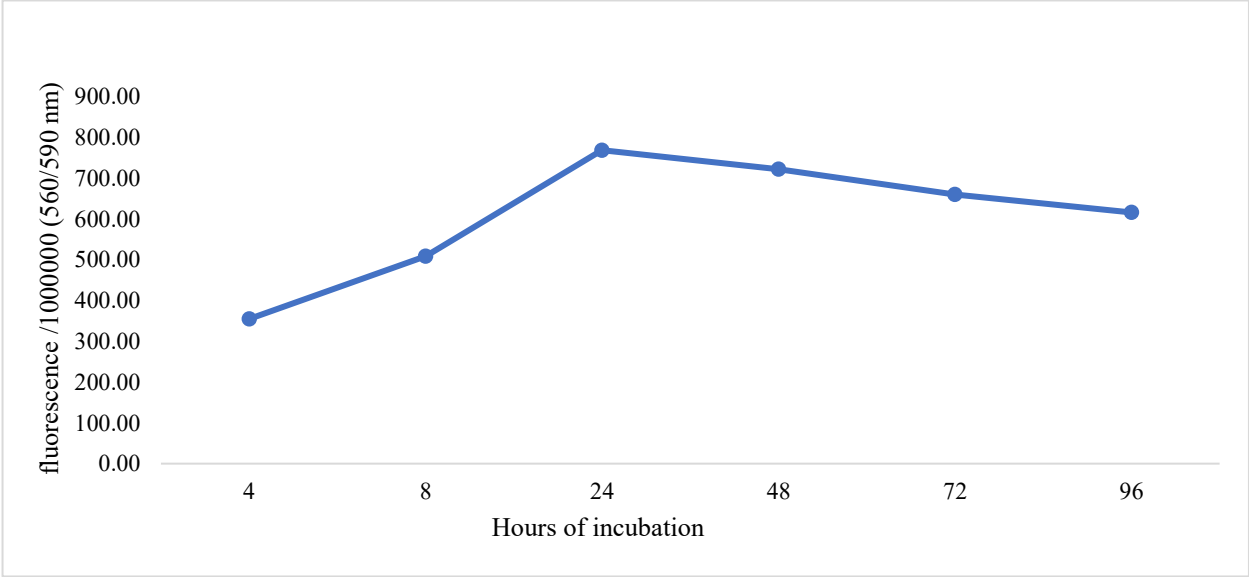

Figure 13. Average Celltiter-Blue fluorescence values and standard deviations /1000000 for 10 M HepG2 cells /ml bioink recorded at (560/590 nm) after different hours of incubation

Celltiter Blue's manufacturer's protocol states incubating cells with Celltiter Blue reagent for 1-4 hours. But as 3D bioprinted cells are imbedded in hydrogel, optimal incubation time needed to be evaluated. Maximum fluorescence was detected after 24 hours of incubation with Celltiter Blue reagent. After this point, fluorescence seemed to decline slightly probably due to photobleaching as a result of repeated fluorescence measurements and exposure to light during plate handling. Therefore, in later experiments, constructs were incubated for 24 hours before fluorescence was read using a plate reader.

5.1.2. Lactate dehydrogenase (LDH) Cytotoxicity Analysis

5.1.2.1. LDH cytotoxicity assay validation with HepG2 & LX-2 cells in 2D

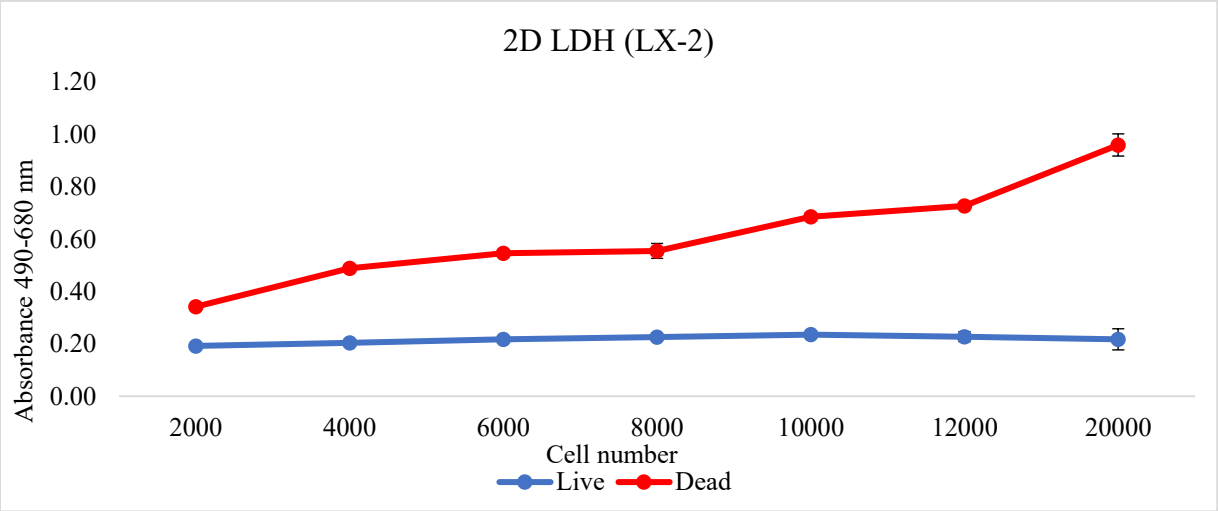

Figure 14. Average LDH absorbance values measured at 490-680nm for LX-2 cells plated in 2D in cell in a series of densities (2000-20000 cells/well). One set of triplicates was lysed (red) while the other set was kept alive (blue).

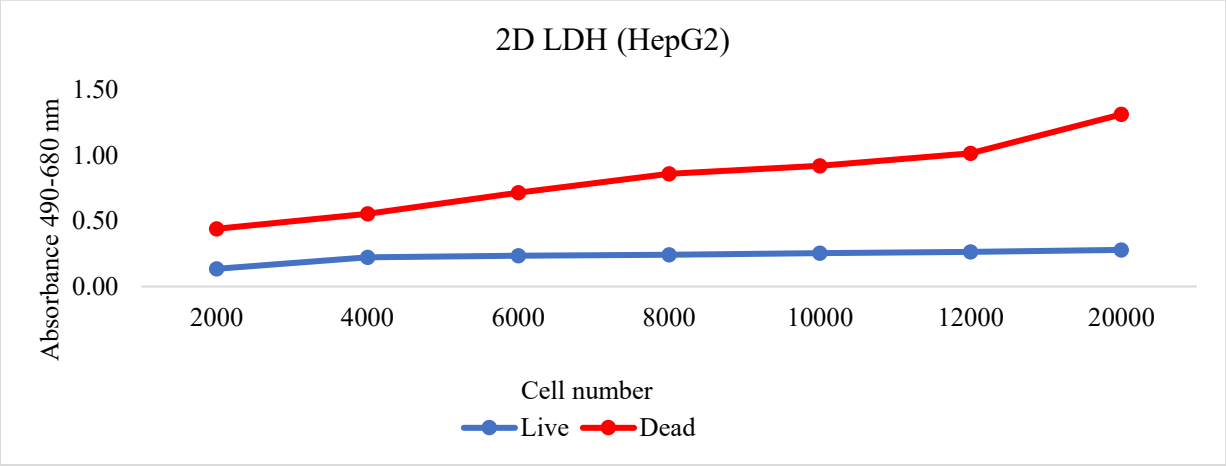

Figure 15. Average LDH absorbance values measured at 490-680nm for HepG2 cells plated in 2D in a series of densities (2000-20000 cells/well). One set of triplicates was lysed (red) while the other set was kept alive (blue).

Figures 14 and 15 show a clear increase in amount of LDH excreted into the spent medium with increasing number of lysed LX-2 and HepG2 cells. While amount of LDH in spent medium taken from live cells remains constant despite an increase in cell density. This indicates that both LX-2 and HepG2 cells do not produce LDH unless the cells are dead/dying. And that the LDH assay can be successfully used to determine cytotoxicity of LX-2 and HepG2 cell.

5.1.2.2. LDH cytotoxicity assay validation with HepG2 & LX-2 cells in 3D

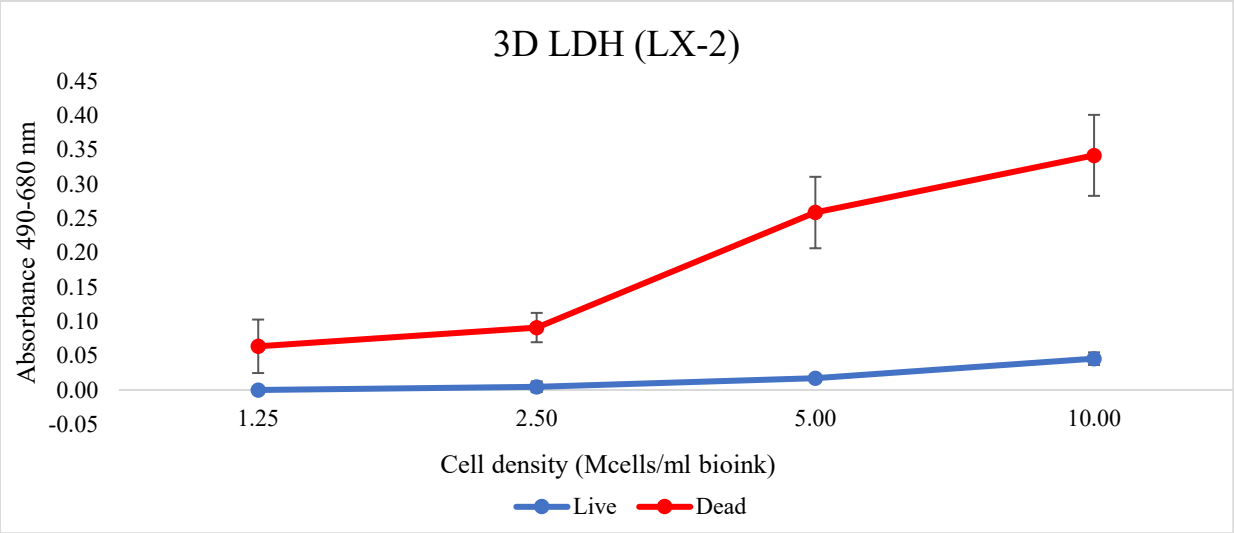

Figure 14. Average LDH absorbance values measured at 490-680nm for LX-2 cells plated bioprinted in 4 different cell densities. One set of triplicates was lysed (red) while the other set was kept alive (blue).

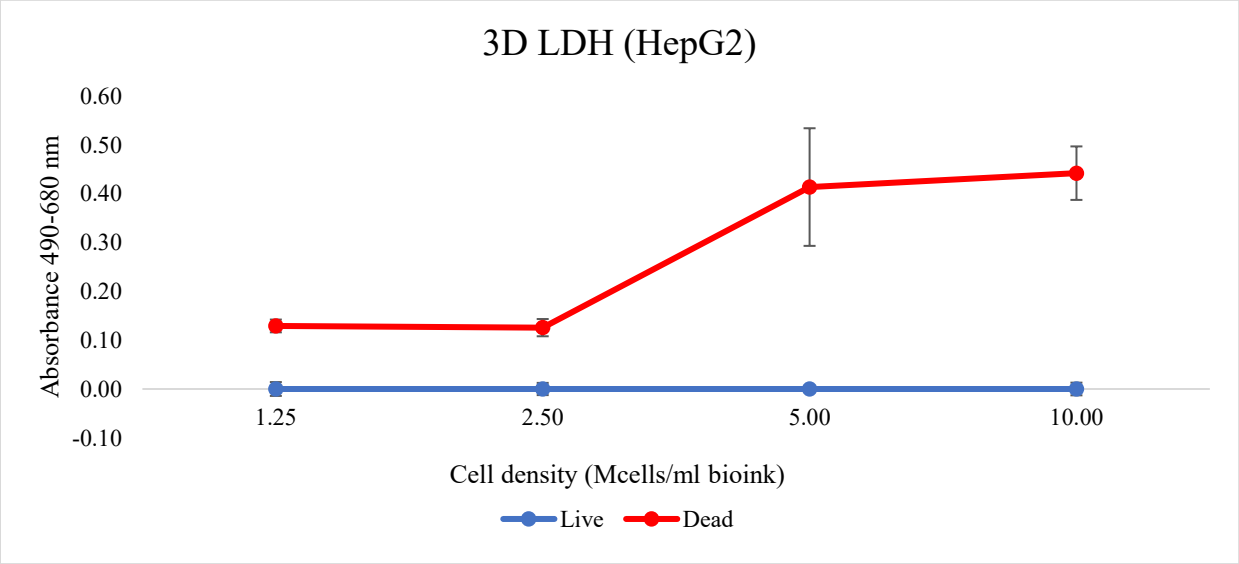

Figure 15. Average LDH absorbance values measured at 490-680nm for HepG2 cells plated bioprinted in 4 different cell densities. One set of triplicates was lysed (red) while the other set was kept alive (blue).

As cells were imbedded in a hydrogel, incubation time with the lysis buffer was extended to 3 hours instead of the 45 minutes used for the cells in 2D. This is to ensure that the lysis buffer diffuses inside the constructs and reaches all cells within the bioprinted structure. 3D bioprinted LX-2 and HepG2 cells exhibit similar behavior to cells plated in 2D. The level of LDH measured in spent medium increases with an increase in density of lysed cells and remains constant for live

cells despite increase in cellular density. This confirms that LDH assay can be used reliably to investigate cytotoxicity of bioprinted LX-2 and HepG2 cells.

5.1.2.3. Validating effectiveness of LDH cytotoxicity assay to detect change in LDH levels due to cellular distress

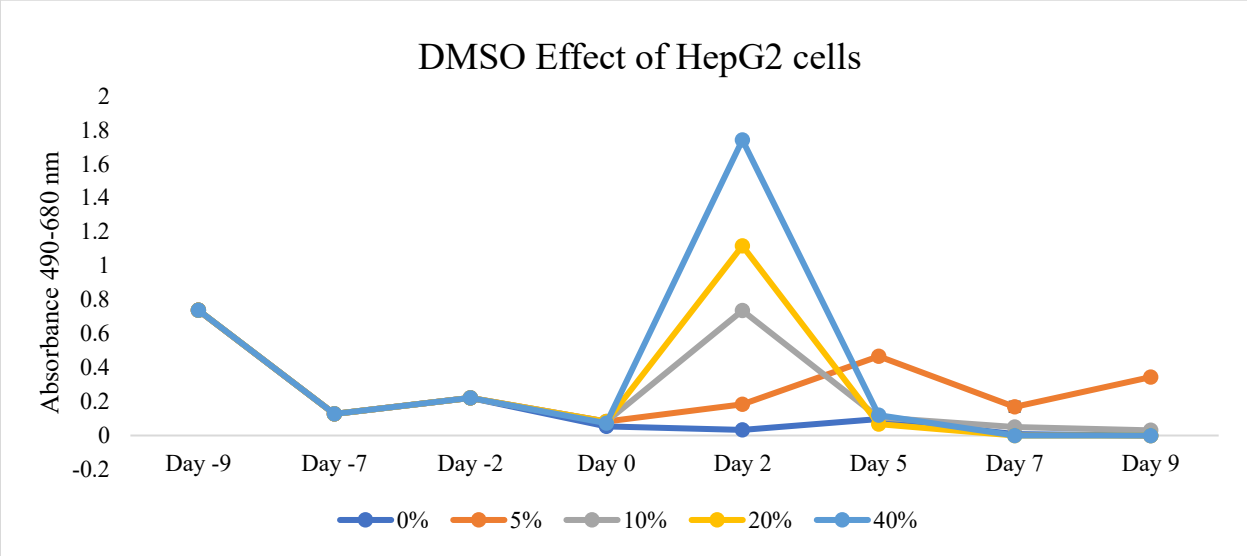

Figure 16. Average LDH absorbance values measured at 490-680nm for 10 M/ml HepG2 cells bioprinted and cultured for 19 days and doused in different concentrations of DMSO on day 0 (day 10 after bioprinting).

Bioprinted HepG2 cells were cultured for 9 days before being doused with different concentrations of DMSO. Spent medium samples were collected over the course of 19 days. LDH levels were found to be elevated on day -9 (day 1 after bioprinting). This was expected as the bioprinting process is stressful for cells and causes cellular damage and death for a significant number of the bioprinted cells. LDH levels go down after that an remain relatively constant for the next 7 days. On day zero (day 10 after bioprinting), constructs were doused with DMSO which is toxic to cells in high concentration. Spent medium collected on day 2 after addition of DMSO shows a spike in LDH levels corresponding to the percentage of DMSO added. On days 5-9 after addition of DMSO, LDH amount goes down to the low level observed before addition of DMSO.

Constructs doused with 5% of DMSO demonstrated a delayed effect and maximum LDH levels were detected on day 5 after addition of DMSO instead of day 2 as with the cells doused with higher amounts of DMSO. This maybe because DMSO levels were not high enough to elicit immediate cell death but caused certain metabolic changes that resulted in a higher number of cells dying later on.

Similar to the Celltiter Blue assay, the LDH cytotoxicity assay results reflect the state of cells in the entire bioprinted construct and can therefore provide reliable information about cellular cytotoxicity which when coupled with Celltiter Blue viability results gives a much more complete and representative picture of the wellbeing of the bioprinted cells compared to Live/Dead staining. LDH assay is used nondestructively on spent media. This is highly desirable as constructs would not need to be sacrificed and the same construct can be monitored overtime. LDH cytotoxicity

assay can also be used to investigate cellular proliferation. However, this would require lysing the bioprinted cells and measuring LDH quantity released into the spent medium. Therefore, monitoring cellular proliferation through the LDH assay cannot be achieved nondestructively.

5.1.3. Bicinchoninic acid (BCA) protein concentration analysis

5.1.3.1. BCA protein concentration analysis on bioprinted constructs

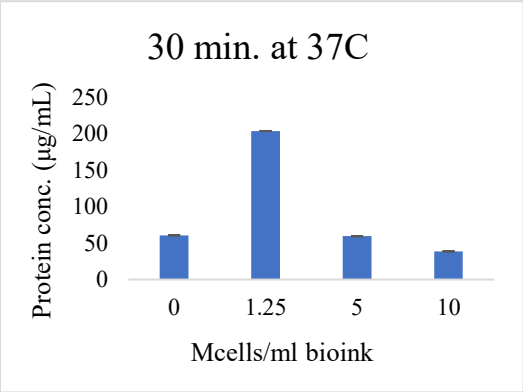

Figure 17. Average protein concentrations (µg/ml) found in constructs bioprinted with different cells densities of LX-2 cells. After incubation for 30 min. at 37°C using the manufacturer's microplate method.

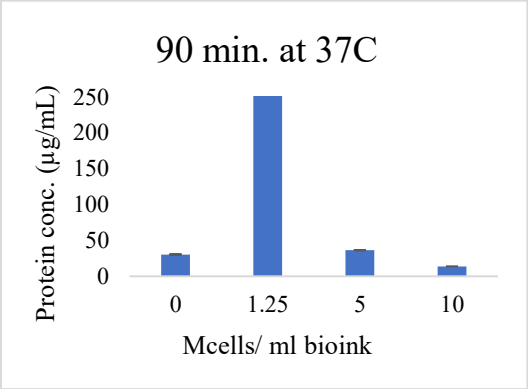

Figure 18. Average protein concentrations (µg/ml) found in constructs bioprinted with different cells densities of LX-2 cells. After incubation for 90 min. at 37°C using the manufacturer's microplate method.

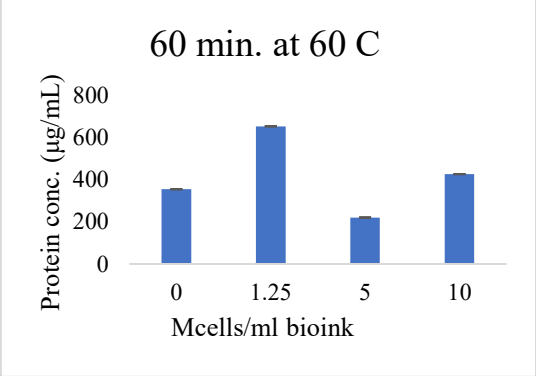

Figure 19. Average protein concentrations (µg/ml) found in constructs bioprinted with different cells densities of LX-2 cells. After incubation for 60 min. at 60°C using the manufacturer's microplate method.

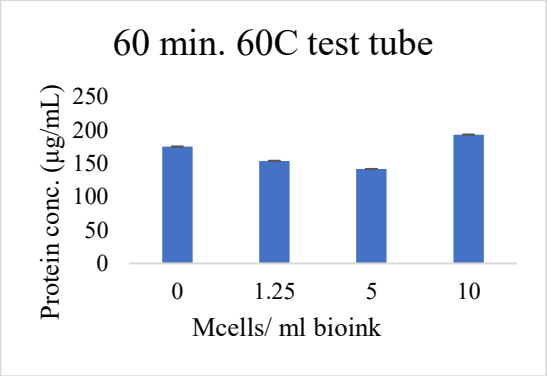

Figure 20. Average protein concentrations (µg/ml) found in constructs bioprinted with different cells densities of LX-2 cells. After incubation for 60 min. at 60°C using the manufacturer's test tube method.

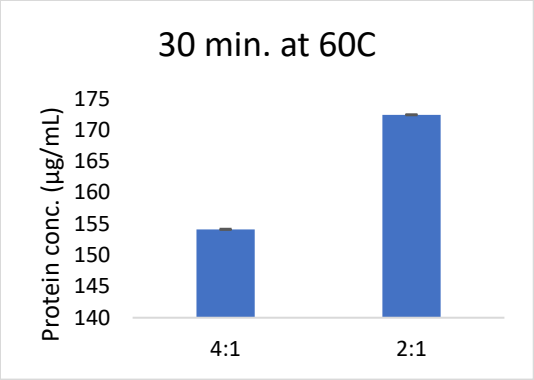

Figure 21. Average protein concentrations (µg/ml) found in bioprinted constructs containing 10M HepG2 & LX-2 cocultures (2:1 &4:1)/ml bioink. After incubation for 30 min. at 60°C using the manufacturer's microplate method.

LX-2 cells were bioprinted in a series of densities (1.25,2.5,5 and 10 M cells/ml bioink). Triplicates of each cellular density were collected. BCA protein assay was used to investigate protein deposition inside the constructs using different procedures offered by the manufacturer. It was found that incubating samples at 60°C greatly increased the sensitivity of the assay vs incubation 37°C. Using the microplate method resulted in higher sensitivity compared to the test tube method.

It can be noticed that the results do not show an increase in protein deposition corresponding to the increase in cell density as was expected. Instead protein concentrations seem to be random. This can be due to the fact that the cells were only cultured for 4 days and therefore did not deposit much protein and most of the protein detected is the protein present in the bioink itself.

Interestingly however is the fact that the protein concentration for the 1.25 M/ml was the highest among all densities. This is because incubation with PBS and pipetting was not enough to lyse the constructs properly and that resulted in a large piece of the structure ending up in the 1.25Mcells/ml well. This highlighted the necessity of lysing the structures more effectively. Therefore, the constructs were in later attempts sonicated for 1 hour prior to pipetting. This led to a much easier and faster disintegration of the constructs resulting in a more homogeneous solution. A filtration step using syringes and sterile filters was also attempted. This turned out to be a very time-consuming and labor-intensive step. Therefore, due to the high number of samples in each experiment this was considered to be impractical to implement.

Next, triplicates of 2:1 and 4:1 HepG2 and LX-2 cocultures that had been cultured for 21 days were used. This time the constructs were sonicated for an hour after the 3-hour incubation with PBS (-/-). This resulted in a much more homogeneous solution. The constructs were incubated for 30 minutes at 60°C. It was found that the protein concentration in the 2:1 construct was higher than the 4:1 construct as expected.

One concern about using the BCA protein assay on bioprinted constructs is the fact that the bioink itself contains proteins which will interfere with the obtained results. This would be a huge drawback if the aim of the project was to determine the exact amount of protein deposited by the cells in the constructs. But since the aim in this project was to monitor the increase in protein deposition overtime and in different conditions to determine the effect of the different conditions on protein deposition then, the BCA protein assay would still be able to give informative, reliable results especially since the same kind of bioink was used in all conditions.

5.1.3.2. BCA protein concentration analysis on spent medium

In an attempt to optimize BCA assay to be used nondestructively on spent medium, medium samples were collected over the course of 9 days of culturing 10 Mcells/ml bioink of bioprinted HepG2 cells. BCA protein assay was used under different conditions.

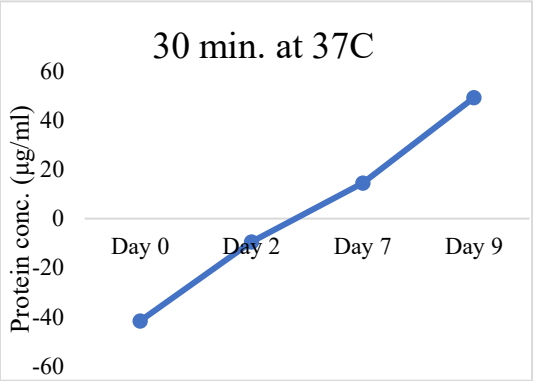

Figure 22. Average protein concentrations (µg/ml) in spent medium taken from bioprinted 10M HepG2 cells/ml bioink. After incubation for 30 min. at 37°C using the manufacturer's microplate method.

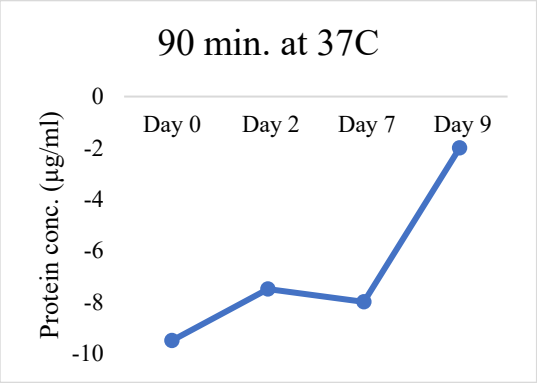

Figure 23. Average protein concentrations (µg/ml) in spent medium taken from bioprinted 10M HepG2 cells/ml bioink. After incubation for 90 min. at 37°C using the manufacturer's microplate method.

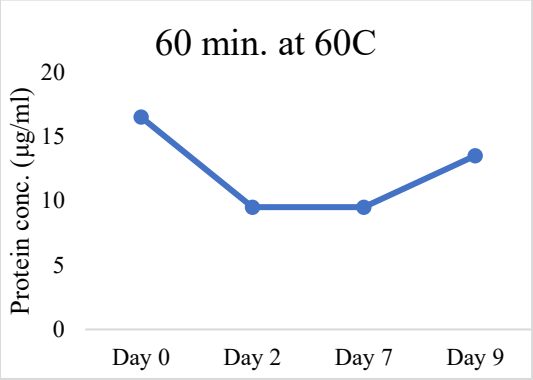

Figure 24. Average protein concentrations (µg/ml) in spent medium taken from bioprinted 10M HepG2 cells/ml bioink. After incubation for 60 min. at 60°C using the manufacturer's microplate method.

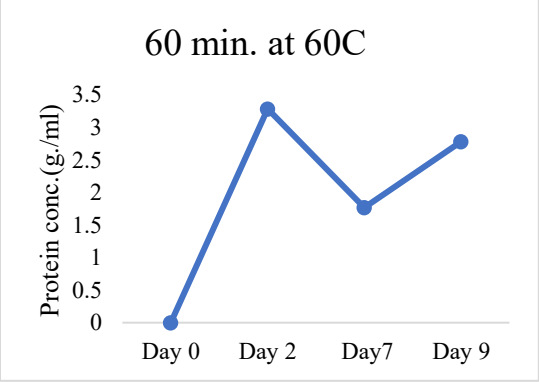

Figure 25. Average protein concentrations (µg/ml) in spent medium taken from bioprinted 10M HepG2 cells/ml bioink. After incubation for 60 min. at 60°C using the manufacturer's test tube method.

Protein concentrations detected in the medium were very high and out of the range of the generated standard curves. This is due to the fact that the media are already rich with many different kinds of proteins and amino acids such as Fetal bovine serum (FBS) and L-glutamate used to supplement the media. Therefore, fresh medium controls were used in order to be able to determine the amount of proteins excreted by the cells only. Incubation at 37°C yielded spent medium protein concentrations that were lower than those in the fresh medium controls resulting in negative values for the protein concentrations which is obviously not possible. Incubation at 60°C resulted higher sensitivity. Protein concentrations although were extremely low were positive values.

For the next attempt medium samples were diluted to increase sensitivity. Spent medium was collected from 2:1 and 4:1 cocultures and HepG2 monoculture after being cultured for 7 days. Detected protein concentrations in the spent medium samples were still consistently lower compared to fresh medium samples which did not lead to any useful information. This is probably because the proteins in the spent medium had been taken up and utilized by the cells. It was therefore evident that the BCA protein assay could not be used to detect protein deposition into the medium.

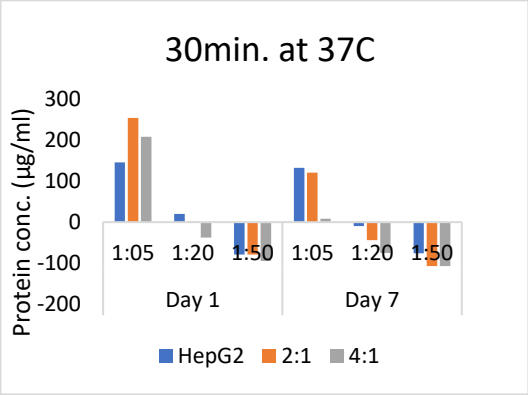

Figure 26. Average protein concentrations (µg/ml) in spent medium taken from bioprinted HepG2 cells, 2:1 HepG2:LX2 coculture and 4:1 HepG2:LX2 coculture with cell density of 10Mcells/ml bioink. Medium was diluted to the ff ratios: 1:5,1:20,1:50 and incubated for 30 min. at 37°C using the manufacturer's microplate method.

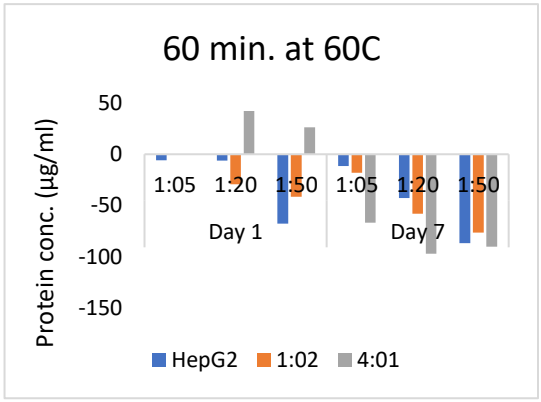

Figure 27. Average protein concentrations (µg/ml) in spent medium taken from bioprinted 10M HepG2 cells, 2:1 HepG2:LX2 coculture and 4:1 HepG2:LX2 coculture with cell density of 10Mcells/ml bioink. Medium was diluted to the ff ratios: 1:5,1:20,1:50 and incubated for 60 min. at 60°C using the manufacturer's microplate method.

5.1.4. Actin/NucBlue staining

1 Drop of Actin stain | 2 Drops of Actin stain

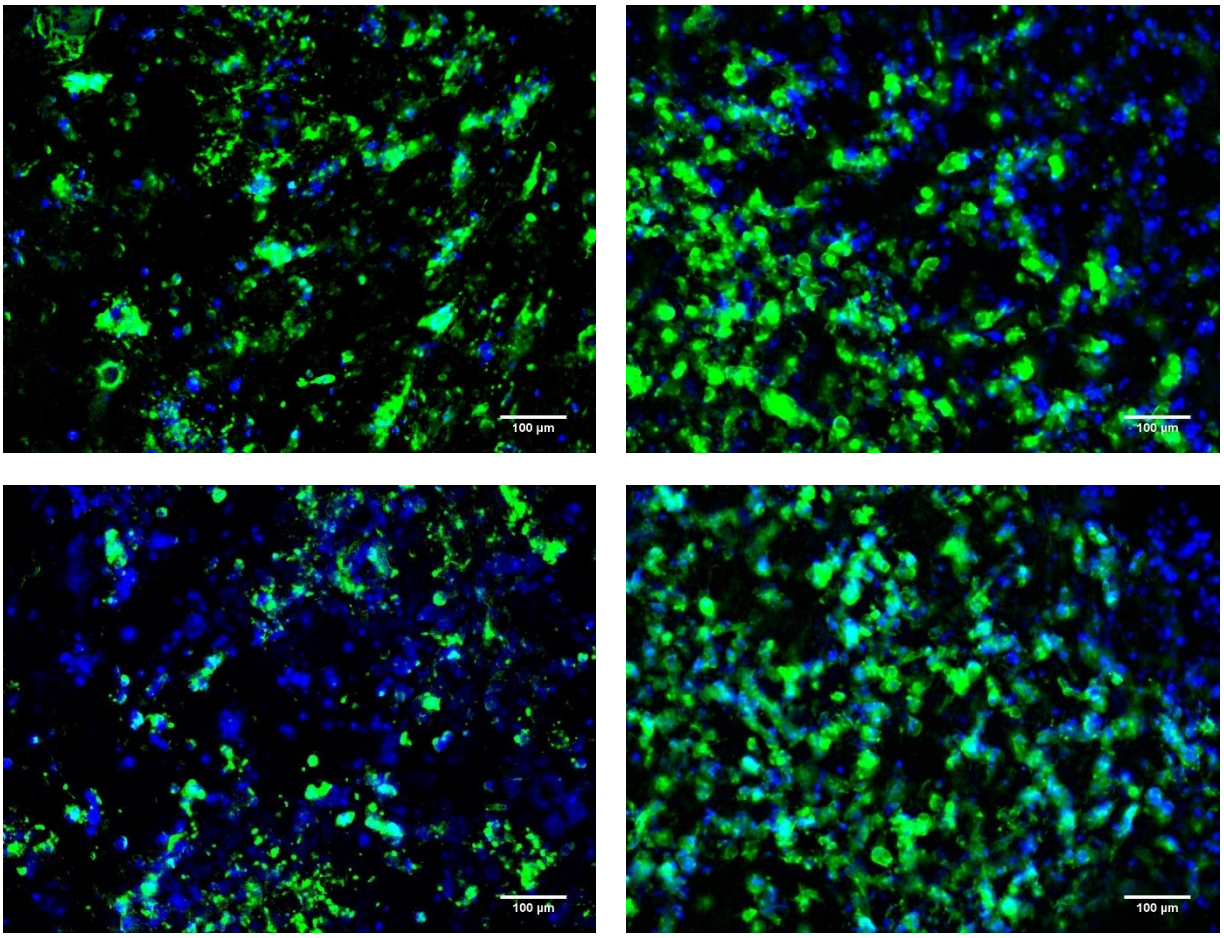

Figure 28. 10M /ml LX-2 cells stained with Actin/NucBlue on day 7 stained with 1 or 2 drops of ActinGreen. Images were taken at 10x magnification.

Figure 29 shows that staining bioprinted constructs with 1 drop of ActinGreen results in the same brightness and clarity of the images compared to staining with 2 drops of ActinGreen. Experiment also showed that incubation of fixed constructs in ethanol or HBSS (+/+) does not make a difference in the quality of the resulting images. Therefore, experimental samples were stained with 1 drop of ActinGreen and kept in HBSS (+/+) until imaging.

5.2. Experimental results

5.2.1. Viability

5.2.1.1. Live/Dead analysis

Construct samples were collected in duplicates for live/dead analysis on days 1,7, and 20 for each of the three replicate experiments. The average cell count and viability values can be seen in table

4 and are also presented in the form of a bar graph (figure 29). Images depicting viability at Day 20 can be seen in figure 30. Complete values and images for the individual print sessions can be seen in Appendix 9.2.1

Table 4. Average cell count and viability				
		Average Cell count		Average Viability (%)
	Days	Live	Dead	
HePG2	Day 1	279.17	330.67	54.07
	Day 7	176.33	133.00	62.92
	Day 20 C	244.33	302.33	46.93
	Day 20 I	205.17	151.67	60.29
2:1	Day 1	314.33	347.17	55.52
	Day 7	407.67	300.17	59.80
	Day 20 C	283.67	409.00	41.23
	Day 20 I	315.67	354.50	46.64
4:1	Day 1	198.17	402.00	38.43
	Day 7	235.67	135.17	66.63
	Day 20 C	404.83	424.67	47.11
	Day 20 I	328.33	284.67	52.60
Average live/dead cell count and standard deviation for three replicate experiments on days 1,7 and 20 (Induction(I) & Control (C)) for HepG2, 2:1 and 4:1 conditions.				

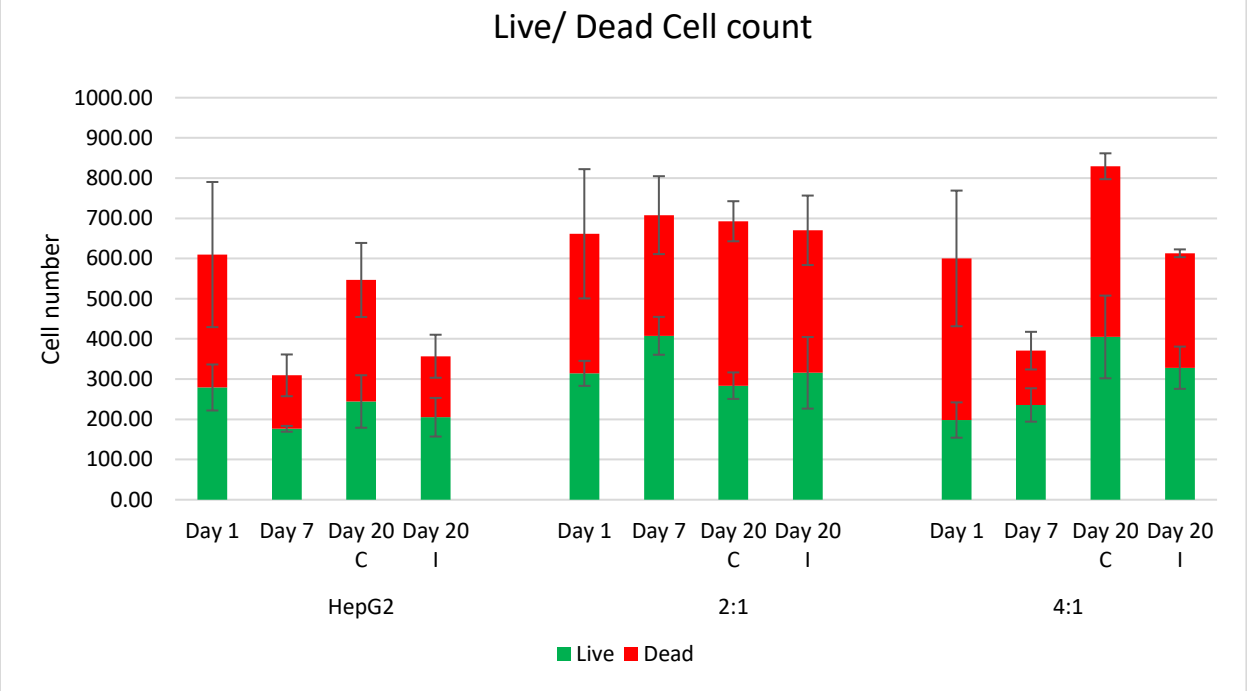

Figure 29. Average cell count for three replicate experiments showing live (green) and dead (red) cells on days 1,7 and 20 (Induction & Control) for HepG2, 2:1 and 4:1 conditions.

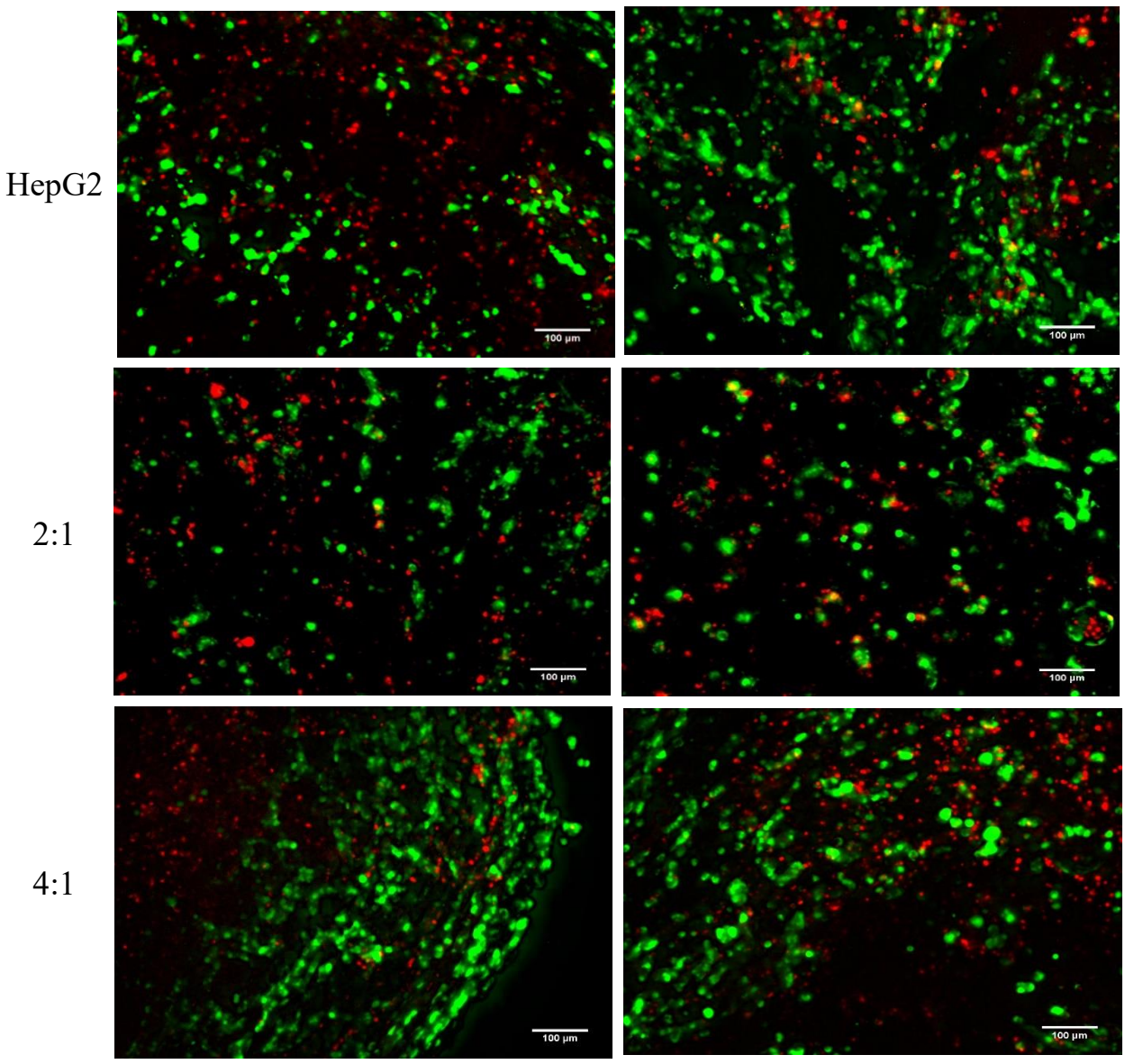

Figure 30. Day 20 live/dead images for HepG2 control, 2:1 coculture ratio, 4:1 coculture ratio. Live cells can be seen in green and dead cells in red. Images were taken at 10x magnification

In all conditions of the experiment, cell viability was maintained at 40-60% throughout the culture period. Viability is probably higher than the numbers shown in table 4, as can be seen from figure 30 and Appendix 9.2.1.2 but the image analysis software used counts cell clusters as single cells. As the cells were stretching and clustering, as can be seen from figure 3, the software could not count them correctly.

As seen in table 4, at day 20, the viability was highest for the HepG2 condition followed by the 4:1 condition. This shows that an increase in the number of LX-2 cells has a negative effect on overall viability. The viability was always slightly higher in the induced group compared to the control group within each condition. However, the differences were not significant. The images do not show a clear distinction between the induced and control groups in any of the three cell conditions. More quantitative viability was determined with CellTiter-Blue®.

5.1.2. Celltiter-Blue®

Construct samples were collected in triplicates for experiment 3 and the Celltiter blue assay was run on days 1,7,14,20. Results can be seen in figure 31. Complete numbers can be seen in Appendix 9.2.2

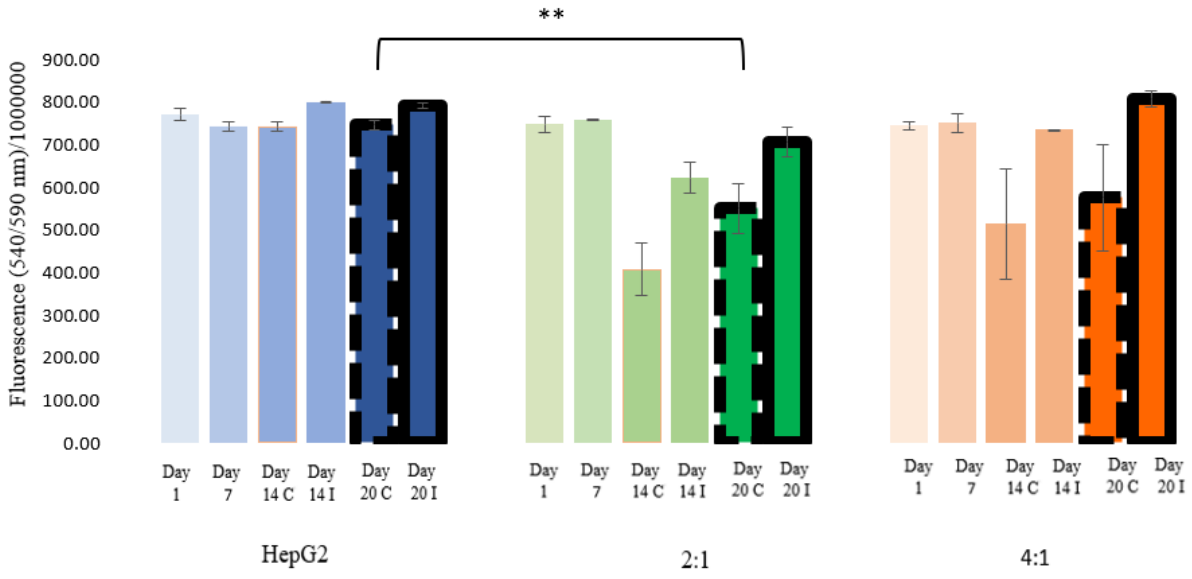

Figure 31. Average Celltiter-Blue fluorescence values/1000000 on days 1,7,14 (I&C) and 20 (I&C) for HepG2, 2:1 coculture ratio and 4:1 coculture ratio. n=3, **indicates p> 0.01

A fourth print session was carried out for the purpose of validating Celltiter blue results. The constructs were cultured for 14 days and not induced with TGF-β. Only effect of coculture ratios was investigated. (Figure 32)

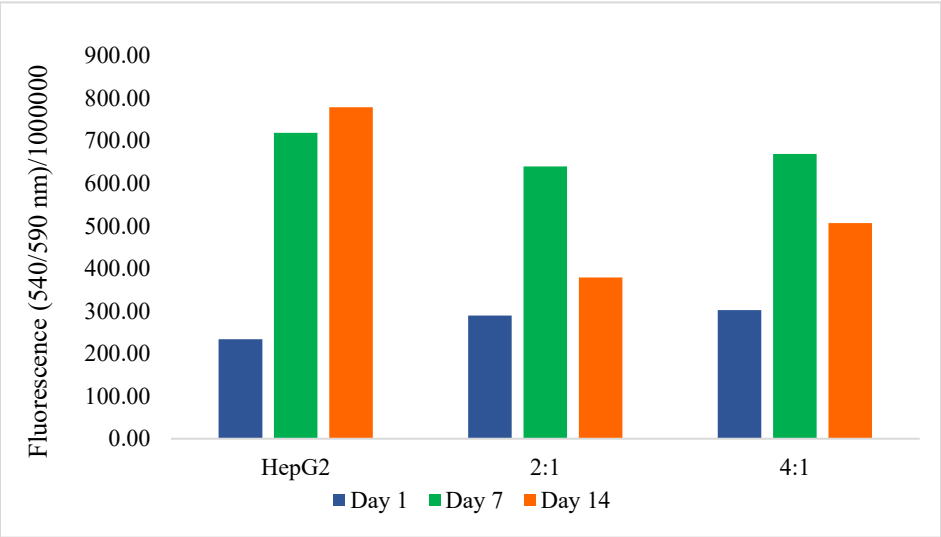

Figure 32. Celltiter-Blue fluorescence results for experiment 4

As seen from figures 31, at day 20 the 2:1 condition that contained the highest number of LX-2 cells was significantly less viable compared to the HepG2 condition that contained no LX-2 cells (two-way ANOVA, p-value=0.008). This demonstrates that an increase in LX-2 number negatively affects overall viability. Results from the extra print validate this. It can be seen from figure 32 that the greatest viability was exhibited in the HepG2 condition while the 2:1 condition exhibited the lowest viability. This is in agreement with what has already been demonstrated in the Live/Dead results. Also, figure 31 shows that the viability at days 1 and 7 was high with no observed difference in all three conditions. At day 14, the viability dropped for both coculture ratios but remained high for the HepG2 control. One explanation for this could be that over the course of 14 days, LX-2 cells had proliferated to reach a high enough number to negatively affect overall viability. This further supports the theory that an increase in LX-2 numbers influences overall cell viability causing it to decrease. We can also see that the viability for the induced group is higher than the control group especially in the cocultures (2:1 and 4:1). This is expected as the growth factor TGF-β causes cell proliferation in LX-2 cells [35].

Figure 32 does not show a gradual increase in HepG2 numbers over the course of 20 days as was expected. This could be because Celltiter-Blue® was saturated meaning that not enough Celltiter blue was added to reflect the increased cell number in later days. Therefore, the obtained numbers may not be not be a realistic representation of the actual HepG2 numbers in the later days of the experiment. Perhaps further optimization is required by using a higher quantity of Celltiter-Blue® or a shorter incubation time.

5.2. Cytotoxicity

Lactate dehydrogenase (LDH) Cytotoxicity Assay

Medium samples of were collected in triplicates on days 1, 7, 12, 16 and 20 for each of the three replicate experiments to determine cell cytoxicity non-invasively. Average LDH levels can be seen in Figure 33. (detailed data in Appendix 9.2.3.)

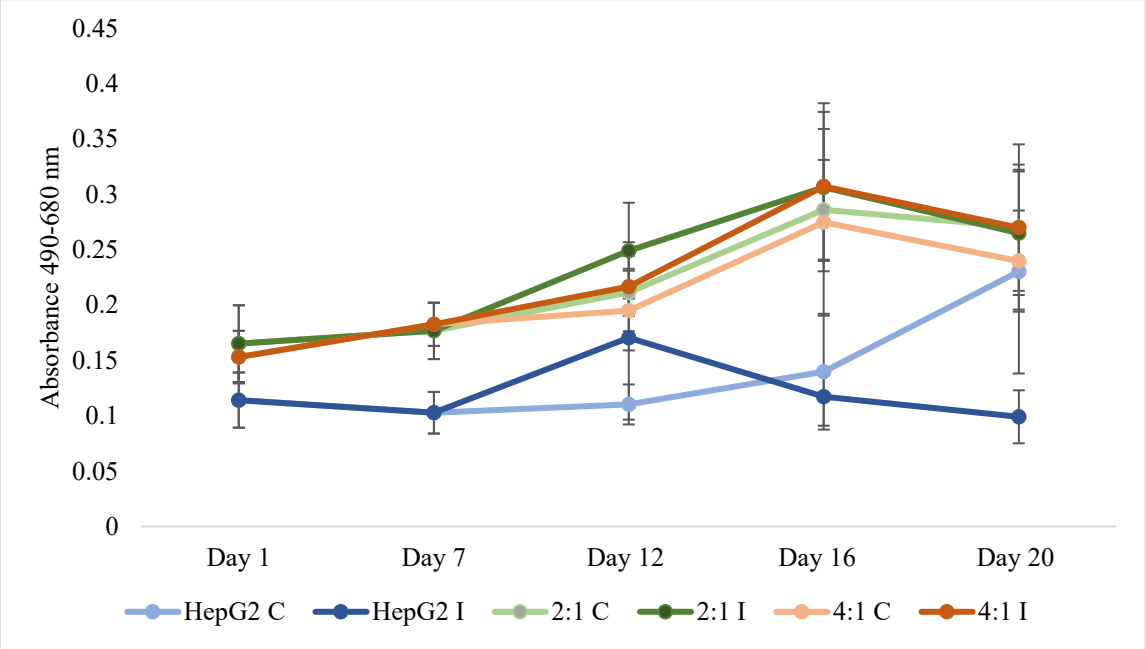

Figure 33. Average absorbance values (490-680 nm) depicting LDH levels on days 1,7,12 (I&C),16(I&C) and 20 (I&C) for HepG2, 2:1 coculture ratio and 4:1 coculture ratio. n=3, *indicates p> 0.05

LDH levels were consistently higher for cocultures conditions particularly, on days 16 and 20 compared to HepG2 monoculture conditions. On day 16 there was a significant difference (two-way ANOVA, p-value=0.02) between the 2:1 and the HepG2 groups. This further supports the theory that cell death occurs to a much greater extent in the 2:1 condition with the highest number of LX-2s compared with HepG2 condition that has no LX-2s.

On day 20 the LDH levels for HepG2(C) are much higher compared to the HepG2 (I) (fig.33). Suggesting that the induction with TGF-β has influenced the HepG2 cellular metabolism. However, no significant difference between the induced and control HepG2 groups was observed.

Results from the LDH cytotoxicity assay mirror the viability results from both the Live/Dead and Celltiter blue experiments. All three assays suggest that for some reason an increase in LX-2 cell number causes a decrease in overall cellular viability. One possible explanation for this is that LX-2 cells produce ECM proteins particularly when they are activated into myofibroblasts. The

accumulation of ECM could displace the HepG2 cells, disrupt their function and eventually cause hepatocyte cell death. It is well known that accumulation of ECM in liver fibrosis leads to disruption of hepatocyte function due to the change in liver architecture and thus cell-matrix interaction which leads to an increase in hepatocyte cell death [8] [14] [36] [78]. Research by *Norona et al.* showed that an increase in LDH levels corelated with a decrease in albumin production which is indicative of hepatocellular death. *Norona et al.* also demonstrated that collagen deposition in bioprinted fibrotic liver tissue models corelated with hepatocellular damage [28].

It can be seen that using the LDH cytotoxicity assay in conjunction with a viability assay such as Celltiter blue is very useful as it can provide valuable information that when in corroboration with the viability result gives more credibility and reliability to overall results and end conclusions.

5.3. Protein production

5.3.1. Bicinchoninic acid (BCA) protein assay on constructs

Construct samples were collected in triplicates on days 7, 12,16 and 20 for each of the three replicate experiments for measuring total protein production. Average protein concentrations can be seen in Figure 34. (detailed data in Appendix 9.2.4.1.)

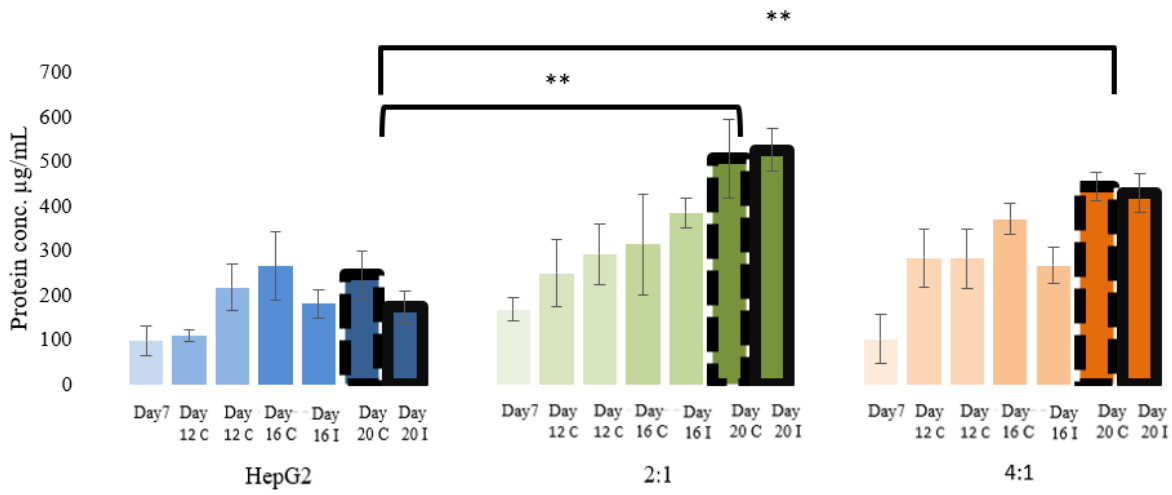

Figure 34. Average protein concentration (µg/mL) on days 8,12 (I&C),16(I&C) and 20 (I&C) for HepG2, 2:1 coculture ratio and 4:1 coculture ratio. n=3, **indicates p> 0.01

Protein concentrations were found to be higher in the coculture conditions particularly in the 2:1 condition compared to the HepG2 control condition (Two-way ANOVA, p-value=0.002 for the 2:1 ratio and p-value= 0.001 for the 4:1 ratio). As stated earlier, this can be a possible explanation to the decrease in viability and increase in cytotoxicity that was found in the 2:1 condition i.e. where LX-2 numbers are the highest. A similar effect was observed by *Norona et al.* who found that the increased production of extracellular proteins inside the bioprinted fibrotic liver tissue constructs negatively influenced hepatocellular health and viability [28]

Although there was a clear difference between the two coculture ratios, there did not seem to be a significant difference in protein deposition between the group that was induced with TGF-β versus the control group. This was unexpected as addition of the growth factor TGF-β was intended to induce fibrosis in the structure and thus increase collagen production by LX-2 cells. The fact that there did not seem to be a difference in protein production, viability or cytotoxicity between the group induced with TGF-β and the control group suggests that the concentration of TGF-β added was insufficient or that a different pro-fibrotic compound is needed to activate the LX-2 cells which would trigger the rest of the cascade of events that would lead to fibrosis which is characterized by accumulation of collagen and hepatocellular cell death.

Although the BCA protein assay did seem to give informative quantitative data, it does have several drawbacks. First, it was unable give any qualitative data on the types of proteins measured inside the constructs. This was limiting as it was collagen in particular that was relevant for this project and not overall protein deposition. Not being able to identify the proteins present prevented us from distinguishing between the protein deposited by the cells and the protein present in the bioink to begin with. However, this was not a huge limitation for this particular project. As previously mentioned, we aimed to identify a trend in the increase in protein deposition over time in different conditions. In other experiments that require the determination of the exact amount of protein deposited inside a construct, however, this assay may not be as useful as the protein content of the bioink will interfere with the results.

Another difficulty faced when implementing this assay is the need to lyse the constructs. Lysing the bioprinted constructs resulted in a nonhomogeneous solution that contained small differently sized particles of bioink. Although sonication of the construct did alleviate this problem there were still visible particles in the solution. If these particles end up in the sample wells, they cause inaccurately high readings. More optimization is maybe required to lyse the constructs more efficiently. Perhaps longer incubation times with PBS (-/-) or a longer sonication is required.

5.3.2. Bicinchoninic acid (BCA) protein assay on spent medium

Optimization attempts had indicated that the BCA protein assay would not be useful in detecting the amount of proteins expressed by the cells into the spent medium. But it was noticed in the optimization attempts that fresh medium samples almost always contained higher protein concentrations compared to spent medium samples. This is probably due to cells utilizing proteins in the medium. Therefore, BCA protein assay was used on the collected medium samples to examine if a trend in protein concentration could be observed i.e. less protein content in samples collected from later days in the experiments when cell number would be higher. If more cells in the constructs lead to more protein being used up and thus less protein content detected in spent medium, then this assay could be used nondestructively to detect proliferation. However, results seemed random and inconsistent. This may partly be due to the fact that fresh medium protein concentration is not consistent to begin with. Batch and lot variations in FBS for example could very likely lead to protein concentration variations. Therefore, The BCA protein assay cannot be used on spent medium to give any useful information.

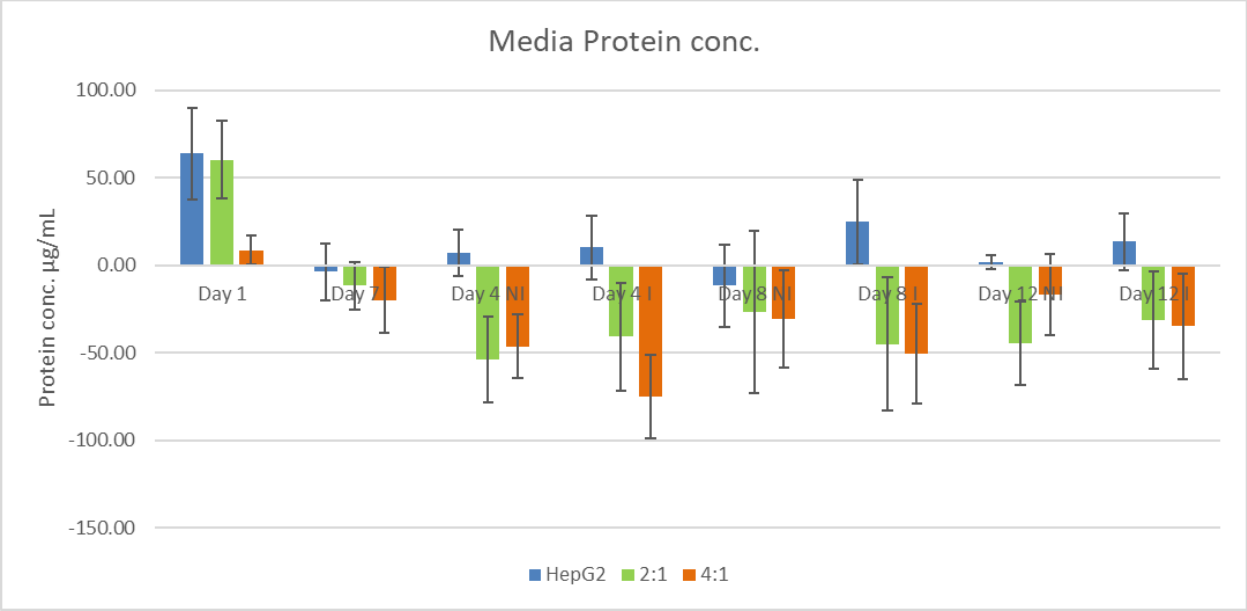

Figure 39. Average media protein concentrations for three replicate experiments

5.4. Morphology

Actin/NucBlue staining

Samples were transferred to a 96 well plate and fixed on days 7, 18 and 20 in triplicates to perform staining. Figure 40 is a summary of the representative images for day 20 (individual images are in Appendix 9.4.5)

Clusters could be seen forming in all 6 conditions but more so in the 2:1 condition. At day 20, 2:1 clusters seemed very compact and tightly packed compared to the 4:1 clusters that were looser and contained more separated cells (this can be seen more clearly in figure 41). This is probably due to the fact that the 2:1 condition has more LX-2 cells compared to the 4:1 condition. Activated LX-2 cells are myofibroblasts that stretch out and proliferate quickly [36]. This could therefore lead to the formation of denser clusters.

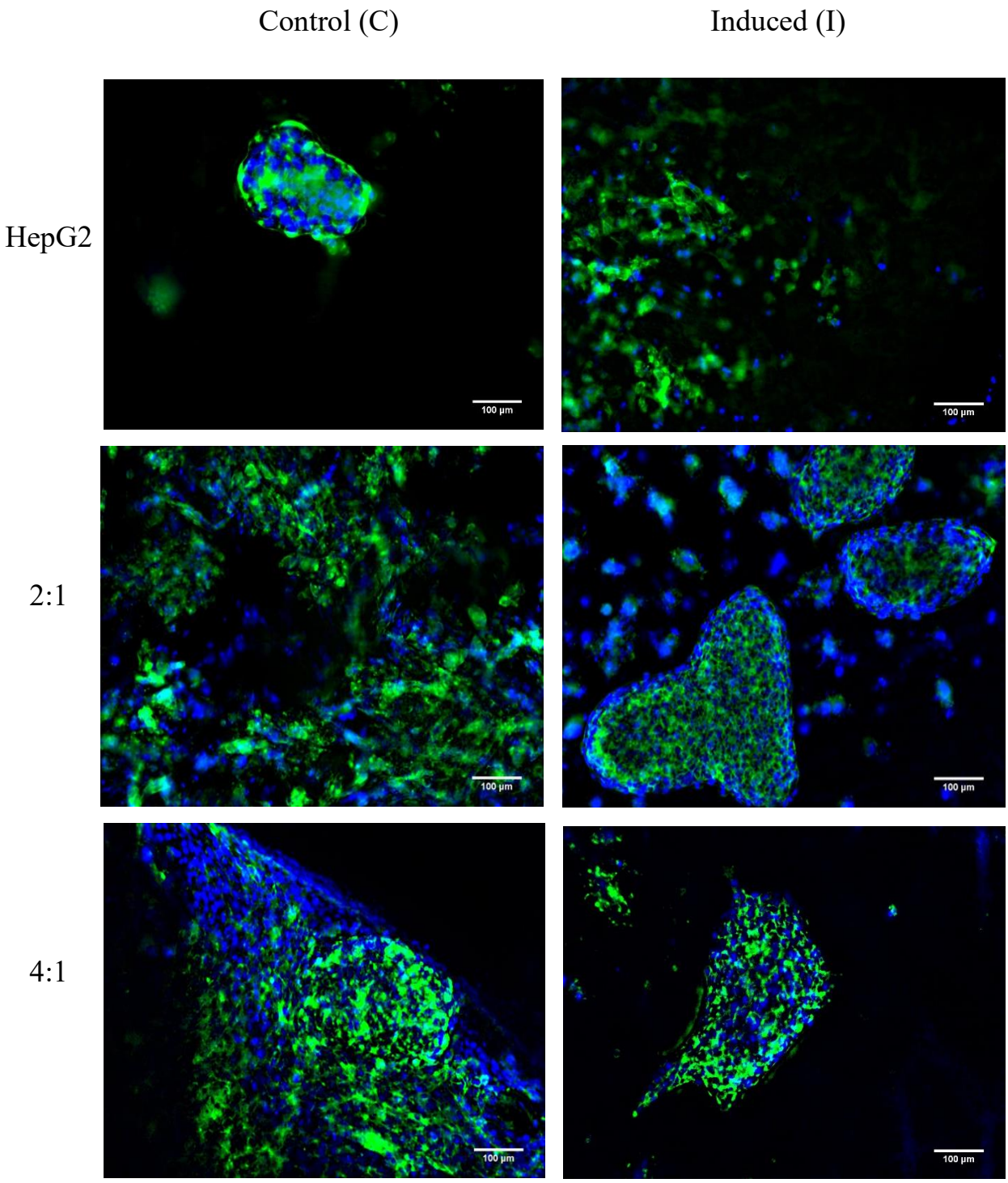

Figure 40. HepG2, 2:1 and 4:1 Actin/NucBlue stained constructs on day 20. Images were taken at 10x magnification.

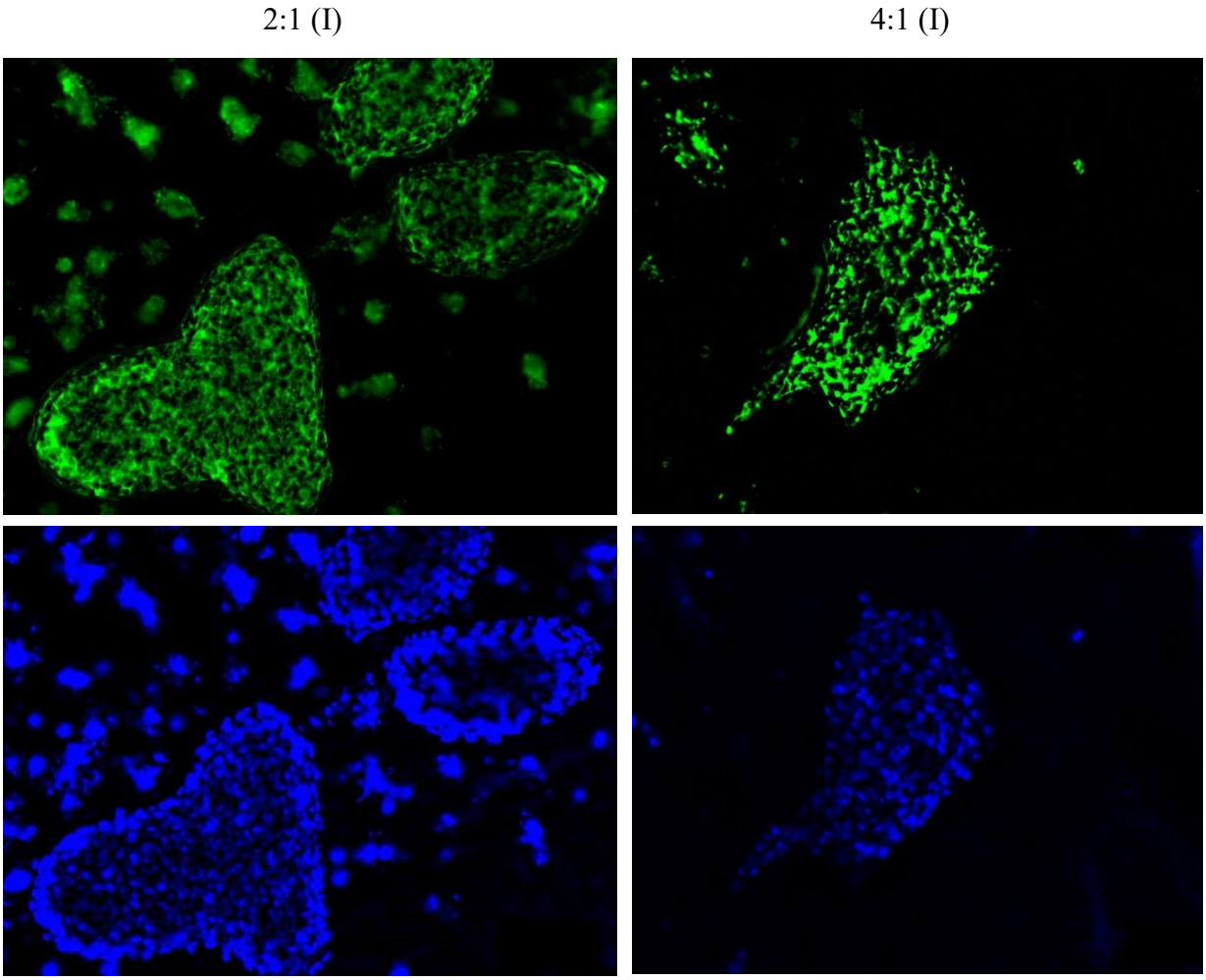

Figure 41. 4:1 (I) and 2:1(I) Actin (green) and NucBlue (blue) stained images on day 20.

6. Conclusions

The aim of this project was to investigate the effect of the growth factor TGF-β on 3D bioprinted liver tissue models to produce 3D fibrotic liver models. Two different coculture ratios of hepatocytes and hepatic stellate cells were investigated. Different assays that can be used to assess the produced fibrotic liver model were evaluated and optimized.

It was possible to adapt Celltiter-Blue, LDH cytotoxicity assay and NucBlue/ActinGreen staining to be used on 3D bioprinted structures with minor modification. However, adaptation of the BCA assay required lysis of the bioprinted constructs which presented a challenge. The developed construct lysis process can perhaps be further improved. Nevertheless, the BCA protein assay was able to provide informative, quantitative data when used to investigate protein deposition inside

the bioprinted structure. It was not possible however, to use the BCA protein assay nondestructively on spent medium for investigating cellular protein assessment.

The results indicate that the 2:1 HepG2 to LX-2 coculture ratio shows greater potential in simulating liver fibrosis compared to the 4:1 HepG2 to LX-2 ratio. The viability results from both Live/Dead analysis and Celltiter-Blue® showed that the lowest cell viability was exhibited in the 2:1 coculture ratio. This was further corroborated by the LDH cytotoxicity assay that showed the greatest increase in cytotoxicity to be in the 2:1 coculture ratio. The BCA protein analysis results that show that the greatest amount of protein deposition was in the 2:1 ratio. Actin/NucBlue staining showed that the morphology of the 2:1 clusters was denser and more compact compared to the other conditions. As the 2:1 condition contained the greatest number of LX-2 cells, it may be assumed that the compact morphology of the clusters is due to proliferation of the LX-2 cells. This seems to be consistent with what is agreed upon in the literature which is that ECM protein production (scar tissue formation) which is the most distinctive features of liver fibrosis disrupts the hepatic architecture leading to hepatocellular damage and death [8] [14] [36] [78].

However, the assay results cannot decisively conclude this. The viability assays assessed overall viability for both the HepG2 and LX-2 cells. Therefore, it cannot be definitely stated that HepG2 viability in particular was negatively affected. The BCA protein analysis results showed elevated total protein concentration deposited inside the constructs in the 2:1 condition without giving an indication of the quality of the proteins. Liver fibrosis is characterized by the accumulation of collagen (I &III) in particular. As the BCA protein assay was unable to confirm this, one cannot conclude that fibrosis did indeed occur.

In addition, there did not seem to be a significant difference between the group in which fibrosis was induced (I) compared to the control group (C) within each condition in any of the cell conditions investigated. This indicates that fibrosis may have not been induced despite the addition of TGF-β.

7. Future studies

Further investigation on fibrosis induction is needed to determine if fibrosis was indeed induced by TGF- β. The optimal concentration of TGF-β needed to induce fibrosis also needs to be investigated. 10 ng/ml has been used in the literature to induce fibrosis in 3D bioprinted structures [28]. It might also be useful to explore other compounds for fibrosis induction. Examples used repeatedly in the literature include methotrexate, thioacetamide [41] [43].

Adjusting the composition of the bioink to make it more customized to liver cells by incorporation of additional liver specific ECM components might be beneficial. Changing the printing pattern might also provide better results. Mixing the two cell types in separate bioinks and printing the LX-2 cells as a border with the HepG2 cells in the center as was done by *Norona et al.* and *Nguyen et al.* might provide a compartmentalized, more native like structure to the bioprinted constructs as opposed to mixing both cell types in the same bioink and printing them as discs [28] [43]. This way, monitoring the migration of LX-2 cells into the HepG2 cell compartment, through fluorescently labeling the cells for example, could be used as an indication of fibrosis.

Leit et al. used hepatocyte specific medium in culturing control hepatocyte, stellate cell cocultures (that were not meant to be induced) to ensure that the HSCs remain quiescent [13]. *Mazzocchi et al.* used well plates coated with polydimethylsiloxane (PDMS) to prevent cell outgrowth out of the bioprinted constructs onto the plastic substrate [53]. Implementing such changes might produce better results.

Assays that can analyze and characterize fibrosis specific properties should be used. Albumin production to monitor hepatocyte functionality and collagen deposition by stellate cells are important to measure. α-smooth muscle actin is produced by stellate cells when they are activated and is therefore frequently used as an activation marker. Also, as inflammation is strongly linked to fibrosis, cytokines could be measured in spent medium to assess the progression of fibrosis. ELISA, qPCR and immunohistochemistry among other assays have been used in the literature to monitor the previously mentioned properties [28] [13] [39] [41].

If the above-mentioned changes produce promising results then more cell types could be included to produce a more representative model. Examples in the literature of cell types used in addition to hepatocytes and stellate cells to produce liver tissue models include Kupffer cells and endothelial cells [28] [41] [43].

8. Reference list

1. Gray's Anatomy: A classic medical textbook online | Mo Costandi [Internet]. [cited 2018 Sep 25]. Available from: https://neurophilosophy.wordpress.com/2006/11/11/grays-anatomy-a-classic-medical-textbook-online/
2. Liver: Anatomy and Functions | Johns Hopkins Medicine Health Library [Internet]. [cited 2018 Sep 25]. Available from: https://www.hopkinsmedicine.org/healthlibrary/conditions/liver_biliary_and_pancreatic_disorders/liver_anatomy_and_functions_85,P00676
3. Liver – Anatomy and Function of the Human Liver [Internet]. InnerBody. [cited 2018 Sep 25]. Available from: http://www.innerbody.com/image_digeov/card10-new2.html
4. Mitra V, Metcalf J. Metabolic functions of the liver. Anaesthesia & Intensive Care Medicine. 2012 Feb 1;13(2):54–5.
5. Metabolic Functions of the Liver [Internet]. [cited 2018 Sep 28]. Available from: http://www.vivo.colostate.edu/hbooks/pathphys/digestion/liver/metabolic.html
6. How the Liver Detoxifies | Life Extension [Internet]. [cited 2018 Oct 2]. Available from: https://www.lifeextension.com/Protocols/Gastrointestinal/Liver-Degenerative-Disease/Page-04
7. Gao B. Basic liver immunology. Cell Mol Immunol. 2016 May;13(3):265–6.
8. van Grunsven LA. 3D in vitro models of liver fibrosis. Adv Drug Deliv Rev. 2017 01;121:133–46.
9. Mazza G, Al-Akkad W, Rombouts K. Engineering in vitro models of hepatofibrogenesis. Adv Drug Deliv Rev. 2017 01;121:147–57.
10. What is liver fibrosis? [Internet]. [cited 2019 Feb 2]. Available from: https://www.healthcare.siemens.com/clinical-specialities/liver-disease/what-is-liver-fibrosis
11. Drew L. Drug development: Sprint finish. Nature. 2017 Nov 22;551: S86.
12. NASH prevalence: Key figures | The NASH Education Program™ [Internet]. The NASH Education Program. [cited 2018 Dec 8].
13. Leite SB, Roosens T, El Taghdouini A, Mannaerts I, Smout AJ, Najimi M, et al. Novel human hepatic organoid model enables testing of drug-induced liver fibrosis in vitro. Biomaterials. 2016 Feb;78:1–10
14. Bataller R, Brenner DA. Liver fibrosis. J Clin Invest. 2005 Feb 1;115(2):209–18.
15. Choudhury D, Tun HW, Wang T, Naing MW. Organ-Derived Decellularized Extracellular Matrix: A Game Changer for Bioink Manufacturing? Trends Biotechnol. 2018 Aug;36(8):787–805.
16. Williams D, Thayer P, Martinez H, Gatenholm E, Khademhosseini A. A perspective on the physical, mechanical and biological specifications of bioinks and the development of functional tissues in 3D bioprinting. Bioprinting. 2018 Mar 1; 9:19–36.
17. Rimann M, Bono E, Annaheim H, Bleisch M, Graf-Hausner U. Standardized 3D Bioprinting of Soft Tissue Models with Human Primary Cells. J Lab Autom. 2016 Aug 1;21(4):496–509
18. The liver - Canadian Cancer Society [Internet]. www.cancer.ca. [cited 2018 Sep 25]. Available from: http://www.cancer.ca/en/cancer-information/cancer-type/liver/liver-cancer/the-liver/?region=on

19. Jones J. Couinaud classification of hepatic segments | Radiology Reference Article | Radiop aedia.org [Internet]. Radiopaedia. [cited 2018 Sep 25]. Available from: https://radiopaedia.org/articles/couinaud-classification-of-hepatic-segments
20. Lobules of liver [Internet]. IMAIOS. [cited 2018 Sep 25].
21. File:2423 Microscopic Anatomy of Liver.jpg - Wikimedia Commons [Internet]. [cited 2019 Jan 23]. Available from: https://www.imaios.com/en/e-Anatomy/Anatomical-Parts/Lobules-of-liver
22. Anatomy and physiology of the liver [Internet]. [cited 2018 Sep 25]. Available from: http://www.rnceus.com/ld/ldanat.html#Link790739Context
23. Zhou Z, Xu M-J, Gao B. Hepatocytes: a key cell type for innate immunity. Cellular & Molecular Immunology. 2016 May;13(3):301–15.
24. Hepatocytes: Liver Epithelial Cells - LabCE.com, Laboratory Continuing Education [Internet]. [cited 2018 Nov 7]. Available from: https://www.labce.com/spg665068_hepatocytes_liver_epithelial_cells.aspx
25. Paxton S, Peckham M, Adele K. The Leeds Histology Guide. 2003 [cited 2018 Nov 7]. Available from: https://www.histology.leeds.ac.uk/digestive/liver_hepatocyte.php
26. Soldatow VY, LeCluyse EL, Griffith LG, Rusyn I. In vitro models for liver toxicity testing. Toxicol Res (Camb). 2013 Jan 1;2(1):23–39.
27. Guguen-Guillouzo C, Guillouzo A. General review on in vitro hepatocyte models and their applications. Methods Mol Biol. 2010;640:1–40.
28. Norona L, Nguyen D, Gerber D, C. Presnell S, L. LeCluyse E. Modeling compound-induced fibrogenesis in vitro using three-dimensional bioprinted human liver tissues. Toxicological Sciences. 2016 Sep 7;154:kfw169
29. Weiskirchen R, Tacke F. Cellular and molecular functions of hepatic stellate cells in inflammatory responses and liver immunology. Hepatobiliary Surg Nutr. 2014 Dec;3(6):344–63.
30. Senoo H. Structure and function of hepatic stellate cells. Med Electron Microsc. 2004 Mar;37(1):3–15.
31. Hepatic Stellate Cells | Yin Lab [Internet]. [cited 2018 Nov 7]. Available from: https://www.cincinnatichildrens.org/research/divisions/g/gastroenterology/labs/yin/stellate
32. Hughes P, Marshall D, Reid Y, Parkes H, Gelber C. The costs of using unauthenticated, over-passaged cell lines: how much more data do we need? BioTechniques. 2007 Nov;43(5):575, 577–8, 581-582 passim.
33. Kaur G, Dufour JM. Cell lines. Spermatogenesis. 2012 Jan 1;2(1):1–5.
34. Hepatic stellate cell. In: Wikipedia [Internet]. 2019 [cited 2019 Apr 7]. Available from: https://en.wikipedia.org/w/index.php?title=Hepatic_stellate_cell&oldid=879505441
35. Iredale JP. Models of liver fibrosis: exploring the dynamic nature of inflammation and repair in a solid organ. J Clin Invest. 2007 Mar;117(3):539–48.
36. Zhou W-C, Zhang Q-B, Qiao L. Pathogenesis of liver cirrhosis. World J Gastroenterol. 2014 Jun 21;20(23):7312–24.
37. Brunt EM. Nonalcoholic steatohepatitis. Semin Liver Dis. 2004 Feb;24(1):3–20.
38. Sasseville VG, Lane JH, Kadambi VJ, Bouchard P, Lee FW, Balani SK, et al. Testing paradigm for prediction of development-limiting barriers and human drug toxicity. Chemico-Biological Interactions. 2004 Nov 1;150(1):9–25.

39. Barbero-Becerra VJ, Giraudi PJ, Chávez-Tapia NC, Uribe M, Tiribelli C, Rosso N. The interplay between hepatic stellate cells and hepatocytes in an in vitro model of NASH. Toxicology in Vitro. 2015 Oct 1;29(7):1753–8.
40. Giraudi PJ, Barbero Becerra VJ, Marin V, Chavez-Tapia NC, Tiribelli C, Rosso N. The importance of the interaction between hepatocyte and hepatic stellate cells in fibrogenesis induced by fatty accumulation. Experimental and Molecular Pathology. 2015 Feb 1;98(1):85–92.
41. Prestigiacomo V, Weston A, Messner S, Lampart F, Suter-Dick L. Pro-fibrotic compounds induce stellate cell activation, ECM-remodelling and Nrf2 activation in a human 3D-multicellular model of liver fibrosis. PLoS ONE. 2017;12(6):e0179995. 2018 Dec 9];12(6).
42. Woodrow KA, Wood MJ, Saucier-Sawyer JK, Solbrig C, Saltzman WM. Biodegradable meshes printed with extracellular matrix proteins support micropatterned hepatocyte cultures. Tissue Eng Part A. 2009 May;15(5):1169–79.
43. Nguyen DG, Funk J, Robbins JB, Crogan-Grundy C, Presnell SC, Singer T, et al. Bioprinted 3D Primary Liver Tissues Allow Assessment of Organ-Level Response to Clinical Drug Induced Toxicity In Vitro. PLoS ONE. 2016;11(7):e0158674.
44. Liaw C-Y, Ji S, Guvendiren M. Engineering 3D Hydrogels for Personalized In Vitro Human Tissue Models. Advanced Healthcare Materials. 2018;7(4):1701165.
45. Grix T, Ruppelt A, Thomas A, Amler A-K, Noichl BP, Lauster R, et al. Bioprinting Perfusion-Enabled Liver Equivalents for Advanced Organ-on-a-Chip Applications. Genes (Basel). 2018 Mar 22;9(4).
46. Kang K, Kim Y, Jeon H, Lee SB, Kim JS, Park SA, et al. Three-Dimensional Bioprinting of Hepatic Structures with Directly Converted Hepatocyte-Like Cells. Tissue Eng Part A. 2018;24(7–8):576–83.
47. Pati F, Gantelius J, Svahn HA. 3D Bioprinting of Tissue/Organ Models. Angewandte Chemie International Edition. 2016;55(15):4650–65.
48. Thiele GM, Duryee MJ, Thiele GE, Tuma DJ, Klassen LW. Review: Precision Cut Liver Slices for the Evaluation of Fatty Liver and Fibrosis. Curr Mol Pharmacol. 2017;10(3):249
49. Westra IM, Mutsaers HAM, Luangmonkong T, Hadi M, Oosterhuis D, de Jong KP, et al. Human precision-cut liver slices as a model to test antifibrotic drugs in the early onset of liver fibrosis. Toxicol In Vitro. 2016 Sep; 35:77–85.
50. Riccalton-Banks L, Liew C, Bhandari R, Fry J, Shakesheff K. Long-term culture of functional liver tissue: three-dimensional coculture of primary hepatocytes and stellate cells. Tissue Eng. 2003 Jun;9(3):401–10.
51. Bell CC, Hendriks DFG, Moro SML, Ellis E, Walsh J, Renblom A, et al. Characterization of primary human hepatocyte spheroids as a model system for drug-induced liver injury, liver function and disease. Sci Rep. 2016 04;6:25187.
52. Baze A, Parmentier C, Hendriks DFG, Hurrell T, Heyd B, Bachellier P, et al. Three-Dimensional Spheroid Primary Human Hepatocytes in Monoculture and Coculture with Nonparenchymal Cells. Tissue Engineering Part C: Methods. 2018 Aug 13;24(9):534–45.
53. Mazzocchi A, Devarasetty M, Huntwork R, Soker S, Skardal A. Optimization of collagen type I-hyaluronan hybrid bioink for 3D bioprinted liver microenvironments. Biofabrication. 2018 Oct 30;11(1):015003.

54. Bishop ES, Mostafa S, Pakvasa M, Luu HH, Lee MJ, Wolf JM, et al. 3-D bioprinting technologies in tissue engineering and regenerative medicine: Current and future trends. Genes & Diseases. 2017 Dec 1;4(4):185–95.
55. Li J, Chen M, Fan X, Zhou H. Recent advances in bioprinting techniques: approaches, applications and future prospects. J Transl Med. 2016 20;14:271.
56. Adepu S, Dhiman N, Laha A, Sharma CS, Ramakrishna S, Khandelwal M. Three-dimensional bioprinting for bone tissue regeneration. Current Opinion in Biomedical Engineering. 2017 Jun 1;2:22–8.
57. Starly B, Shirwaiker R. Chapter 3 - 3D Bioprinting Techniques. In: Zhang LG, Fisher JP, Leong KW, editors. 3D Bioprinting and Nanotechnology in Tissue Engineering and Regenerative Medicine [Internet]. Academic Press; 2015 [cited 2019 Jan 24].
58. Gopinathan J, Noh I. Recent trends in bioinks for 3D printing. Biomaterials Research. 2018 Apr 6;22(1):11.
59. Gungor-Ozkerim PS, Inci I, Zhang YS, Khademhosseini A, Dokmeci MR. Bioinks for 3D bioprinting: an overview. Biomater Sci. 2018 May 1;6(5):915–46.
60. Biolaminin 111 LN [Internet]. BioLamina. [cited 2019 Mar 30]. Available from: http://www.biolamina.com/laminin-ln-111
61. Biolaminin 121 LN [Internet]. BioLamina. [cited 2019 Mar 30]. Available from: http://www.biolamina.com/biolaminin-121
62. Narayanan LK, Thompson TL, Shirwaiker RA, Starly B. Label free process monitoring of 3D bioprinted engineered constructs via dielectric impedance spectroscopy. Biofabrication. 2018 28;10(3):035012.
63. Wang MO, Vorwald CE, Dreher ML, Mott EJ, Cheng M-H, Cinar A, et al. Evaluating 3D-Printed Biomaterials as Scaffolds for Vascularized Bone Tissue Engineering. Advanced Materials. 2015;27(1):138–44.
64. Quinn KP, Bellas E, Fourligas N, Lee K, Kaplan DL, Georgakoudi I. Characterization of metabolic changes associated with the functional development of 3D engineered tissues by non-invasive, dynamic measurement of individual cell redox ratios. Biomaterials. 2012 Jul 1;33(21):5341–8.
65. Ng KW, Leong DTW, Hutmacher DW. The challenge to measure cell proliferation in two and three dimensions. Tissue Eng. 2005 Feb;11(1–2):182–91.
66. Simmons AD, Williams C, Degoix A, Sikavitsas VI. Sensing metabolites for the monitoring of tissue engineered construct cellularity in perfusion bioreactors. Biosensors and Bioelectronics. 2017 Apr 15;90:443–9.
67. Correa D, Somoza RA, Caplan AI. Nondestructive/Noninvasive Imaging Evaluation of Cellular Differentiation Progression During In Vitro Mesenchymal Stem Cell-Derived Chondrogenesis. Tissue Eng Part A. 2018;24(7–8):662–71.
68. Blum JS, Temenoff JS, Park H, Jansen JA, Mikos AG, Barry MA. Development and characterization of enhanced green fluorescent protein and luciferase expressing cell line for non-destructive evaluation of tissue engineering constructs. Biomaterials. 2004 Dec;25(27):5809–19.
69. CellTiter-Blue® Cell Viability Assay [Internet]. [cited 2018 Sep 11]. Available from: https://worldwide.promega.com/products/cell-health-assays/cell-viability-and-cytotoxicity-assays/celltiter_blue-cell-viability-assay/

70. Calcein AM Cell Viability Assay Kit [Internet]. Biotium. [cited 2018 Sep 11]. Available from: https://biotium.com/product/calcein-am-cell-viability-assay-kit/
71. MLive/Dead Cell Double Staining Kit 04511 [Internet]. Sigma-Aldrich. [cited 2018 Sep 6]. Available from: https://www.sigmaaldrich.com/catalog/product/sigma/04511
72. Pierce LDH Cytotoxicity Assay Kit - Thermo Fisher Scientific [Internet]. [cited 2018 Sep 6]. Available from: https://www.thermofisher.com/order/catalog/product/88953
73. Pierce BCA Protein Assay Kit - Thermo Fisher Scientific [Internet]. [cited 2018 Sep 6]. Available from: https://www.thermofisher.com/order/catalog/product/23225
74. ActinGreen 488 ReadyProbes Reagent - Thermo Fisher Scientific [Internet]. [cited 2019 Jan 26]. Available from: https://www.thermofisher.com/order/catalog/product/R37110NucBlue Live ReadyProbes Reagent - Thermo Fisher Scientific [Internet]. [cited 2019 Jan 26].
75. NucBlue Live ReadyProbes Reagent - Thermo Fisher Scientific [Internet]. [cited 2019 Jan 26]. Available from: https://www.thermofisher.com/order/catalog/product/R37605
76. Masuma R, Kashima S, Kurasaki M, Okuno T. Effects of UV wavelength on cell damages caused by UV irradiation in PC12 cells. Journal of Photochemistry and Photobiology B: Biology. 2013 Aug 5;125:202–8.
77. Bardsley K, et al. Current State-of-the-Art 3D Tissue Models and Their Compatibility with Live Cell Imaging. Adv Exp Med Biol. 2017;1035:3-18.
78. Campana L, Iredale JP. Extracellular Matrix Metabolism and Fibrotic Disease. Curr Pathobiol Rep. 2014 Dec 1;2(4):217–24

9. Appendix

9.1. Protocols

9.1.1. liver tissue model 3D bioprinting protocol

Table 5. Liver tissue model 3D bioprinting protocol using 10 M HepG2 and LX2 cells/ml of GelXA LN 111/121

	Step	Material	Description
1	Preparation of cell-laden bioink.	▪ HepG2 and LX2 cells ▪ Cell culture medium ▪ GelXA bioink ▪ 1 ml syringes with luer lock connections ▪ Female/Female luer lock adaptor	❖ Warm stock GelXA in a water bath or incubator to 37 °C (Always keep GelXA protected from light) ❖ Place GelXA cartridge in a sterile 50 ml Falcon tube and centrifuge at 1000 g for 5 minutes to remove any air bubbles. ❖ Obtain cell pellet with total cell count ❖ Determine the volume of the cell pellet using a pipette and adjust ❖ Calculate desired cell concentration per ml of GelXA Transfer appropriate cell suspension using a pipette to a sterile 1ml syringe. Adjust volume with additional medium to obtain 50µl (The volume of the cell suspension to be added to GelXA should not exceed 10% of the desired volume of cell-laden bioink.) ❖ Connect a female/female luer connector to a new 1ml syringe and transfer 450µl of the pre-warmed Gel-XA from the stock Gel-XA syringe ❖ Attach the bioink syringe to the syringe with cell suspension ❖ Mix by alternating dispensing of one syringe into the other
2	Set up of the Bioprinter	▪ BIO X	❖ Pneumatic-driven micro-extrusion. ❖ Printing pressure: 10-15 kPa. ❖ Printing speed: 15mm/s. ❖ Infill: disable ❖ Printhead temperature: Room temperature (22°C). ❖ Print bed temperature: Room temperature (22°C).
3	Printing	▪ Print file ▪ UV shielding cartridges, 3CC ▪ Sterile Conical 22G Bioprinting nozzles. ▪ 48 well plate	❖ Transfer the cell-laden bioink back into a UV shielding cartridges, 3CC. ❖ Load the cartridge into the printhead holder and calibrate the printhead. Start bioprinting. ❖ Print the constructs

4	Crosslinking	▪ $CaCl_2$ Crosslinking Solution ▪ Cell culture medium	❖ Submerge the cell-laden constructs in an ionic solution of 50mM CaCl2 for 1 minute. ❖ Remove crosslinking solution and add appropriate culture medium.
5	Incubation	Incubator	❖ Incubate the constructs in corresponding growth medium in standard culture conditions (37°C, 5% CO2 and 95% relative humidity). Use 100µl/well.

9.1.2. Live/Dead staining protocol

Table 6. Live/Dead staining protocol using Calcein AM and PI

	Step	Material	Description
1	Stock solution preparation	▪ Calcein AM ▪ DMSO ▪ PI ▪ HBSS +/+	❖ Dissolve 1 vial of 50 µg of Calcein AM in 50,3 µl DMSO ❖ Weigh up 2 mg of PI in an Eppendorf tube. ❖ Add 1 ml of HBSS+/+ to the tube with PI and gently mix. ❖ Store Calcein AM solution at -20 °C and PI solution at 4 °C
2	Pre-washing	▪ HBSS +/+	❖ Move constructs to be analyzed to a 96 well plate ❖ add HBSS+/+, wash for 15 min at 37 °C
3	Preparation of green staining solution	▪ 1,5 µl of Calcein AM stock solution ▪ 6 ml cell FBS free culture medium	❖ Place Calcein AM stock solution at RT to thaw. ❖ Pre-warm FBS free cell culture medium to 37 °C ❖ Add 1,5 µl Calcein AM (1mM) into the 6 ml of the pre-warmed cell culture medium in 15 ml Falcon tube
4	Staining	▪ Calcein AM green staining solution	❖ Remove HBSS+/+ from constructs and add enough green staining solution to cover the constructs ❖ Incubate the constructs in the incubator for 1 hour
5	Preparation of red staining solution	▪ 50 µl of PI stock solution ▪ 5 ml FBS free cell culture medium	❖ Pre-warm FBS free cell culture medium to 37 °C ❖ Add 50 µl of PI into 5 ml of the pre-warmed cell culture medium in 15 ml Falcon tube

6	Staining	▪ PI red staining solution	❖ Remove green staining solution and add enough red PI staining solution to cover constructs ❖ incubate for 5 min at RT.
7	Washing	▪ HBSS +/+	❖ Remove red PI staining solution and wash twice for 15 min in HBSS +/+ ❖ Keep in HBSS+/+ until imaging

9.1.3. Celltiter-Blue® protocol

Table 7. Protocol for Celltiter-Blue® viability assay on 3D bioprinted constructs

	Step	**Material**	**Description**
1	Reagent preparation	▪ Celltiter-Blue® reagent	❖ Thaw Celltiter-Blue® reagent and bring to RT. (Celltiter-Blue® reagent should be protected from light at all times)
2	Addition of reagent	▪ Thawed Celltiter-Blue® reagent ▪ Pre-warmed Cell culture medium ▪ Reservoir for reagent ▪ 96 well plate ▪ Plate reader	❖ Move constructs to be analyzed to 96 well plate ❖ Add 100 µl of pre-warmed cell culture medium to each sample well (if test compounds are to be added to constructs, the final volume of added compounds and medium should be 100 µl in each well.) ❖ Pour estimated amount of required Celltiter-Blue® reagent into a reservoir. ❖ Add 20µl of Celltiter-Blue® to each sample well ❖ Cover plate and shake for 30 seconds using the plate reader
3	Incubation	▪ Incubator	❖ Place the 96 well plate in the incubator and incubate overnight.
4	Reading	▪ Plate reader	❖ Shake plate for 30 seconds using a plate reader then record fluorescence at 560/590 nm

9.1.4. Lactate dehydrogenase (LDH) Cytotoxicity Analysis protocol

Table 8. Protocol for LDH cytotoxicity assay on spent medium

	Step	Material	Description
1	Reaction mixture preparation	▪ Substrate Mix vial ▪ 11.4ml ultrapure water ▪ Assay buffer vial (0.6 ml) ▪ 15 ml falcon tube	❖ Dissolve vial of substrate mix in 11.4 ml ultrapure water in 15 ml falcon tube. ❖ Thaw Assay buffer vial and bring to RT. (Assay buffer must be protected from light at all times). ❖ Combine Assay buffer (0.6ml) with 11.4 ml Substrate Mix to produce 12ml of Reaction Mixture. Note: Keep reaction mixture protected from light. Remaining reaction mixture can be stored at -20°C for 3-4 weeks with tolerance for 3 freeze/thaw cycles.
2	Addition of reaction mixture	▪ Reaction mixture ▪ 96 well plate ▪ Reservoir	❖ Transfer 50µl of each medium sample as well as fresh medium controls to a 96 well plate. ❖ Pour estimated amount of required reaction mixture into a reservoir. ❖ Using a multichannel pipet add 50µl of reaction mixture to each sample well.
3	Incubation	▪ Aluminum foil	❖ Cover plate with aluminum foil and incubate for 30 minutes at RT.
4	Adding stop solution	▪ Stop solution ▪ Reservoir	❖ Pour estimated required amount of stop solution into a reservoir ❖ Add 50µl of stop solution to each sample well Note: Break any bubbles in the wells by a syringe needle before reading
5	Reading	▪ Plate reader	❖ Read absorbance at 490 nm and 680nm. Note: Subtract the 680nm (background) absorbance values from the 490nm absorbance values to determine LDH activity

9.1.5. Bicinchoninic acid (BCA) protein concentration analysis protocol

Table 9. Protocol for BCA protein assay on 3D bioprinted constructs

	Step	Material	Description
1	Working reagent preparation	▪ BCA Reagent A ▪ BCA Reagent B	❖ Mix 50 parts BCA Reagent A with 1 part BCA Reagent B to prepare Working Reagent (WR)
2	Preparation of protein standards	▪ Ampule of Bovine serum albumin (BSA) ▪ 2.75 ml PBS ▪ 6 Eppendorf tubes	❖ Prepare series of protein standards by following the dilution scheme shown in table 10
3	Addition of PBS to constructs	▪ Eppendorf tubes ▪ PBS	❖ Move constructs to be analyzed to Eppendorf tubes. ❖ Add 200µl of PBS to each tube. ❖ Incubate constructs in PBS for 4 hours at RT.
4	Sonication	▪ Sonicator	❖ Sonicate Eppendorf tubes for 1 hour.
5	Lysing constructs	▪ Pipette	❖ Pipette the PBS in each Eppendorf tube up and down until the constructs disintegrate.
6	Plate reader preparation	▪ Plate reader	❖ Set plate reader to heat up to 60°C.
7	Addition of working reagent	▪ Working reagent ▪ 96 well plate	❖ Transfer 25µl of each construct sample solution and protein standard to a 96 well plate ❖ Add 200µl of WR to each well.
8	Incubation	▪ Plate reader	❖ Cover well plate and place in the pre heated incubator ❖ Shake plate for 30 seconds ❖ Incubate plate at 60°C for 30 Minutes in the plate reader
9	Cooling		❖ Take out the plate from the plate reader and allow to cool down to RT
10	Reading	▪ Plate reader	❖ Remove plate cover and place the plate back into the plate reader ❖ Measure absorbance at 580nm using the plate reader

Table 10. Dilution scheme for BCA protein assay (working range: 5-250 µg/ml)

Vial	Volume of Diluent (µL)	Volume and Source of BSA (µL)	Final BSA Concentration (µg/mL)
A	700	100 of Stock	250
B	400	400 of vial A dilution	125
C	450	300 of vial B dilution	50
D	400	400 of vial C dilution	25
E	400	100 of vial D dilution	5
F	400	0	0 = Blank

9.1.6. Actin/NucBlue staining protocol

Table 11. Protocol for Actin/NucBlue staining on 3D bioprinted constructs

	Title	Material	Description
1	Sample fixation	▪ 4% PFA ▪ 48 well plate	❖ Transfer constructs to be stained to a 48 well plate ❖ Add 500µl of 4% PFA or enough to cover constructs ❖ Incubate in RT overnight
2	Washing	▪ HBSS +/+	❖ Wash constructs with HBSS+/+ 3 times for 10 minutes at a time ❖ Keep constructs in HBSS+/+ at 4°C until staining
3	Preparation of Actin staining solution	▪ ActinGreen™ ▪ HBSS+/+ ▪ 15 ml falcon tube	❖ Add 1 drop of ActinGreen™ for each ml of HBSS+/+ (Keep actin solution protected from light at all times)
5	Actin staining	▪ Actin staining solution	❖ Remove HBSS+/+ from the constructs and add 500 µl of Actin staining solution or enough to cover constructs ❖ Incubate constructs overnight at RT
6	Preparation NucBlue staining solution	▪ NucBlue™ ▪ HBSS+/+ ▪ 15 ml falcon tube	❖ Add 1 drop of NucBlue™ for each ml of HBSS+/+ (keep NucBlue solution protected from light at all times)
7	NucBlue staining	▪ NucBlue staining solution	▪ Remove Actin staining solution and 500µl of NucBlue staining solution or enough to cover construct ▪ Incubate constructs for 1 hour at RT

8	Washing	▪ HBSS +/+	▪ Wash constructs with HBSS+/+ three times for 10 minutes at a time ▪ Keep constructs in HBSS+/+ until imaging

9.2. Complete results of 3D bioprinting experiments

9.2.1 Live/Dead analysis cell count and viability results

9.2.1.1

Table 12. Experiment 1 cell count and viability values for 10M HepG2 /ml GelXA

HepG2							
			Cell no.	Total cell no.	Viability (%)	Avg. cell no.	Avg. vaiability (%)
Day 1	1.00	Live	143.00	226.00	63.27	253.00	61.64
		Dead	83.00				
	2.00	Live	168.00	280.00	60.00		
		Dead	112.00				
Day 7	1.00	Live	212.00	363.00	58.40	381.50	50.70
		Dead	151.00				
	2.00	Live	172.00	400.00	43.00		
		Dead	228.00				
Day 20 I	1.00	Live	420.00	808.00	51.98	711.00	55.47
		Dead	388.00				
	2.00	Live	362.00	614.00	58.96		
		Dead	252.00				
Day 20 C	1.00	Live	284.00	666.00	42.64	567.00	55.62
		Dead	382.00				
	2.00	Live	321.00	468.00	68.59		
		Dead	147.00				

Table 13. Experiment 1 cell count and viability values for 10M 2HepG2 :1 LX-2 /ml GelXA

2:1							
			Cell no.	Total cell no.	Viability (%)	Avg. cell no.	Avg. vaiability (%)
Day 1	1.00	Live	219.00	354.00	61.86	325.00	77.89
		Dead	135.00				
	2.00	Live	278.00	296.00	93.92		
		Dead	18.00				
Day 7	1.00	Live	504.00	577.00	87.35	593.50	87.03
		Dead	73.00				
	2.00	Live	529.00	610.00	86.72		
		Dead	81.00				
Day 20 I	1.00	Live	433.00	970.00	44.64	811.00	44.18
		Dead	537.00				
	2.00	Live	285.00	652.00	43.71		
		Dead	367.00				
Day 20 C	1.00	Live	496.00	1083.00	45.80	1068.00	48.83
		Dead	587.00				
	2.00	Live	546.00	1053.00	51.85		
		Dead	507.00				

Table 14. Experiment 1 cell count and viability values for 10M 4HepG2 :1 LX-2 /ml GelXA

4:1							
			Cell no.	Total cell no.	Viability (%)	Avg. cell no.	Avg. vaiability (%)
Day 1	1.00	Live	153.00	252.00	60.71	203.00	43.67
		Dead	99.00				
	2.00	Live	41.00	154.00	26.62		
		Dead	113.00				
Day 7	1.00	Live	143.00	199.00	71.86	193.50	77.15
		Dead	56.00				
	2.00	Live	155.00	188.00	82.45		
		Dead	33.00				
Day 20 I	1.00	Live	229.00	579.00	39.55	701.00	36.66
		Dead	350.00				
	2.00	Live	278.00	823.00	33.78		
		Dead	545.00				
Day 20 C	1.00	Live	417.00	743.00	56.12	698.00	59.46
		Dead	326.00				
	2.00	Live	410.00	653.00	62.79		
		Dead	243.00				

Table 15. Experiment 2 cell count and viability values for 10M HepG2 /ml GelXA

HepG2							
			No. of cells	Total cell no.	Viability (%)	Avg. cell no.	Avg. vaiability (%)
Day 1	1	Live	398	1207	32.97	1047	27.93
		Dead	809				
	2	Live	203	887	22.89		
		Dead	684				
Day 7	1	Live	150	155	96.77	186.5	93.57
		Dead	5				
	2	Live	197	218	90.37		
		Dead	21				
Day 21 C	1	Live	157	271	57.93	250.5	55.92
		Dead	114				
	2	Live	124	230	53.91		
		Dead	106				
Day 21 I	1	Live	166	189	87.83	162	64.29
		Dead	23				
	2	Live	55	135	40.74		
		Dead	80				

Table 16. Experiment 2 cell count and viability values for 10M 2HepG2 :1 LX-2 /ml GelXA

2:1							
			No. of cells	Total cell no.	Viability (%)	Avg. cell no.	Avg. vaiability (%)
Day 1	1.00	Live	280.00	1126.00	24.87	1025.00	32.18
		Dead	846.00				
	2.00	Live	365.00	924.00	39.50		
		Dead	559.00				
Day 7	1.00	Live	372.00	550.00	67.64	551.50	64.02
		Dead	178.00				
	2.00	Live	334.00	553.00	60.40		
		Dead	219.00				
Day 21 C	1.00	Live	221.00	323.00	68.42	550.50	52.85
		Dead	102.00				
	2.00	Live	290.00	778.00	37.28		
		Dead	488.00				
Day 21 I	1.00	Live	114.00	380.00	30.00	414.00	47.25
		Dead	266.00				
	2.00	Live	289.00	448.00	64.51		
		Dead	159.00				

Table 17. Experiment 2 cell count and viability values for 10M 4HepG2 :1 LX-2 /ml GelXA

4:1							
			No. of cells	Total cell no.	Viability (%)	Avg. cell no.	Avg. vaiability (%)
Day 1	1	Live	215	918	23.42	1012.5	23.95
		Dead	703				
	2	Live	271	1107	24.48		
		Dead	836				
Day 7	1	Live	261	356	73.31	373	65.63
		Dead	95				
	2	Live	226	390	57.95		
		Dead	164				
Day 21 C	1	Live	503	1003	50.15	1113.5	56.73
		Dead	500				
	2	Live	775	1224	63.32		
		Dead	449				
Day 21I	1	Live	486	657	73.97	626	56.73
		Dead	171				
	2	Live	235	595	39.50		
		Dead	360				

Table 18. Experiment 3 cell count and viability values for 10M HepG2 /ml GelXA

HepG2							
			No. of cells	Total cell no.	Viability (%)	Avg. cell no.	Avg. vaiability (%)
Day 1	1	Live	310	491	63.14	529.5	71.44
		Dead	181				
	2	Live	453	568	79.75		
		Dead	115				
Day 7	1	Live	152	367	41.42	360	45.50
		Dead	215				
	2	Live	175	353	49.58		
		Dead	178				
Day 21 C	1	Live	193	554	34.84	678.5	30.49
		Dead	361				
	2	Live	210	803	26.15		
		Dead	593				
Day 21 I	1	Live	211	336	62.80	341.5	59.35
		Dead	125				
	2	Live	194	347	55.91		
		Dead	153				

Table 19. Experiment 3 cell count and viability values for 10M 2HepG2 :1 LX-2 /ml GelXA

2:1							
			No. of cells	Total cell no.	Viability (%)	Avg. cell no.	Avg. vaiability (%)
Day 1	1	Live	344	570	60.35	634.5	58.79
		Dead	226				
	2	Live	400	699	57.22		
		Dead	299				
Day 7	1	Live	325	809	40.17	780	45.52
		Dead	484				
	2	Live	382	751	50.87		
		Dead	369				
Day 21 C	1	Live	234	729	32.10	729	32.10
		Dead	495				
	2	Live	239	704	33.95		
		Dead	465				
Day 21 I	1	Live	195	556	35.07	556	35.07
		Dead	361				
	2	Live	254	501	50.70		
		Dead	247				

Table 20. Experiment 3 cell count and viability values for 10M 4HepG2 :1 LX-2 /ml GelXA

4:1							
			No. of cells	Total cell no.	Viability (%)	Avg. cell no.	Avg. vaiability (%)
Day 1	1.00	Live	270.00	598.00	45.15	585.00	43.47
		Dead	328.00				
	2.00	Live	239.00	572.00	41.78		
		Dead	333.00				
Day 7	1.00	Live	306.00	547.00	55.94	546.00	57.60
		Dead	241.00				
	2.00	Live	323.00	545.00	59.27		
		Dead	222.00				
Day 21 C	1.00	Live	163.00	506.00	32.21	674.00	44.67
		Dead	343.00				
	2.00	Live	481.00	842.00	57.13		
		Dead	361.00				
Day 21 I	1.00	Live	255.00	595.00	42.86	515.00	40.62
		Dead	340.00				
	2.00	Live	167.00	435.00	38.39		
		Dead	268.00				

9.2.1.2. Live/Dead images

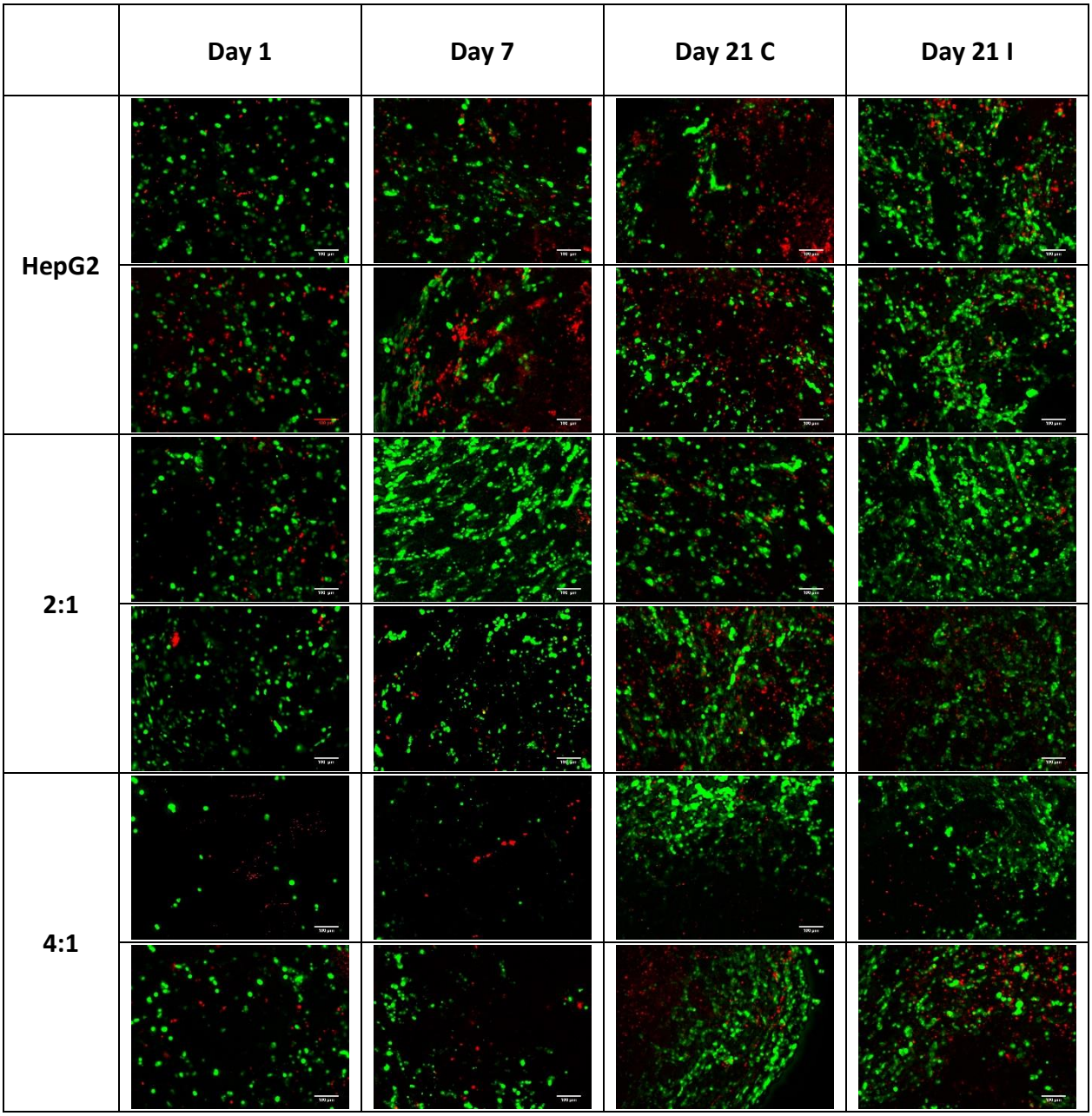

Figure 42. Experiment 1 Live/Dead images

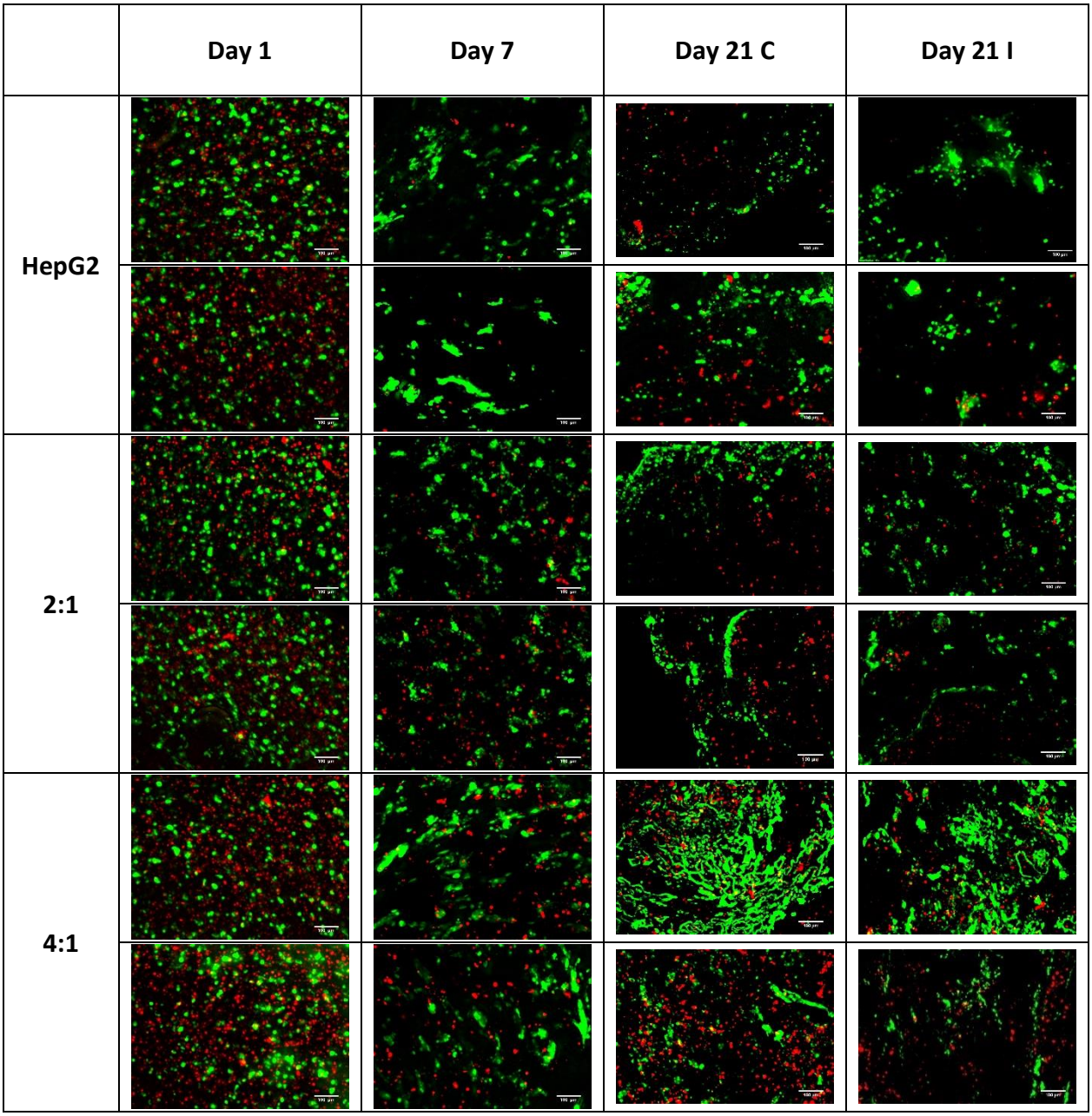

Figure 43. Experiment 2 Live/Dead images

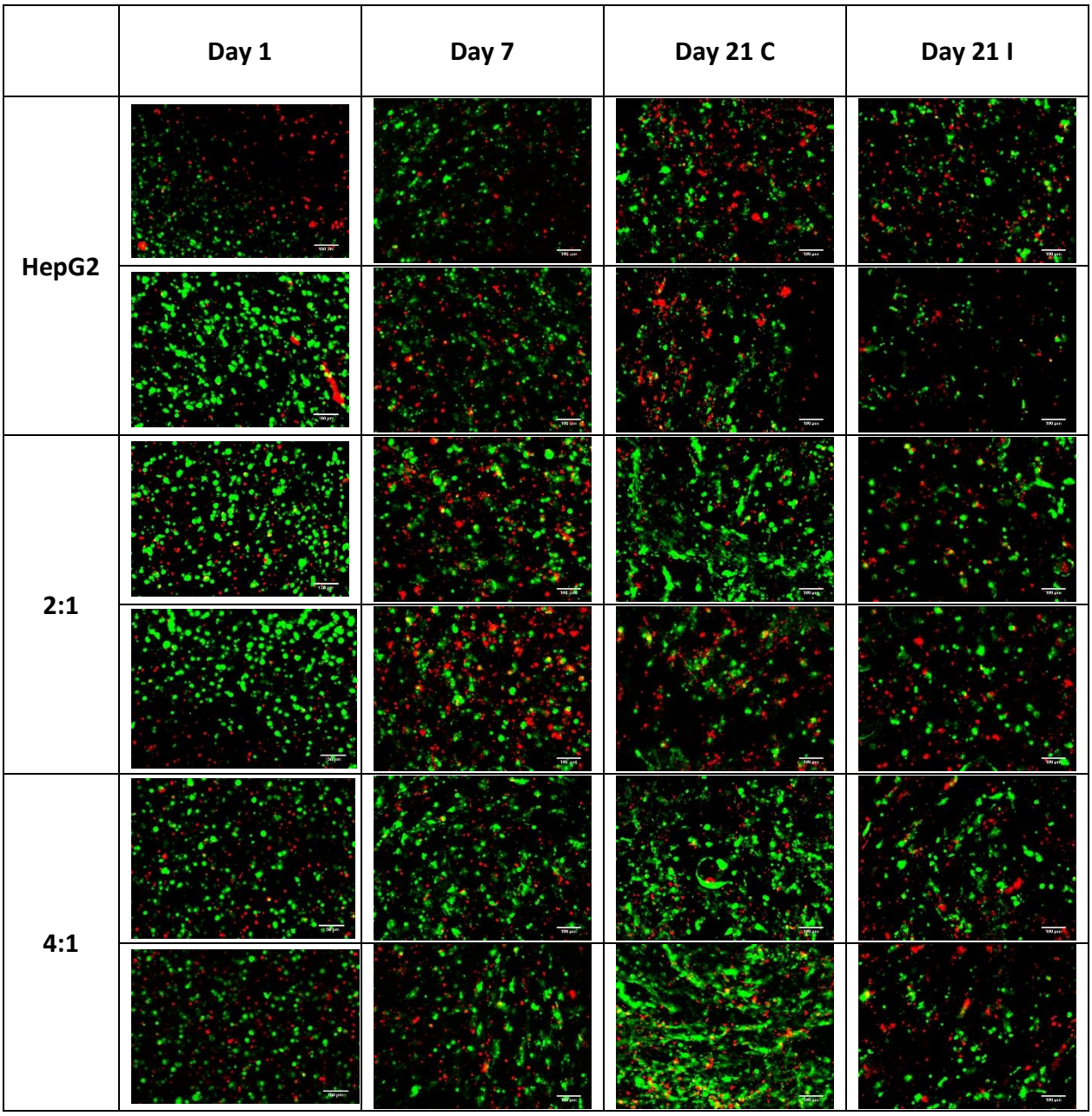

Figure 44. Experiment 3 Live/Dead images

9.2.2. Celltiter-Blue® viability analysis results

Table 21. Average Celltiter-Blue fluorescence values/1000000

Average Fluorescence /1000000			
	HepG2	2:1	4:1
Day 1	769.90	746.7483	743.6307
Day 7	741.39	757.0097	750.5389
Day 14 C	742.10	405.83	511.95
Day 14 I	799.75	620.86	734.81
Day 20 C	745.63	550.11	575.27
Day 20 I	790.47	707.02	806.98

Validation of Celltiter-Blue® results

Table 22 Celltiter-Blue fluorescence values /1000000 for experiment 4

Days	Fluorescence/1000000		
	HepG2	2:01	4:01
Day 1	233.7	289.25	302.05
Day 7	718.62	640.2	668.91
Day 14	779	378.59	506.86

9.2.3. LDH Cytotoxicity assay results

Table 23. Experiment 1 Average absorbance values (490-680 nm) depicting LDH levels

Avg. Absorbance			
	HepG2	2:1	4:1
Day 1	0.065333	0.119667	0.101667
Day 7	0.089	0.145667	0.177333
Day 12 I	0.105333	0.193	0.183333
Day 12 NI	0.1365	0.214	0.13
Day 16 I	0.109333	0.144	0.149667
Day 16 NI	0.084	0.187	0.126
Day 20 I	0.112333	0.193667	0.174
Day 20 NI	0.096333	0.170667	0.130333

Table 24. Experiment 2 Average absorbance values (490-680 nm) depicting LDH levels

LDH			
	HepG2	2:1	4:1
Day 1	0.165	0.131	0.162667
Day 7	0.074	0.149	0.146667
Day 12 I	0.066333	0.205667	0.167333
Day 12 NI	0.069	0.167667	0.170333
Day 16 I	0.069333	0.445	0.485333
Day 16 NI	0.075	0.363	0.388333
Day 20 I	0.046	0.207667	0.28
Day 20 NI	0.154333	0.199	0.231

Table 25. Experiment 3 Average absorbance values (490-680 nm) depicting LDH levels

LDH			
	HepG2	2:1	4:1
Day 1	0.112333	0.245	0.195
Day 7	0.145333	0.235667	0.223667
Day 12 I	0.34	0.349	0.299333
Day 12 NI	0.125333	0.253	0.285
Day 16 I	0.173	0.330667	0.287
Day 16 NI	0.260667	0.308667	0.310333
Day 20 I	0.139	0.393667	0.356
Day 20 NI	0.4403	0.442333	0.358

9.2.4. Bicinchoninic acid (BCA) protein assay results

9.2.4.1. Construct (BCA) protein assay results

Table 26. Experiment 1 average construct protein concentrations

Protein Conc.			
	HepG2	2:1	4:1
Day 0	53.05586	165.0243	13.50815
Day 4 NI	103.1162	402.978	414.4919
Day 4 I	266.15	441.02	426.84
Day 8 NI	423.00	563.84	443.19
Day 8 I	215.75	458.88	256.47
Day 12 NI	215.59	689.66	496.76
Day 12 I	237.78	625.25	331.22

Table 27. Experiment 2 average construct protein concentrations

Protein Conc.			
	HepG2	2:1	4:1
Day 0	63.16811	118.4033	65.22657
Day 4 NI	87.35497	100.0488	157.8571
Day 4 I	97.30	171.07	164.03
Day 8 NI	116.00	125.24	304.01
Day 8 I	106.91	330.42	189.59
Day 12 NI	154.94	338.49	463.71
Day 12 I	93.36	431.12	499.90

Table 28. Experiment 3 average construct protein concentrations

Protein Conc.			
	HepG2	2:1	4:1
Day 0	175.1691	220.0763	225.7607
Day 4 NI	135.5201	245.5142	277.3471
Day 4 I	287.15	264.98	255.32
Day 8 NI	255.3199	254.18	366.59
Day 8 I	220.36	364.46	351.10
Day 12 NI	366.38	493.00	371.28
Day 12 I	189.24	521.64	458.97

9.2.4.2. Media (BCA) protein assay results

Table 29. Average media protein concentrations for three replicate experiments

Avg. conc.		
HepG2	2:1	4:1
63.79	60.11	8.56
-3.62	-11.70	-19.97
7.23	-53.79	-46.27
10.16	-40.61	-74.78
-11.66	-26.56	-30.48
24.82	-44.97	-50.43
1.95	-44.30	-16.66
13.52	-31.25	-34.82

9.2.5. Actin/NucBlue staining images

Day	HepG2	2:1	4:1
Day 8	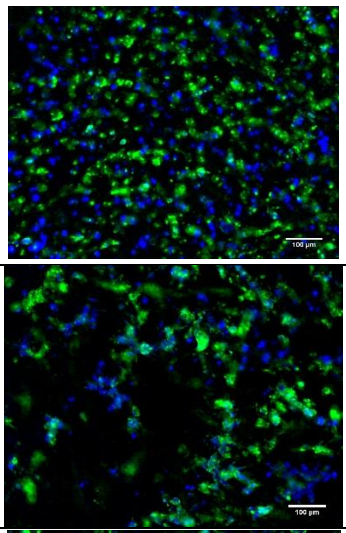	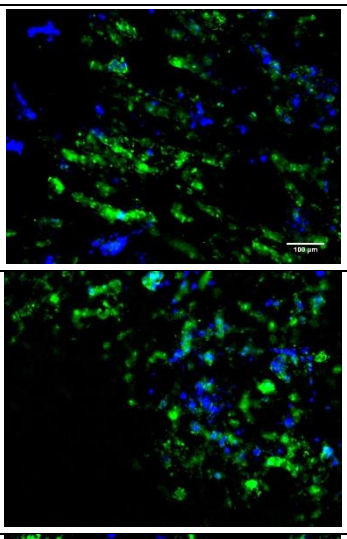	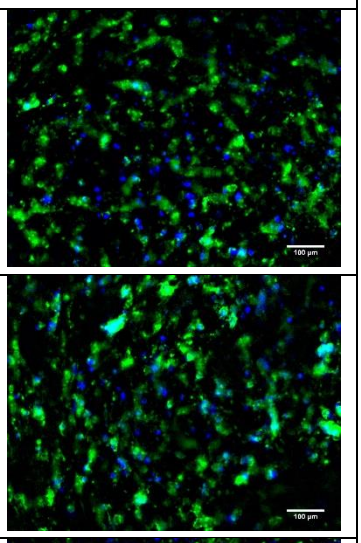
Day 18 C	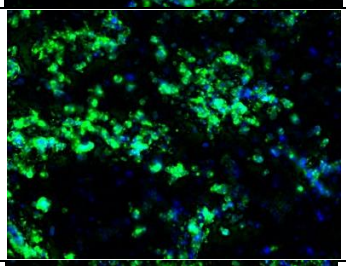	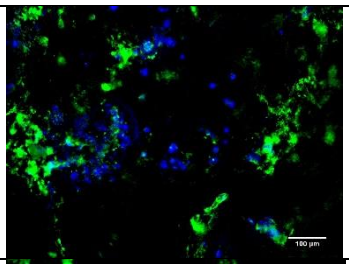	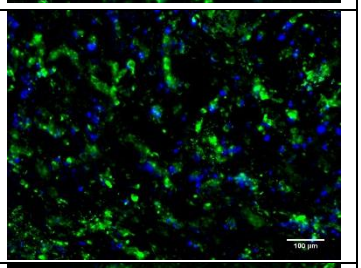
	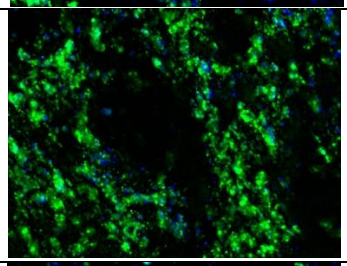	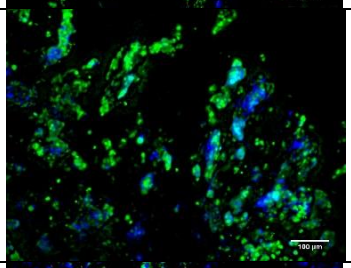	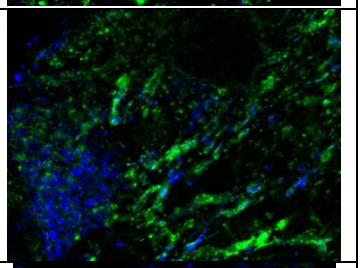
Day 18 I	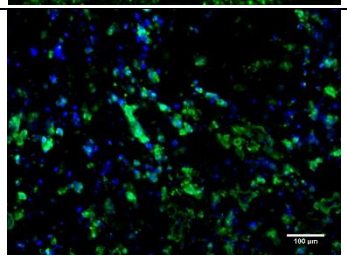	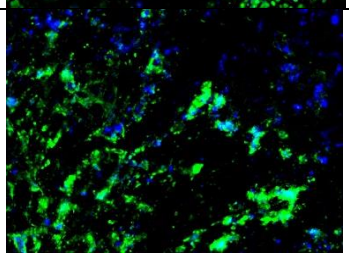	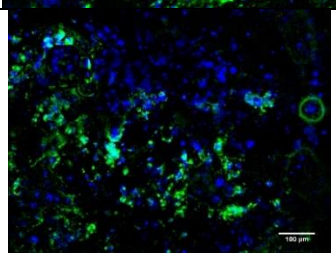
	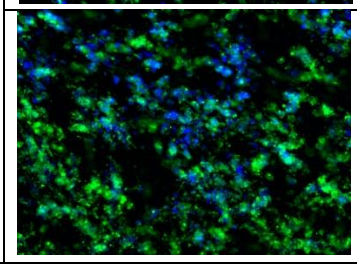	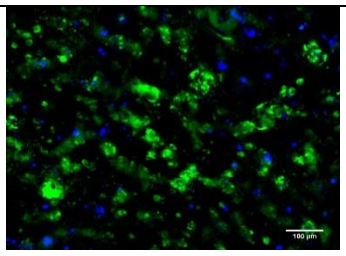	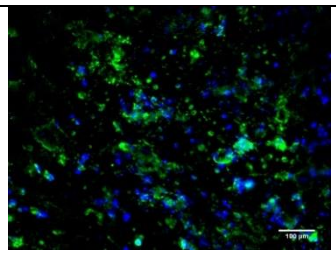

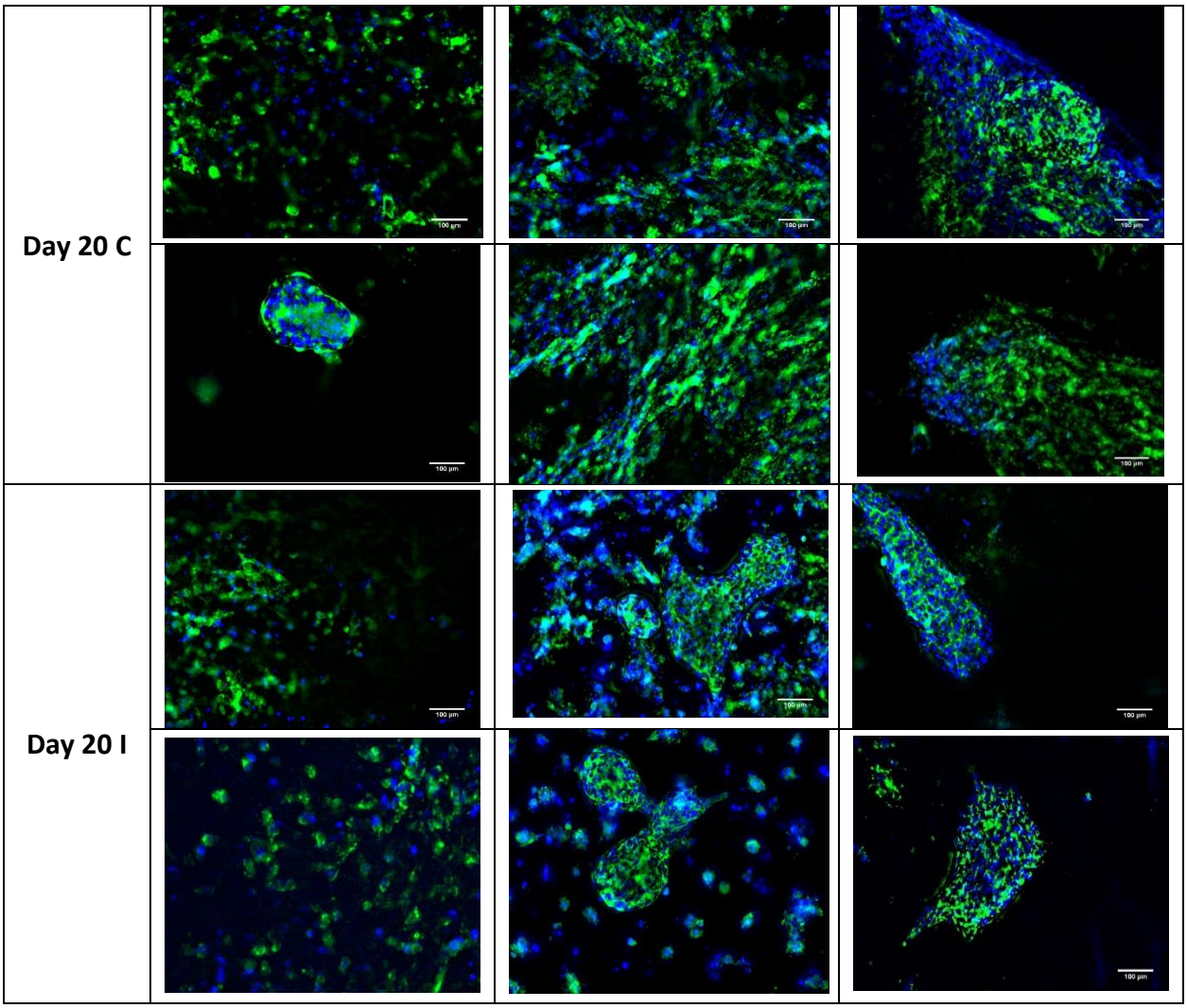

Figure 46. Actin/NucBlue staining images